Marine Ecosystems

Oceanographic monitoring and far-field modelling to inform desalination in Boston Bay

M. Doubell & C. James

Government of South Australia
Department of Primary Industries and Regions

SA Water

SARDI
SOUTH AUSTRALIAN RESEARCH AND DEVELOPMENT INSTITUTE

Oceanographic monitoring and far-field modelling to inform desalination in Boston Bay

Report to SA Water

M. Doubell and C. James

February 2023

This publication may be cited as:
Doubell, M. and James, C. (2023). Oceanographic monitoring and far-field modelling to inform desalination in Boston Bay. Report to SA Water. South Australian Research and Development Institute (Aquatic Sciences), Adelaide. SARDI Publication No. F2022/000347-1. SARDI Research Report Series No. 1165. 71pp.

DISCLAIMER

The authors warrant that they have taken all reasonable care in producing this report. The report has been through the SARDI internal review process and has been formally approved for release by the Research Director, Aquatic and Livestock Sciences. Although all reasonable efforts have been made to ensure quality, SARDI does not warrant that the information in this report is free from errors or omissions. SARDI and its employees do not warrant or make any representation regarding the use, or results of the use, of the information contained herein as regards to its correctness, accuracy, reliability and currency or otherwise. SARDI and its employees expressly disclaim all liability or responsibility to any person using the information or advice. Use of the information and data contained in this report is at the user's sole risk. If users rely on the information, they are responsible for ensuring by independent verification its accuracy, currency or completeness. The SARDI Report Series is an Administrative Report Series which has not been reviewed outside the department and is not considered peer-reviewed literature. Material presented in these Administrative Reports may later be published in formal peer-reviewed scientific literature.

© 2023 SARDI

This work is copyright. Apart from any use as permitted under the *Copyright Act* 1968 (Cth), no part may be reproduced by any process, electronic or otherwise, without the specific written permission of the copyright owner. Neither may information be stored electronically in any form whatsoever without such permission.

Author(s):	M. Doubell and C. James
Reviewer(s):	M. Deveney and R. Kirkwood (SARDI)
Approved by:	S. Goldsworthy Science Leader – Marine Ecosystems
Signed:	
Date:	09 February 2023
Distribution:	SA Water and SARDI Aquatic Sciences.
Circulation:	OFFICIAL Sensitive

ALL ENQUIRIES

South Australian Research and Development Institute - SARDI Aquatic Sciences
2 Hamra Avenue West Beach SA 5024
PO Box 120 Henley Beach SA 5022
P: (08) 8207 5400 **F:** (08) 8207 5415
E: pirsa.sardiaquatics@sa.gov.au **W:** http://www.pir.sa.gov.au/research

TABLE OF CONTENTS

LIST OF FIGURES

LIST OF TABLES

ACKNOWLEDGEMENTS

EXECUTIVE SUMMARY

SA Water are proposing to build a small desalination plant (4-5.3GL per year) with the potential for expansion to 8 GL per year to supplement the existing water supply. Several plant intake and outfall sites in and around Boston Bay (Port Lincoln) are being considered. Given the reduced flushing of the regions surrounding embayment's, the importance of co-located aquaculture industries, and the need to protect receiving ecosystems, there is a need to examine the potential impacts and capacity for the area to host a desalination plant.

In this study, a high-resolution three-dimensional hydrodynamic model for the Port Lincoln region is developed to examine the effect of hydrodynamics on the far-field dispersal of brine discharges for five outfall locations, including inshore outfalls proposed near Billy Lights Point and Point Boston. Hydrodynamic model predictions are additionally used to drive a particle tracking model to understand the far-field connectivity of planktonic larvae, such as the commercially important blue mussel (*Mytilus galloprovincialis*), with proposed intake locations. Comparison of the hydrodynamic model with moored field measurements made over a one-year period showed the model was able to reproduce tidal and lower-frequency (weather-band and seasonal variations) in currents, sea level, temperature, and salinity. The model therefore demonstrated predictive capability for assessing the transport, dispersal and fate of brine discharges and planktonic larvae associated with the operation of the proposed desalination plant.

Using a 5-year model hindcast, far-field predictions of the salinity differences (i.e., anomalies) between a 12 GL per year desalination plant operating at full capacity and a model simulation with no desalination, showed a maximum seasonally-averaged salinity anomaly of 0.44 PSU within 250 to 500m of outfalls. This anomaly is equivalent to a 1.2 % change in the ambient salinity. Maximum seasonally-averaged anomalies were reduced to <0.1 PSU (<0.3% change in the ambient salinity) at distances >1 km from outfalls. At hourly timescales, predicted far-field increases in salinity at distances of ~300 m from outfalls were always <0.9 PSU (<2.5 % change in the ambient salinity) and decreased to <0.4 PSU (<1.1 % change in the ambient salinity) at distances >1 km from outfalls. The predicted changes in salinity due to desalination discharges are within the natural salinity variability of the region determined from the measured data. Salinity observations showed an annual range of 1.46 PSU equivalent to a 4% change in ambient salinity, and variations of ~0.1 and ~0.5 PSU across timescales of several hours to a week, respectively.

Comparison of the brine dispersal patterns from the different outfall locations demonstrated that the spatial extent and magnitude of long-term salinity increases were reduced when outfalls were in offshore waters east of Boston Island. For all outfall locations, salinity increases predicted at distances greater than 250 m from outfalls associated with the 12 GL per year plant modelled in this study were below the less than 5% change in ambient salinity (~1.8 PSU) recommended by the Australian and New Zealand Guidelines for Fresh and Marine Waters and the 1 PSU environmental and ecological tolerance limits for flora and fauna reported in the desalination literature. This suggests, given the small size of the proposed plant (8 GL per year maximum), there are unlikely to be any substantial environmental impacts from brine discharges in the far-field. To adequately minimise salinity increases, however, it will be important that sufficient dilution is achieved by appropriate diffuser designs in the near field.

Biophysical modelling results for planktonic larvae, based on a limited understanding of the spawning characteristics of blue mussels, showed the far-field spatial connectivity of simulated passive larvae with intakes was strongly influenced by tides and the regional circulation patterns. This identified that mussels sourced from Proper Bay and the Boston Bay area inshore from Boston Island had increased connectivity with intakes located near Billy Lights Point and reduced connectivity with the intake located near Point Boston. Similarly, mussels sourced from Louth and Peake Bays had increased connectivity with the intake located near Point Boston and reduced connectivity with intakes located near Billy Lights Point. For all intake locations, the far-field connectivity modelling indicated that less than 0.1% of the particles released over the course of the mussel spawning season may be at risk of coming within a 25 m radius of intakes. Future validation and development of the biophysical model, including *in situ* sampling to understand larval source regions and concentrations and the vertical distribution of mussel larvae, is needed to improve the far-field connectivity modelling to better inform the number of larvae possibly removed by desalination intakes.

The modelling results presented in this study on the potential far-field increases in salinity due to desalination brine outfalls and larval entrainment by intakes should be considered in the context of current and future cumulative environmental impacts in the Port Lincoln region, which is home to South Australia's most valuable and productive aquaculture zone. For example, these impacts include the combined effects resulting from other anthropogenic emissions (e.g., nutrients from tuna and finfish aquaculture, wastewater treatment plants and other sources) and climate change (e.g., marine heatwaves) on the regions ecosystems which remain areas of active research. In

this context, the hydrodynamic model developed in this study for the Port Lincoln region provides an improved tool that can be used to guide, assess, and minimise the potential impacts of desalination (and other anthropogenic point sources) to ensure the health, productivity, and sustainability of the region.

Keywords: hydrodynamic model, larval transport, desalination, brine discharges, dispersal, dilution

1. INTRODUCTION

1.1. Background

Security of water supply is a key priority for SA Water. Existing supplies for regional communities on South Australia's Eyre Peninsula need to be supplemented to ensure future proofing. To achieve this, SA Water plans to build a reverse osmosis desalination plant to initially supply 4-5.3 GL of freshwater per year, with potential for expansion to 8 GL per year. In 2021 a plant planned for construction at Sleaford Bay encountered substantial engineering issues due to geological conditions. Alternative sites in and around Boston Bay (Port Lincoln) are subsequently being considered (Figure 1).
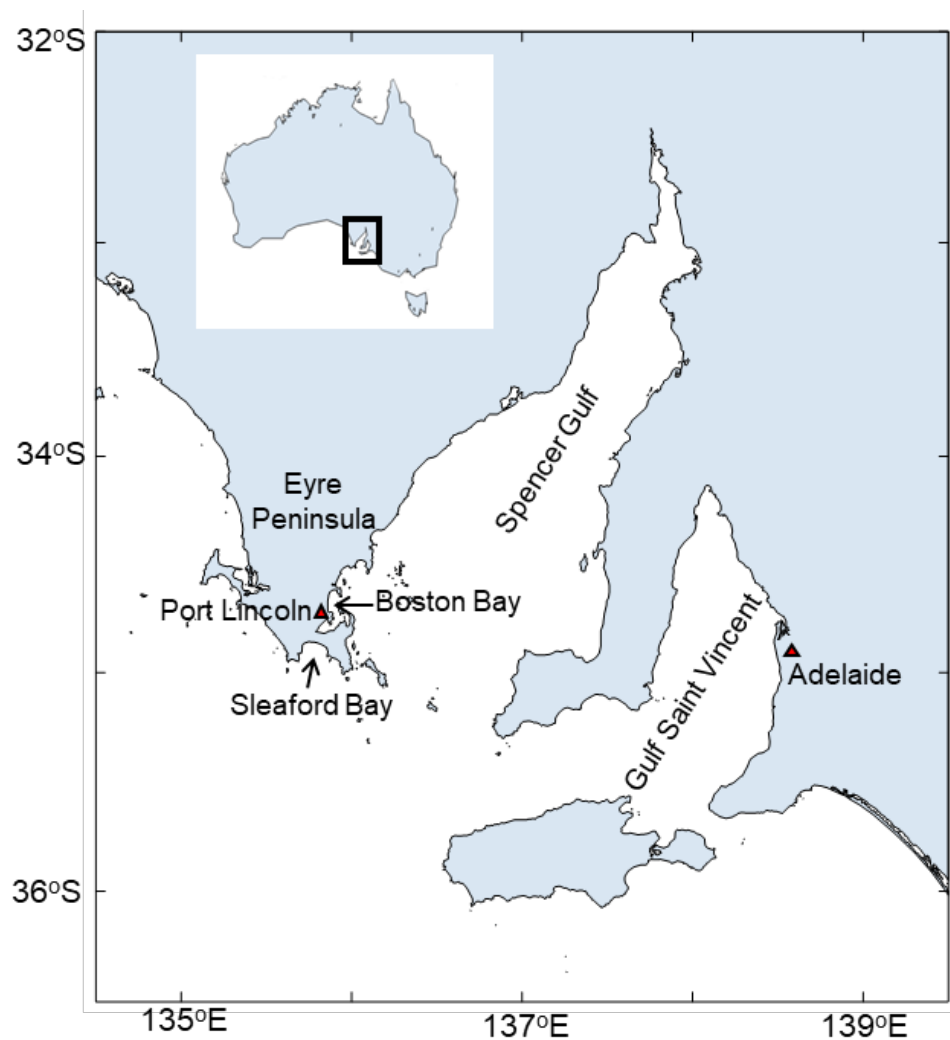
Figure 1. Map showing the location of the Eyre Peninsula region, South Australia.

4

Boston Bay and its adjoining waters are home to South Australia's most valuable and productive aquaculture zone (The Lower Eyre Peninsula Aquaculture Zone) and contain mussel, oyster, abalone, southern bluefin tuna, and other finfish aquaculture. In 2019/20 it was estimated approximately 13,150 tonnes of seafood valued at $180M per annum was produced from this zone (BDO EconSearch, 2020). Oceanographic research has demonstrated that the inshore waters of Boston Bay and adjacent embayments experience reduced flushing both at the site (Middleton et al., 2013, 2014) and bay scale (Herzfeld et al., 2008) relative to adjacent offshore waters. In addition, water quality (Tanner at al. 2020) and seagrass monitoring (Tanner at al. 2019) programs have raised concerns that dissolved nutrient emissions from co-located tuna and other finfish aquaculture, and wastewater treatment plants, are inter-connected and may be having cumulative impacts on the health and ecology of the regions surrounding planktonic and seagrass ecosystems.

Construction and operation of a desalination plant can have environmental and ecological impacts (Lattemann and Höpner 2008; Panagopoulos and Haralambous 2020; Tanner and Drabsch 2021; Omerspahic et al., 2022). In recognition of the reduced flushing of inshore waters and the adjoining co-location of valuable aquaculture industries, there is concern about whether the Port Lincoln region can absorb the outputs of a desalination plant without environmental impacts. Specific concerns raised by the aquaculture industry about the operation of a desalination plant are the potential impacts related to (i) the disposal of high salinity desalination brine and associated harmful chemical contaminants (Mavukkandy et al., 2019) on the receiving marine ecosystem and aquaculture sector, and (ii) the entrainment of the eggs and larvae of marine organisms, such as blue mussels, by the desalination intake.

This study aimed to develop and apply a high-resolution (300m grid resolution) hydrodynamic model for the Port Lincoln region to predict the far-field dispersal of brine outfalls and the far-field transport and connectivity of planktonic larvae. Model results were analysed for several proposed intake and outfall locations to support selection of a site where environmental impacts would be acceptable. Additional outfalls located in offshore waters outside of the embayments were also investigated for comparison with outfalls located closer to the shore. Near-field studies examining the design and application of diffuser systems, that are required to achieve rapid mixing and a 40:1 dilution of brine at the seabed under all conditions over spatial scales of metres to several hundred meters are not resolved by the models applied in this study and are being undertaken separately as part of the engineering design.

1.2. Objectives

The project objectives were to:

1. Use ocean moorings to collect baseline field observations of oceanographic parameters over 12 months.

2. Use the field observations of temperature, salinity, and currents to develop and validate a high-resolution hydrodynamic model for the Boston Bay region (HRBBM).

3. Use the HRBBM to produce a 5-year hindcast simulation and model the far-field dispersion of brine for several proposed desalination plant intake/outfall locations.

4. Use ocean current predictions from the HRBBM to undertake particle tracking studies to better understand the far-field transport and connectivity of planktonic larvae (i.e., blue mussel) with proposed desalination plant intake locations.

2. METHODS

2.1.   Field measurements: ocean moorings

Between 19-July 2021 and 18-August 2022, three oceanographic moorings (SAW1, SAW2, and SAW3) were placed in and around Boston Bay (Figure 2, Table 1). The moorings collected data essential for understanding baseline environmental variability and supporting hydrodynamic model development and validation. Mooring frames (Figure 3) were deployed on the seafloor and, at two locations (SAW1 and SAW2), were equipped with Nortek Acoustic Doppler Current Profilers (ADCP) to measure current speed and direction throughout the water column. At all three locations, conductivity, temperature, and depth (CTD) as well as water quality measures including dissolved oxygen, chlorophyll and turbidity, were measured. All parameters were sampled at sub-hourly intervals (15-30 minutes depending on the sensor). Moorings were serviced at approximately 2-monthly intervals, when data were downloaded, moorings cleaned and sensors either redeployed or exchanged.
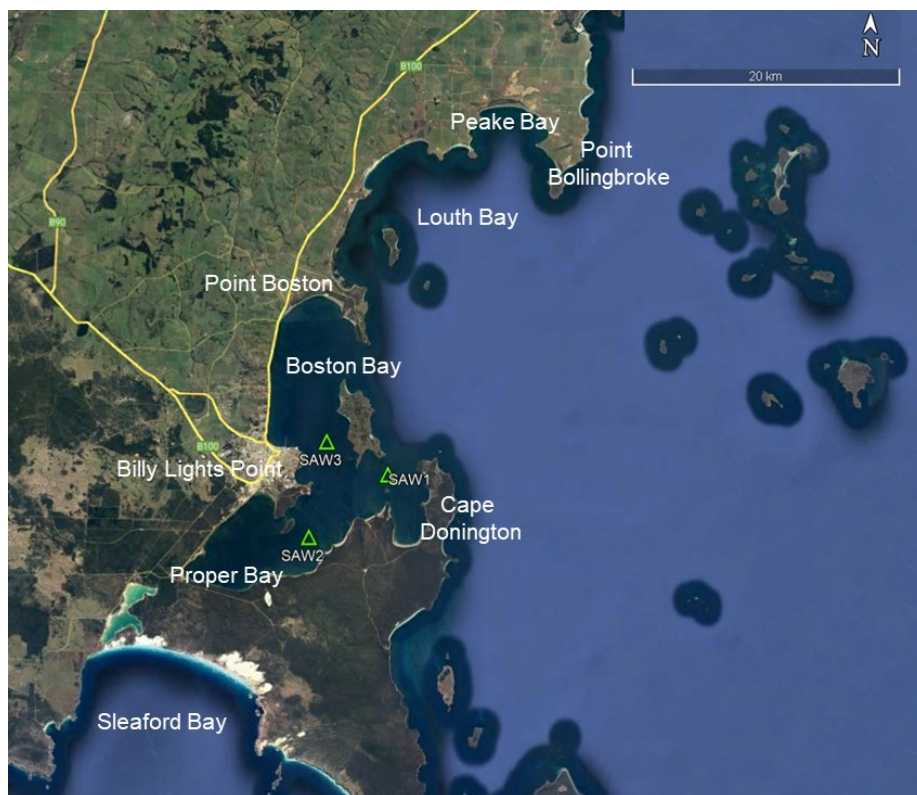
Figure 2. Google Earth image showing Port Lincoln and the surrounding bays. The location of the oceanographic moorings SAW1, SAW2 and SAW3 are indicated by the green triangle markers.

7

Table 1. Description of the mooring locations and ocean sensors used at each mooring.

Mooring Name	Equipment Provider	Sensors	Latitude (°S)	Longitude (° E)	Depth (m)
SAW1	SARDI	- Nortek Signature 500 or 1000 ADCP - Seabird SBE16plus CTD with water quality sensors	34.7381	135.9557	17
SAW2	SA Water	- Nortek Signature 1000 ADCP - YSI EXO2 CTD Sonde with water quality sensors and/or RBR Duo TS loggers	34.7818	135.8917	11
SAW3	SA Water	-YSI EXO2 CTD Sonde with water quality sensors and/or RBR Duo TS loggers	34.7167	135.9042	17

Figure 3. Picture of the coastal ocean mooring deployed at SAW1.

Fouling and sensor calibration issues compromised data quality on occasions, particularly for salinity measurements. For example, Figure 4 shows an example of the step change in salinity of ~1 PSU following a change of sensor at the SAW2 mooring during servicing in September 2021.
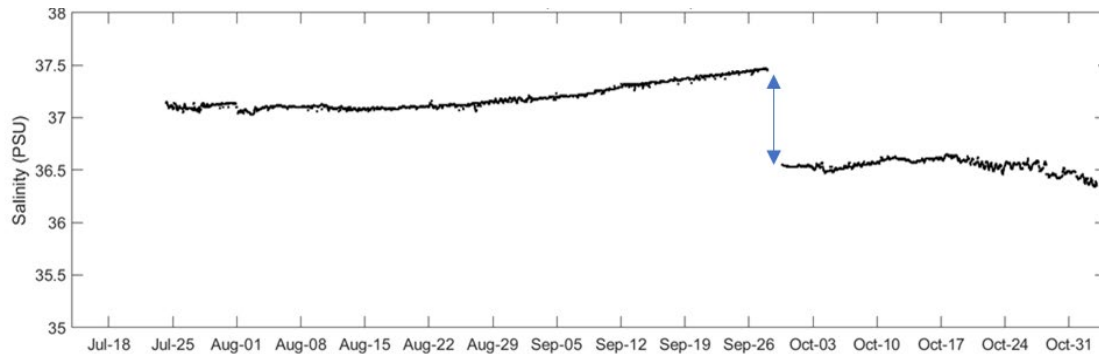
Figure 4. Example of sensor calibration issues which complicate the model validation process. Observed salinities at the SAW2 mooring site showed a distinct step change (indicated by the blue arrow) when sensors were changed during servicing on the on the 28th and 29th of September 2021.

For model validation purposes, calibration errors for each moored temperature and salinity sensor were identified by undertaking tank comparison tests at SARDI using seawater from Gulf Saint Vincent (Table 2). Mean temperature and salinity signals for each moored sensor were averaged over 30-minutes and compared to the SARDI Seabird 19plus profiling CTD which was used as a reference. This CTD is calibrated annually at the CSIRO Oceanographic Calibration Facility and showed strong agreement with *in-situ* bottle samples (Figure 5) taken at the Integrated Marine Observing System (IMOS) Kangaroo Island National Reference Station (r^2 = 0.99, root-mean-square (RMS) error = 0.11 PSU, bias = 0.0003 PSU). Calibration corrections for subsequent deployments were applied using profiles taken with the reference CTD at the start and end of each deployment.

Table 2. Calibration offsets for temperature (^{o}C) and salinity (PSU) for moored instruments.

Sensor	Serial No.	Test date	Salinity Offset	Temperature Offset
SBE16+	50291	15/07/2022	0.004	0.001
SBE16+	50292	18/01/2022	0.004	0.002
EXO2	102998	18/01/2022	0.272	0.038
EXO2	104518	18/01/2022	0.749	-0.008
EXO2	101382	18/01/2022	1.183	0.320
EXO2	103326	18/01/2022	0.989	0.062
RBR Duo	61653	28/04/2022	-0.062	0.013
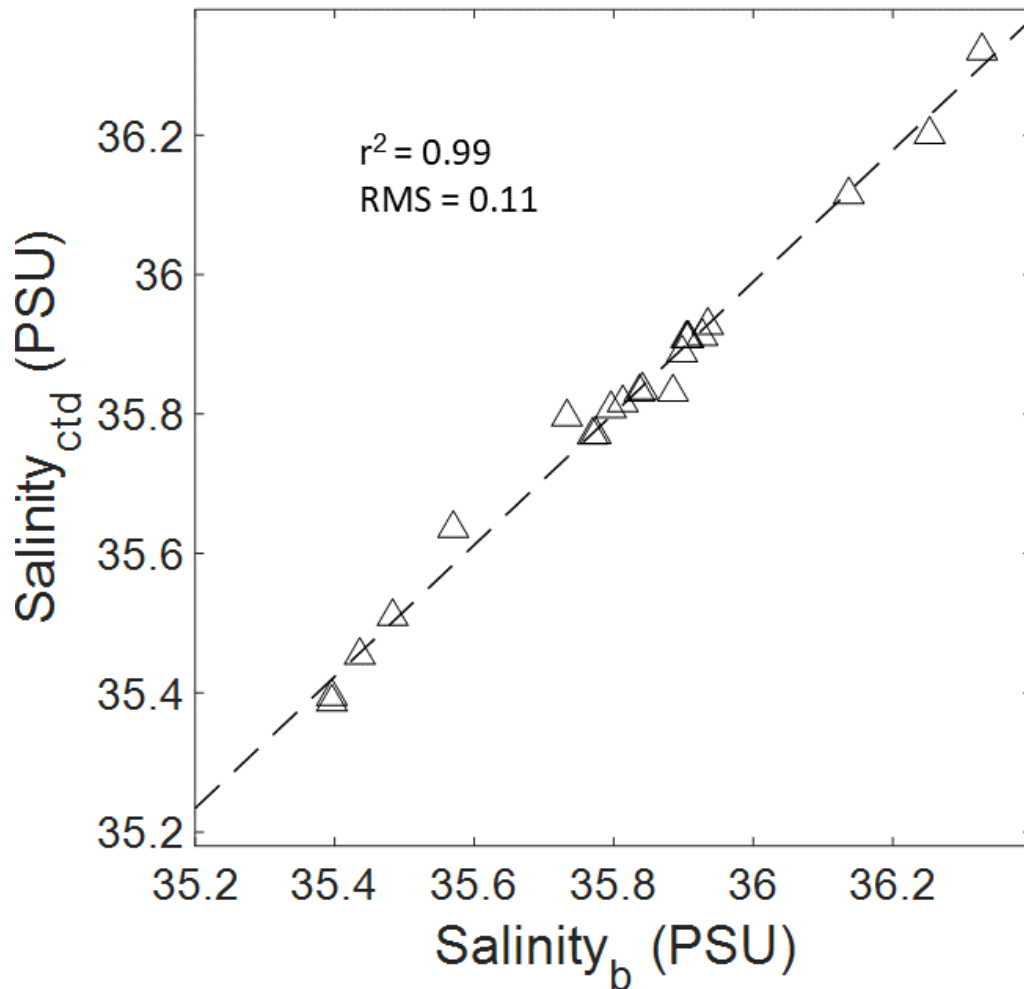
Figure 5. Comparison of salinity measures (PSU) using the SARDI/IMOS Seabird 19plus CTD (SN 6658) with bottle samples (Salinity$_b$) taken between 0 and 100m depth at the IMOS Kangaroo Island National Reference Station across three sampling events (February, May, and August) in 2021. Dashed lines show linear regression. RMS is the root-mean-square error.

2.2.   Ocean modelling system

The open-source Regional Ocean Modelling System (ROMS, https://www.myroms.org/) was used to simulate circulation and mixing in Spencer Gulf. ROMS is a high resolution, three-dimensional, free-surface oceanic model that uses topography-following coordinates in the vertical direction, and orthogonal curvilinear coordinates in the horizontal direction (Shchepetkin & McWilliams 2005; Song & Haidvogel 1994). A nested model approach was applied to increase boundary condition resolution from near-global (non-Arctic) ocean models (10 km grid) to the gulf scale using the 1.5 km resolution version of the Two Gulfs Model (TGM). The bathymetry for the

TGM grid was based on the 0.0025º resolution, Geoscience Australia (GSA), bathymetric grid for Australia Bathymetry (Whiteway 2009). Validation of the TGM has included comparisons against field observations collected by IMOS and other datasets for sea level height, currents, shear, temperature, and salinity. These comparisons have been presented across several peer-reviewed publications (Middleton et al. 2014, McLeay et al. 2016, Rogers et al. 2021) and technical reports (Middleton et al. 2013, 2017; Tanner et al. 2020).

To achieve the finer spatial resolution required to model the potential impact of desalination in Boston Bay, a 2-way nested high-resolution model for Boston Bay (HRBBM) was embedded within the TGM. The HRBBM has a horizontal spatial resolution of 300m and 15 sigma levels in the vertical. Lateral boundary conditions and interior solutions for the HRBBM are exchanged with the TGM and the model is run with a time-step of 40 s. The HRBBM grid allows for wetting and drying (Warner et al. 2013) to improve the simulation of physical processes in the shallow water bays located within the model domain. Improvements to the model's bathymetry was achieved using bathymetric data obtained from the Australian Hydrographic Office (AHO). The AHO bathymetry was adjusted to mean sea level and merged with the GSA bathymetry in the TGM to provide consistency within both models (Figure 6).

Both the TGM and HRBBM were forced with pressure, wind, humidity, heat-fluxes, and precipitation from global atmospheric models provided by the NCEP Climate Forecast System Reanalysis v.2 (Saha et al. 2014). Tidal forcing was provided by the global TPXO9 model (Erofeeva & Egbert 2014). Lateral oceanic boundary conditions and initial fields for TGM (i.e., temperature, salinity, currents, and sea level) were provided by the 10 km resolution Ocean Forecast Australia Model (OFAM). Due to product availability, CSIRO's Blue Link Reanalysis 2020 (BRAN2020; Oke et al., 2013) was used for modelling the years from July 2015 to June 2022 and the CSIRO/Bureau of Meteorology's OceanMAPS v3.4 analysis from July 2022 onwards. Improvement to the model sea surface temperature (SST) was achieved by adjusting the heat-fluxes using remote sensed SST provided by the Level 4 Multi-scale Ultra-high Resolution (MUR) SST Analyses (Chin et al. 2017). The entire desalination hindcast simulation period extended from 1-January 2016 to 1-January 2021. A six-month model spin-up was run, using BRAN-derived initial conditions, from 1-July 2015 to 1-January 2016 to provide artefact free initial conditions for the hindcast simulations. The final hindcast model configuration was

determined using the results of a model validation run from 1-January 2021 to 20-August 2022, for comparison with measurements obtained from the moorings.

For all hindcast configurations model outputs were saved in the following formats to support further analysis. In summary, daily snapshots taken at 00:00 UTC of all model fields across the entire model domain are heavily aliased by the daily tides and were used for producing the 5-year hindcast animations of bottom salinity for each outfall (see Animation 1, Appendix 3). In section 4, three-day averages of all fields across the entire model domain were used to calculate long-term (i.e., seasonal) increases in salinity and to understand the influence of tides on the horizontal dispersal of brine discharges in the vicinity of outfalls. Three-day averages filter out transient features associated with daily tides while preserving the influence of the fortnightly tides including "dodge-tides". Hourly outputs of all fields at specific sites (see Figure 7) were used to perform model validations against measured mooring data (see section 3) and to produce tide resolving salinity-anomaly plots. Hourly velocity fields over 5 months (May-September) for three consecutive years (2016-2018) were used for the particle tracking studies shown in section 5. Hourly outputs of all model fields across the entire model domain for a 3-month period (January-April 2016) were used to understand the sensitivity of far-field salinity increases to brine releases spread over increasing model layers (i.e., depths) in the vertical (see Appendix 2).

For model validation the predictive skill and performance of the HRBBM was assessed using three metrics – the bias, root-mean-square error (RMS) and the coefficient of determination (r^2). Bias is the difference between the mean value predicted by the model and the measured mean, RMS error is the root-mean-square of differences between the model and the measurement, and r^2 is a measure of the fraction of variability (i.e., variance) explained by the model.
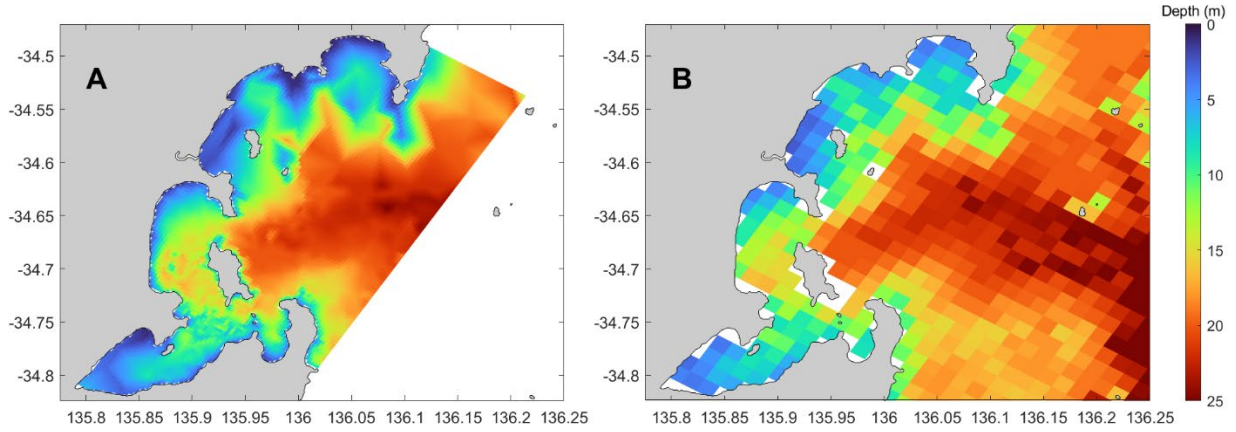
Figure 6. Hydrodynamic model grids developed using the AHO bathymetric datasets for (A) the HRBBM with a horizontal spatial resolution of 300 m and (B) merged with the GSA bathymetry within the corresponding subsection of the TGM with a horizontal spatial resolution of 1500 m.

2.3.   Far-field modelling of desalination discharges

Far-field hydrodynamic modelling to understand the fate and transport of brine discharges was undertaken for three intake and five outfall locations within the greater Port Lincoln region (Figure 7). Brine discharges from the desalination plant were implemented as a point source flux and neglected the impact of density changes on the salt flux (Kämpf et al. 2009) such that:

$$\Delta S = \frac{(Sb-S)q_b}{V}\Delta t \qquad\qquad\qquad (1)$$

where ΔS is the salinity increment for each time step (Δt) within the model, S is the salinity concentration (PSU) in the bottom model grid cell corresponding to the outfall location, Sb is the salinity of the brine discharge, q_b is the brine discharge rate, and V is the volume of the bottom model grid cell. The brine discharge rate was set to the peak outflow for the proposed desalination plant of q_b = 2800 m^3/hr.

A conservative approach was taken by discharging brine into the bottom sigma layer at each outfall location; this maximises the bottom anomaly. Due to the use of a terrain following sigma-coordinate model, the thickness of this bottom layer in the model ranged between 0.4 and 1.6 m across the five outfall sites. Model sensitivity studies to understand the far-field salinity increases associated with brine releases spread vertically over two and three model grid layers from the bottom are shown in Appendix 2. Sb was calculated as a function of the salinity at the intake and

temperature was set to the background water temperature at the outfall. The specified peak plant intake rate of 4191 m³/hr and discharge rate of 2800 m³/hr implies the collection of 1391 m³/hr of freshwater, equivalent to a ~12 GL per year plant operating at an efficiency (E) of 33%. The resultant salinity of discharged brine (Sb) was approximately $(1-E)^{-1}=1.50$ times the intake value.

Table 3. Location of desalination plant intakes and outfalls investigated in this study.

Site Name	Intake		Outfall	
	Longitude (°E)	Latitude (°S)	Longitude (°E)	Latitude (°S)
Billy Lights Point – inshore	135.8855	34.7558	135.8968	34.7484
Billy Lights Point – extension	135.8968	34.7484	135.9202	34.7454
Cape Donington	135.8855	34.7558	136.0102	34.7239
Point Boston – inshore	135.9460	34.6158	135.9466	34.6273
Point Boston – extension	135.9460	34.6158	136.0719	34.6384
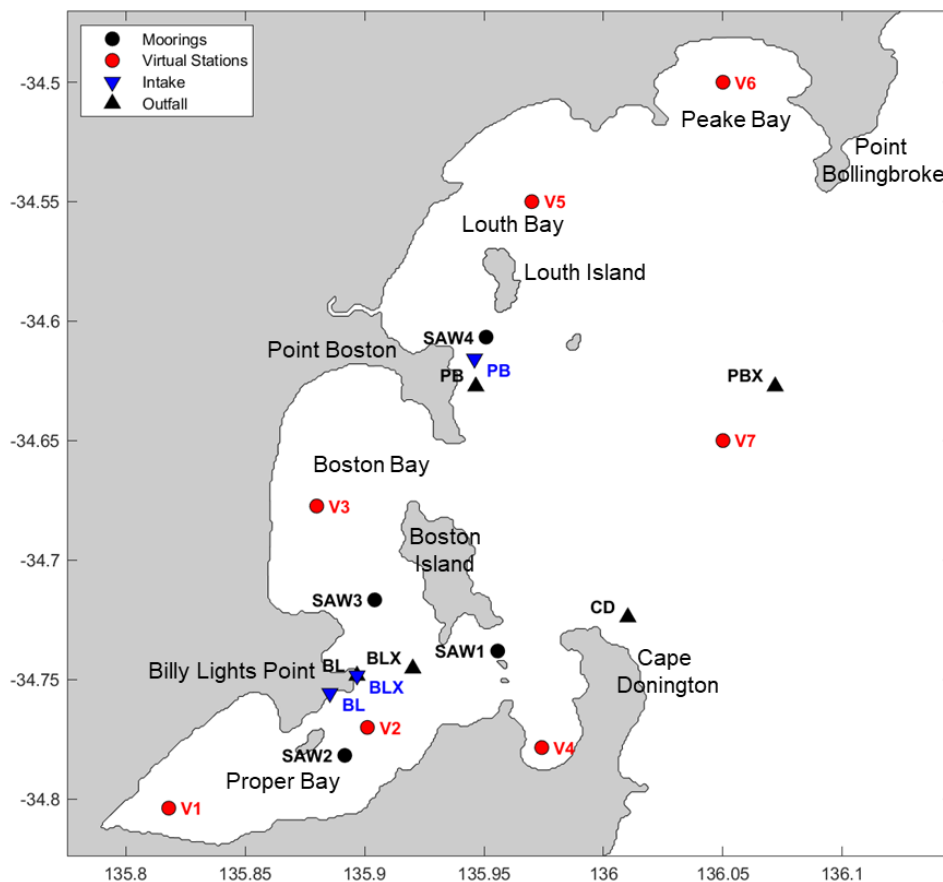
Figure 7. Map of the bays in the Port Lincoln region showing the location of: i) mooring sites (SAW1-4, black circle markers), ii) 'virtual' monitoring sites (V 1-7, red circle markers), iii) potential desalination plant intake (blue triangle markers) and iv) outfall sites (black triangle markers). BL = Billy Lights Point inshore, BLX = Billy Lights Point extension, PB = Point Boston inshore, PBX = Point Boston extension, CD = Cape Donington. No moorings were deployed at a proposed SAW4 site during this study.

14

2.4.   Particle tracking modelling

Dispersal of marine species with a pelagic larval duration is influenced by bio-physical interactions between ocean currents and characteristics of larval behaviour and development (Robins et al., 2013). With an understanding of these characteristics, bio-physical modelling, using outputs from regional hydrodynamic models, have been applied to understand the connectivity and recruitment in South Australia's gulfs of several important commercial species, including Western King prawns (McLeay et al. 2016) and King George Whiting (Rogers et al. 2021).

Spat of free-living blue mussels (*Mytilus galloprovincialis*) are caught and grown-out in aquaculture leases around Boston Bay. Unfortunately, little is known about the pelagic larval duration and development characteristics of the local blue mussel. The biological model for blue mussels used in this study was therefore developed based on discussions with local mussel farmers and the scientific literature for other *Mytilus species.* In summary, blue mussels are expected to be distributed across the intertidal zone of rocky coastlines (Svane 2011). The species uses a broadcast spawning strategy which involves several synchronised mass spawning events to maximise their reproductive success (De Vooys 1999). After spawning, mussel larvae are expected to remain in the water column for 2 to 4 weeks but can take up to 10 weeks to reach final settlement (Seed 1969; Demmer et al. 2022). Although there is limited evidence that planktonic blue mussel larvae can exert some control over their position in the water column (Dobretsov and Miron 2001), mussel larvae are assumed to be passive (i.e., with no active vertical migration behaviour). This is consistent with the approach used in recent particle tracking studies for blue mussels (Coolen et al. 2020; Demmer et al. 2022) and allows generalisation of the results to other species.

Based on this understanding, particle tracking was undertaken to assess the far-field connectivity of the local blue mussel with proposed desalination intake locations. Larval transport was simulated using the larval transport particle tracking model (LTRANS; North et al. 2006; 2008). LTRANS uses ocean current predictions from the HRBBM hydrodynamic model to track the trajectories of particles in three-dimensions and accounts for particle advection and diffusion due to turbulence. Hourly HRBBM outputs were used to run LTRANS which had an internal time step of 120 seconds. LTRANS uses reflective coastal boundary conditions to keep particle trajectories within bounds. As described by North et al. (2008), particles that intersected a coastal boundary were reflected at an angle equal to the angle of approach and at a distance equal to the distance

that the particle had passed the boundary. Particles that passed through vertical boundaries were returned to the water column just above or below the bottom and surface boundary, respectively. Particles that crossed open ocean boundaries were removed from further tracking.

To account for potential interannual differences in the regional circulation on mussel transport, spawning seasons were simulated for three consecutive years (2016, 2017, 2018). Each season included five monthly spawning events, which spanned the period May to September. Monthly spawning events lasted 5-days and involved the daily release of particles. Since blue mussels are expected to be found in the coastal intertidal zone, 10 particles were released each day from HRBBM grid cells within 1 km of the coast. In total 88,350 particles were released during each monthly spawning event. Particle numbers released at each grid point are not representative of actual mussel spat concentrations which are unknown but are expected to be much larger.

Particles were tracked until they exited the model domain. Any particles passing within a radius of 300 m of the proposed desalination intake were counted and removed from further tracking. Finally, to estimate the percentage of particles with connectivity to an intake pipe with a potential entrainment radius of 25 m, the proportion of particles released during each monthly spawning event with connectivity to within 300 m of the intake was downscaled by adjusting for the reduced cross-sectional area of the entrainment zone (i.e., $\pi 25^2 / \pi 300^2$).

3. RESULTS: MODEL VALIDATION

This section provides a comparison of measured and modelled parameters.

3.1.   Sea surface height

Sea level variations at the mooring sites were dominated by the tides with amplitudes up to 1.5 m (Figure 8 and Figure 9). The model performed well and reproduced both the phase and amplitude of the tidal variations with a bias of < 0.01 cm, RMS < 8 cm and $r^2 \geq 0.96$.
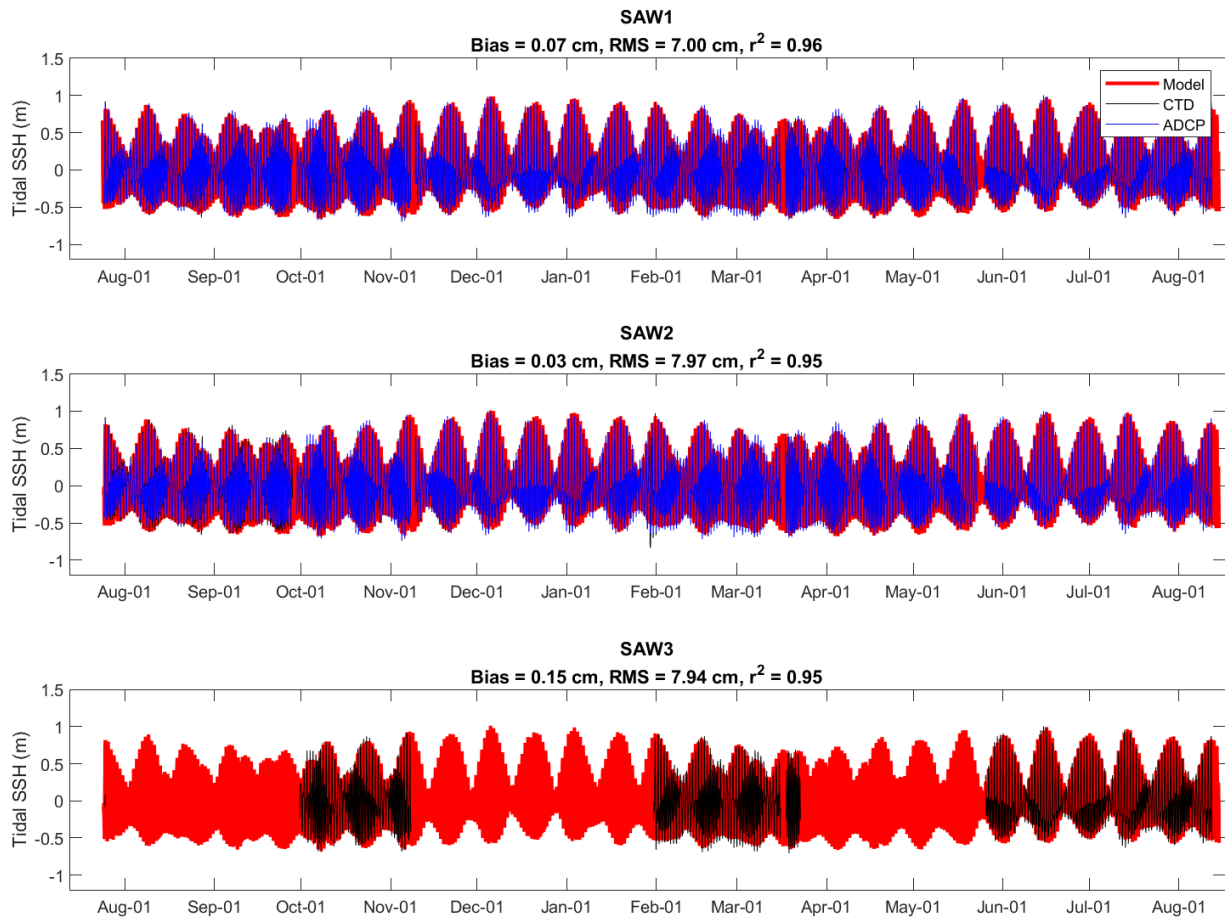
Figure 8. Comparison of measured and modelled Sea Surface Height (SSH, m) at the SAW1, SAW2 and SAW3 moorings.
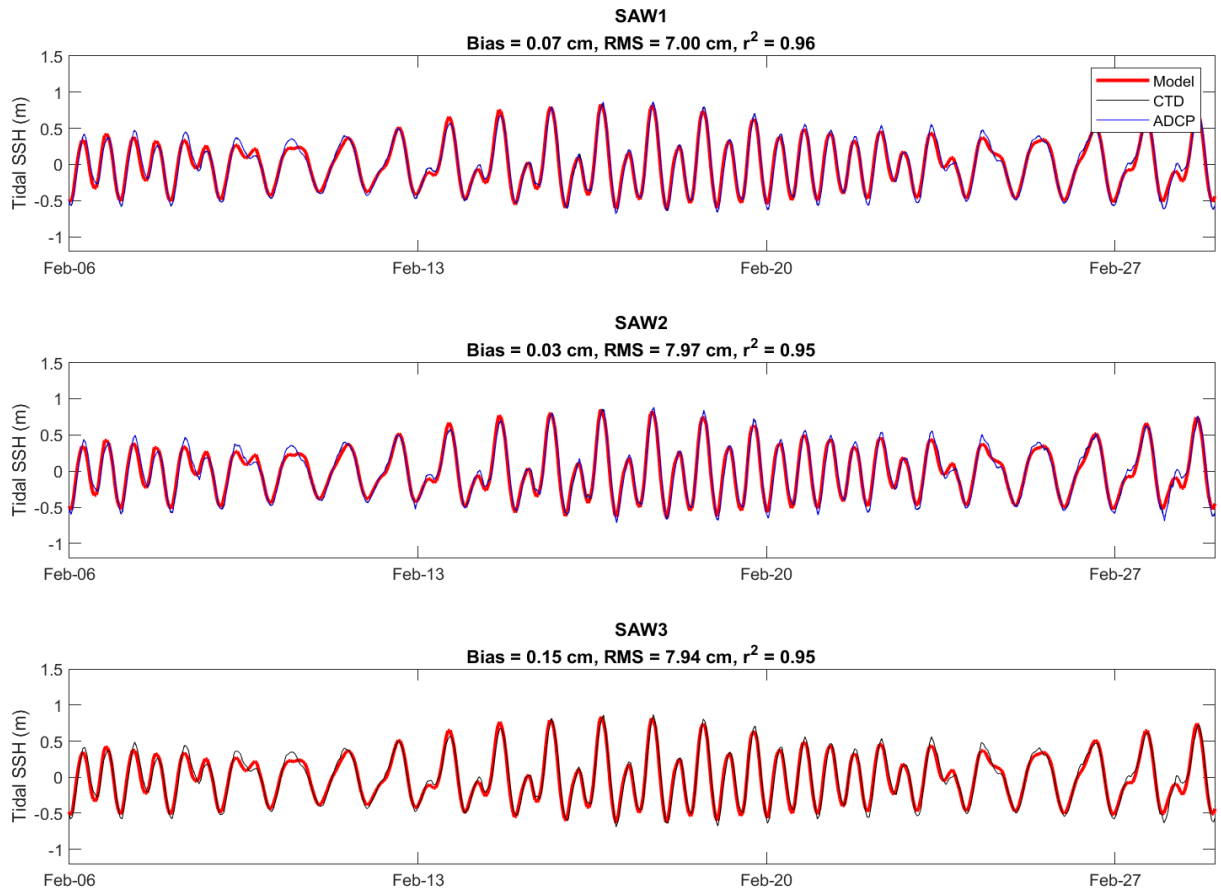
Figure 9. A closer comparison of the measured and modelled Sea Surface Height (SSH, m) at the SAW1, SAW2 and SAW3 moorings (shown in Figure 8) demonstrating the spring-neap tide cycle for the period 6 to 27 February 2022.

Removal of the tidal signal using the Thompson (1983) low-pass filter revealed the low-frequency variability in sea surface height (Figure 10). Unlike tidal fluctuations, which are generally predictable, lower frequency variations in sea surface height are driven by a complex combination of local and remote wind forcing associated with passing atmospheric high- and low-pressure systems referred to as the 'weather-band'. Sea level variations with amplitudes of up to 50 cm measured over periods of 3-20 days were reproduced well by the model, with a bias of ≤ 0.15 cm, RMS < 8 cm and r^2 ≥ 0.94. This result indicated that the model had a strong capability for simulating the dynamics that influenced sea surface height.
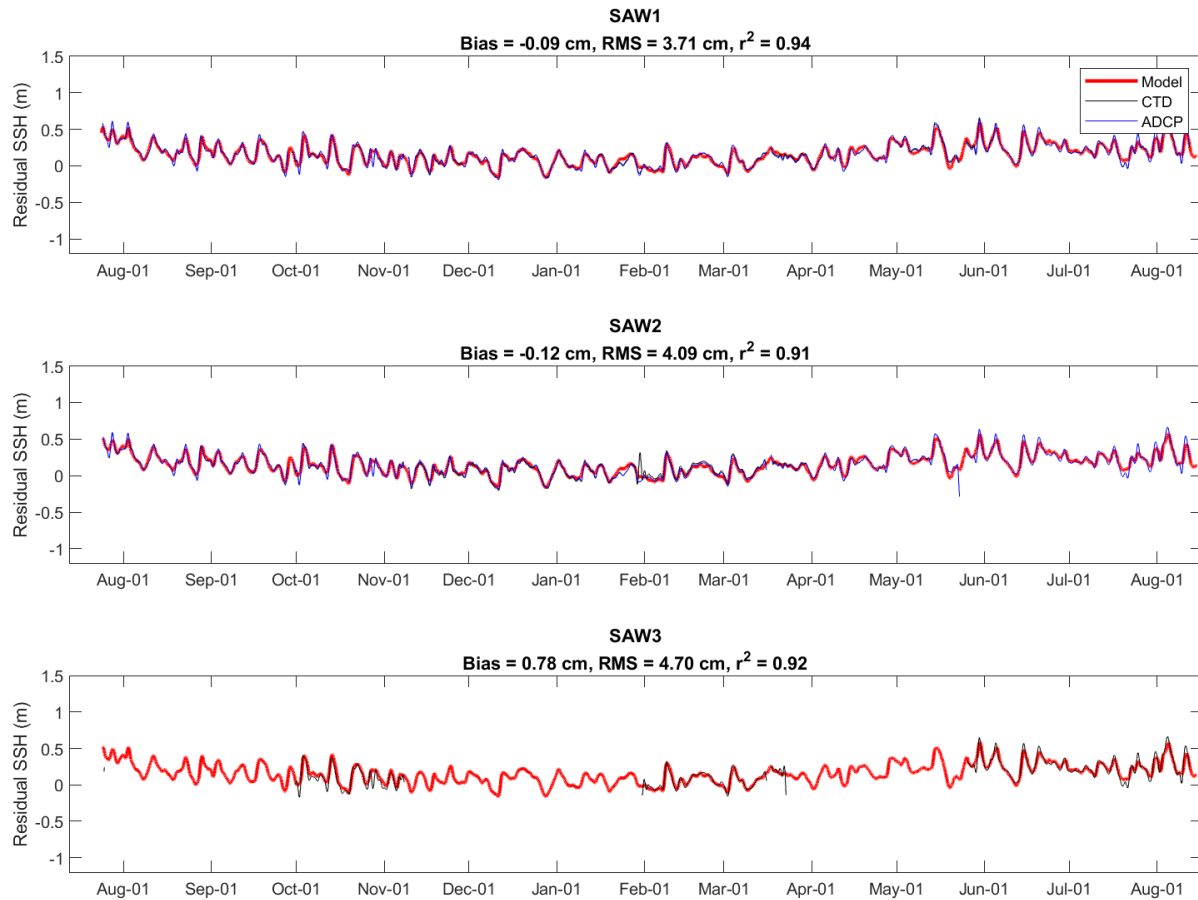
Figure 10. Comparison of measured and modelled low-pass-filtered Sea Surface Height (SSH) (m) at the SAW1, SAW2 and SAW3 moorings.

3.2.   Currents

A comparison of the measured and modelled, depth-averaged tidal currents resolved along the principal axis of observation (i.e., major current direction) are shown in Figure 11 and Figure 12. Tidal currents with amplitudes up to approximately 0.3 m/s and 0.2 m/s were measured at the SAW1 and SAW2 moorings, respectively. The principal axis was aligned to the east/west (with positive values to the east) at the SAW1 mooring and the northeast/southwest (with positive vales to the northeast) at the SAW2 mooring. Model agreement was very good for tidal currents at the SAW2 mooring, with an RMS error = 0.039 m/s (approximately 1/10 of the tidal signal) and r^2 =0.70. Model agreement was slightly less at the SAW1 mooring with an RMS error = 0.075 m/s and r^2 =0.56. Histograms show the model to be in good agreement with the observed current

speeds at both mooring locations (Figure 13), particularly during periods of lower current speeds. The model slightly over-predicted maximum current speeds at SAW1 by up to 0.1 m/s, particularly during spring tides when currents were directed to the west (Figure 12). At both mooring locations the tidal signals fell to close to zero velocity every 14 days during the 'dodge' tide (a neap tide with minimal rise and fall over the course of ~2-3 days) as expected for a tidal signal that is dominated by M2 and S2 semi-diurnal components (Figure 12).
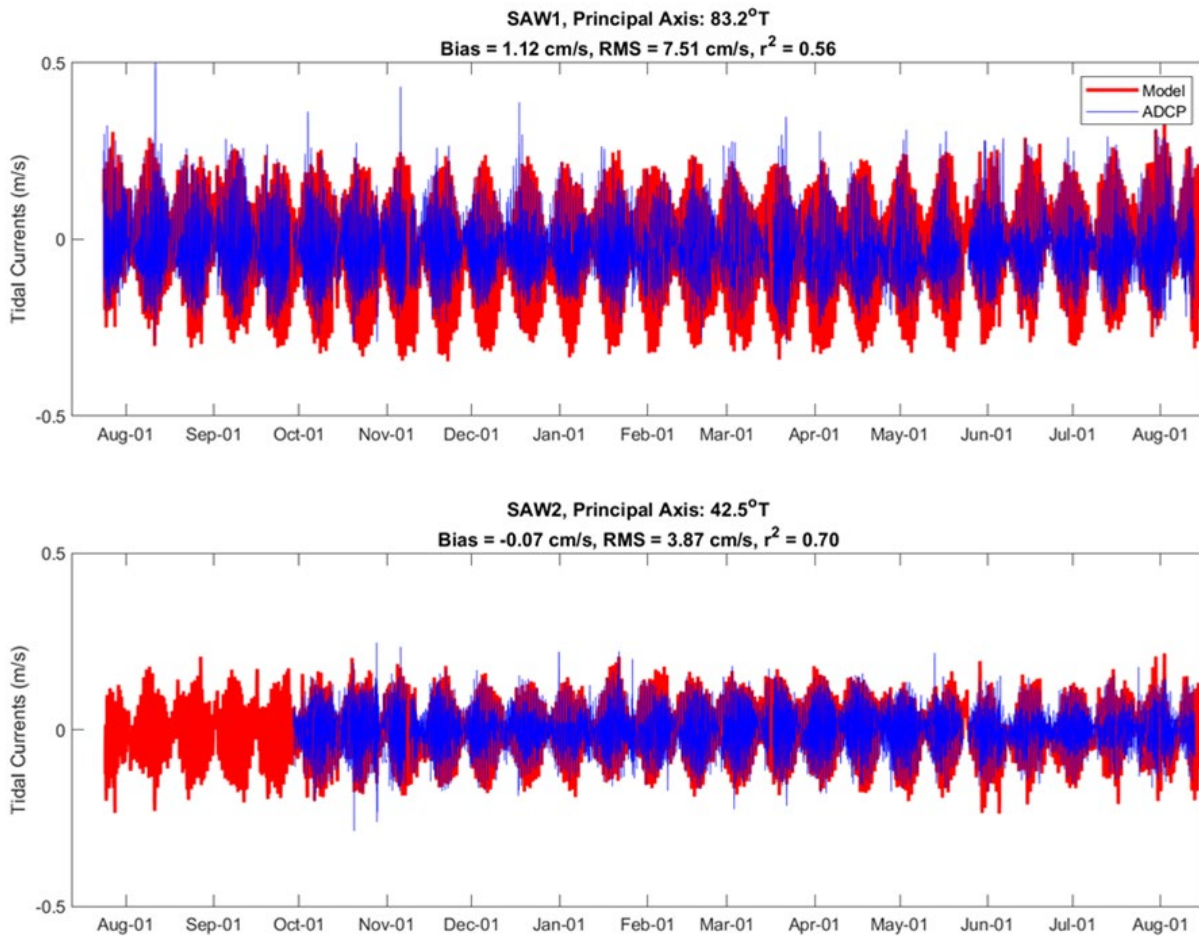
Figure 11. Comparison of the measured and modelled depth-averaged velocity (m/s) resolved along the principal axis at the SAW1and SAW2 moorings. Positive values are to the east at SAW1 and northeast at SAW2.
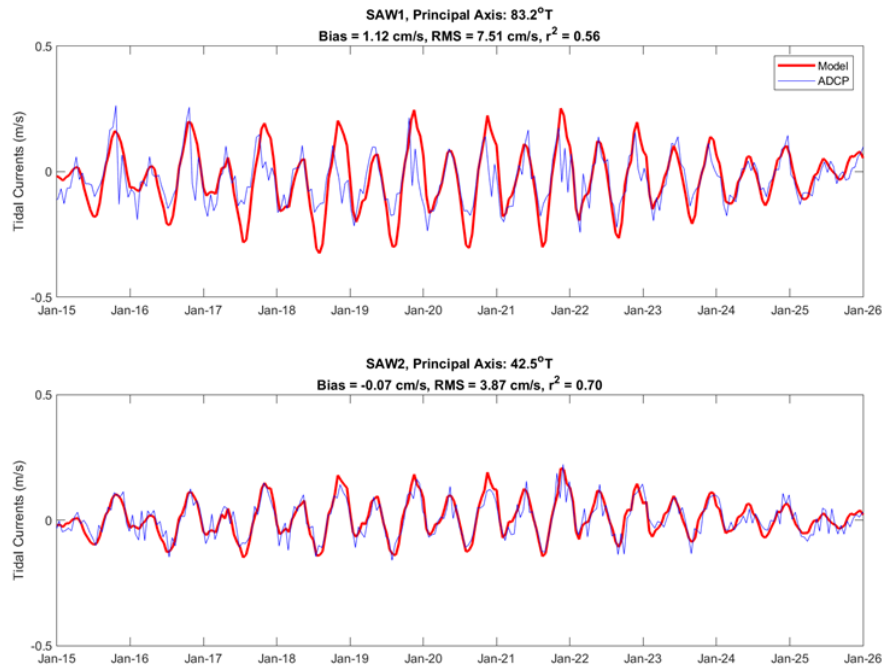
Figure 12. Closer comparison of the measured and modelled depth-averaged velocity (m/s) resolved along the principal axis at the SAW1, SAW2 and SAW3 moorings.
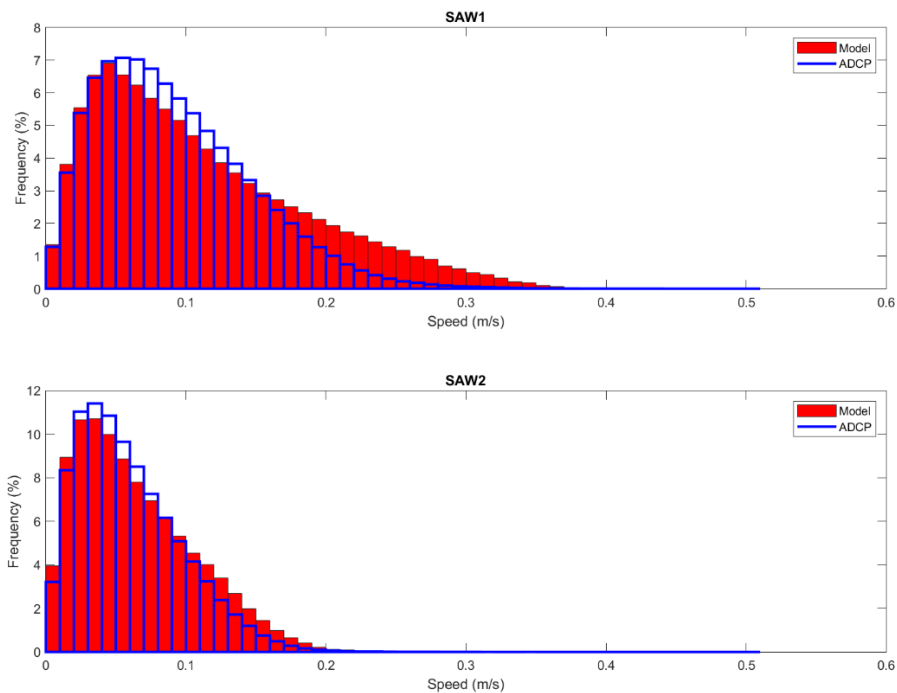
Figure 13. Histogram of current speeds comparing observed values (blue bins) with model (red bins) predictions at the (top panel) SAW1 and bottom panel (SAW2) mooring sites.

Currents driven by weather-band events were weaker than those generated by tides and showed variability over periods of 3-10 days with speeds up to 0.05 m/s measured at the SAW1 mooring and <0.05 m/s at the SAW2 mooring (Figure 14). The model qualitatively reproduced the measured signals but not always the timing. During cooler months the amplitude of the weather band currents were often overpredicted, particularly at the shallower SAW2 mooring. Compared to tidal currents, model agreement for weather-band currents was reduced, as indicated by the RMS errors ≤ 0.03 m/s (approximately 1/2 of the signal) and r^2 ≤ 0.25. The ADCP measurements were noticeably noisier than the model predictions, which may reflect sub grid-scale processes that the model is not able to reproduce.
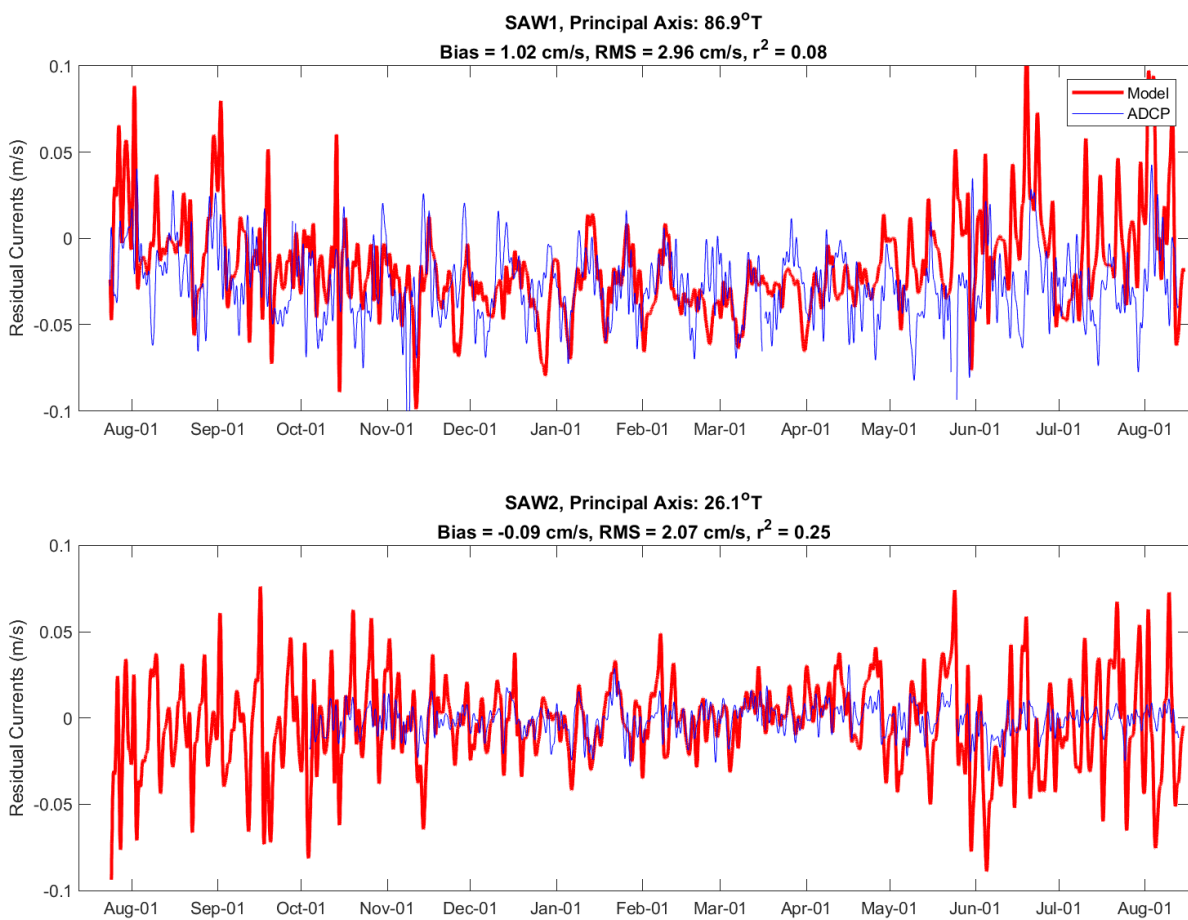
Figure 14. Comparison measured and modelled low-pass-filtered and depth-averaged velocity (m/s) resolved along the principal axis at the SAW1 and SAW2 moorings.

3.3.   Temperature

Accurate prediction of temperature and salinity by the hydrodynamic model is important for modelling the density driven circulation. Measured and modelled temperatures ranged from 12 °C in August to 24 °C in February (Figure 15) and were in excellent agreement, as indicated by the small biases ≤ 0.52 °C and RMS errors ≤0.69 °C, and high r^2 values ≥ 0.98.
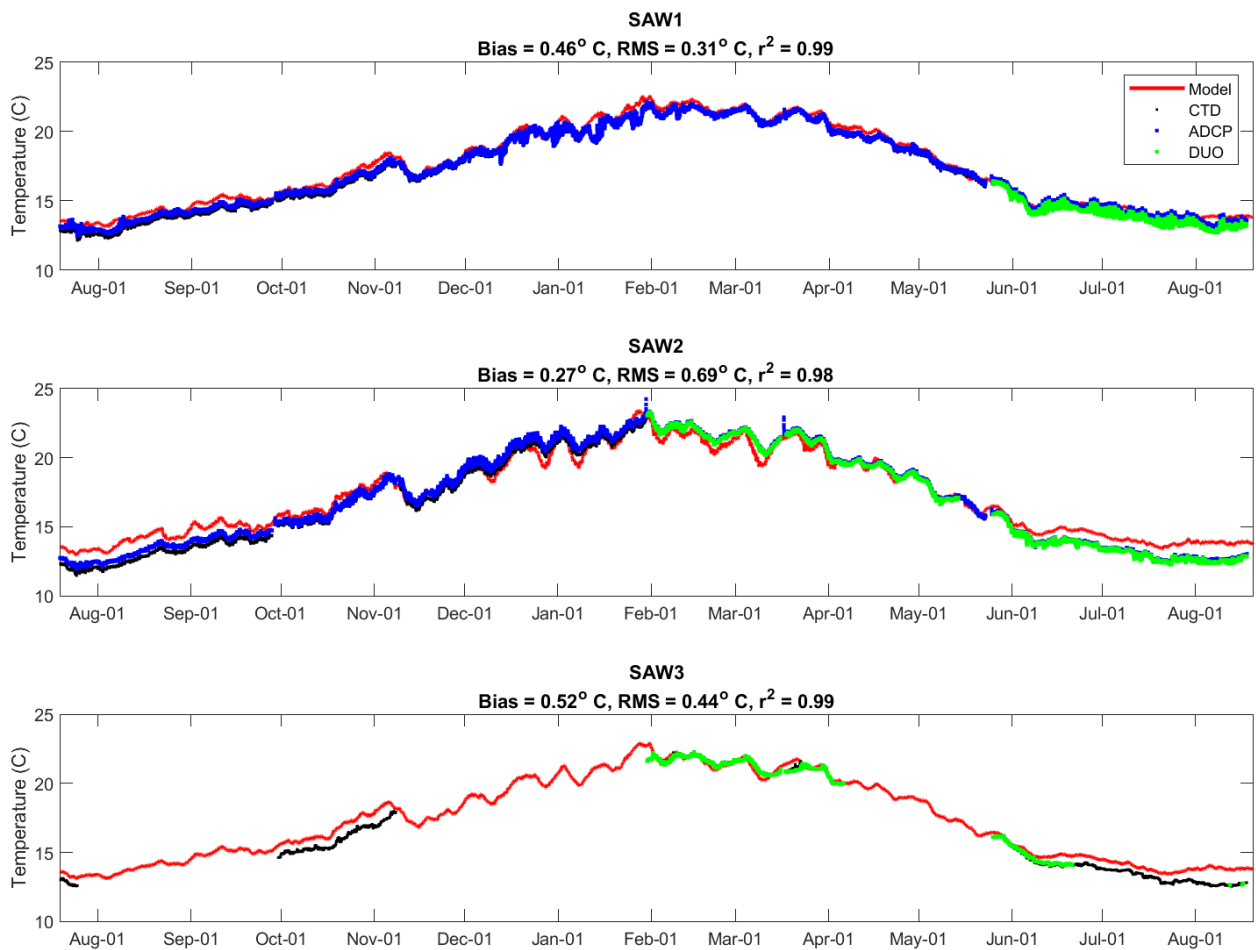
Figure 15. Comparison of the measured and modelled temperature (°C) at the SAW1, SAW2 and SAW3 moorings.

3.4.   Salinity

Measured and modelled salinities at each mooring site are shown in Figure 16. The quality of measured data suffered from calibration and fouling issues, particularly at the SAW3 mooring site. The errors in salinity were in part managed by applying calibration corrections (Table 2) and adjusting for salinity drifts. Following adjustments and the removal of erroneous measurements, the model showed reasonable agreement with the model at the SAW1 and SAW2 moorings, as indicated by biases = 0.06 PSU, RMS errors <0.4 PSU and $r^2 \geq 0.56$. The comparison was less favourable at the SAW3 mooring where the quality of measurements returned was questionable.

Measured salinities at the SAW1 ranged between a minimum (Smin) of 35.82 PSU and maximum (Smax) of 37.28 PSU with an average value (Savg) of 36.23 PSU. The observed annual range was 1.46 PSU and the ambient salinity varied by 4% ([Smax-Smin]/Savg) between the maximum and minimum values. During warmer months, salinity variations of between approximately 0.1 and 0.5 PSU were observed across shorter timescales of hours to weeks, respectively (Figure 17). Both the annual range and observed salinities during warmer months were underpredicted by the model following an intense rain event which occurred in the region on 22-February 2022.

In a comparison with the Port Lincoln automated weather station (PL-AWS), the NCEP Climate Forecast System Reanalysis v.2 (CFSRv2) freshwater flux for this event over-estimated the local rainfall by more than 100% (Figure 18). While most events are well represented by the CFSRv2 grid resolution (~20km), intense precipitation events can be much patchier and can be overestimated by atmospheric models (Davis et al., 2006). In this case, the over-estimate of freshwater flux by CFSRv2 extended over much of Spencer Gulf and probably contributed to the underestimation of salinity for a considerable period. Adjustments for one-off events are not systematic and cannot be applied to the 5-year hindcasts. Because of this, and due to the lack of precipitation measurements over most of the TGM parent grid, the freshwater flux cannot be adjusted to accommodate unpredicted variations in rainfall.
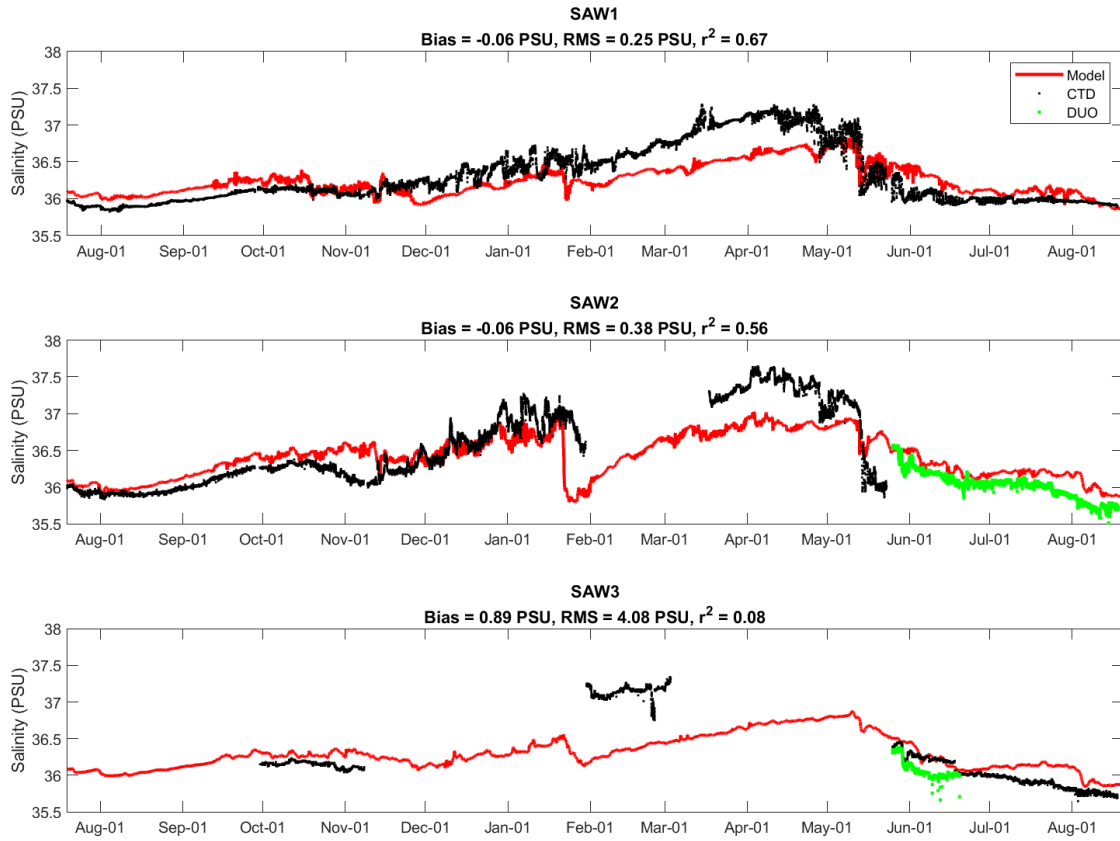
Figure 16. Comparison of the measured and modelled salinity (PSU) at the SAW1, SAW2 and SAW3 moorings.
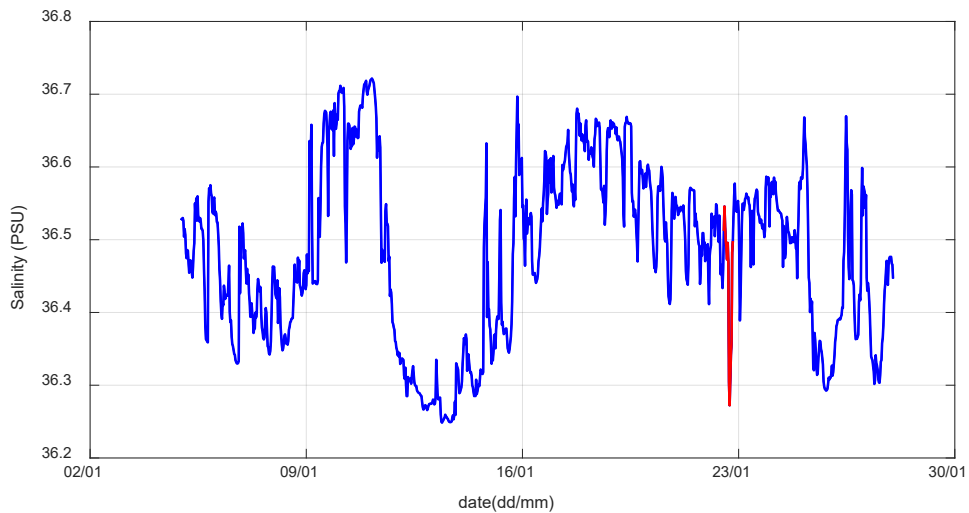
Figure 17. Bottom measurements of salinity (PSU) taken at SAW1 in January 2022. Measurements were made at 30-minute intervals. The salinity decrease on 22-January (red highlight) corresponds with a strong localised precipitation event.

25
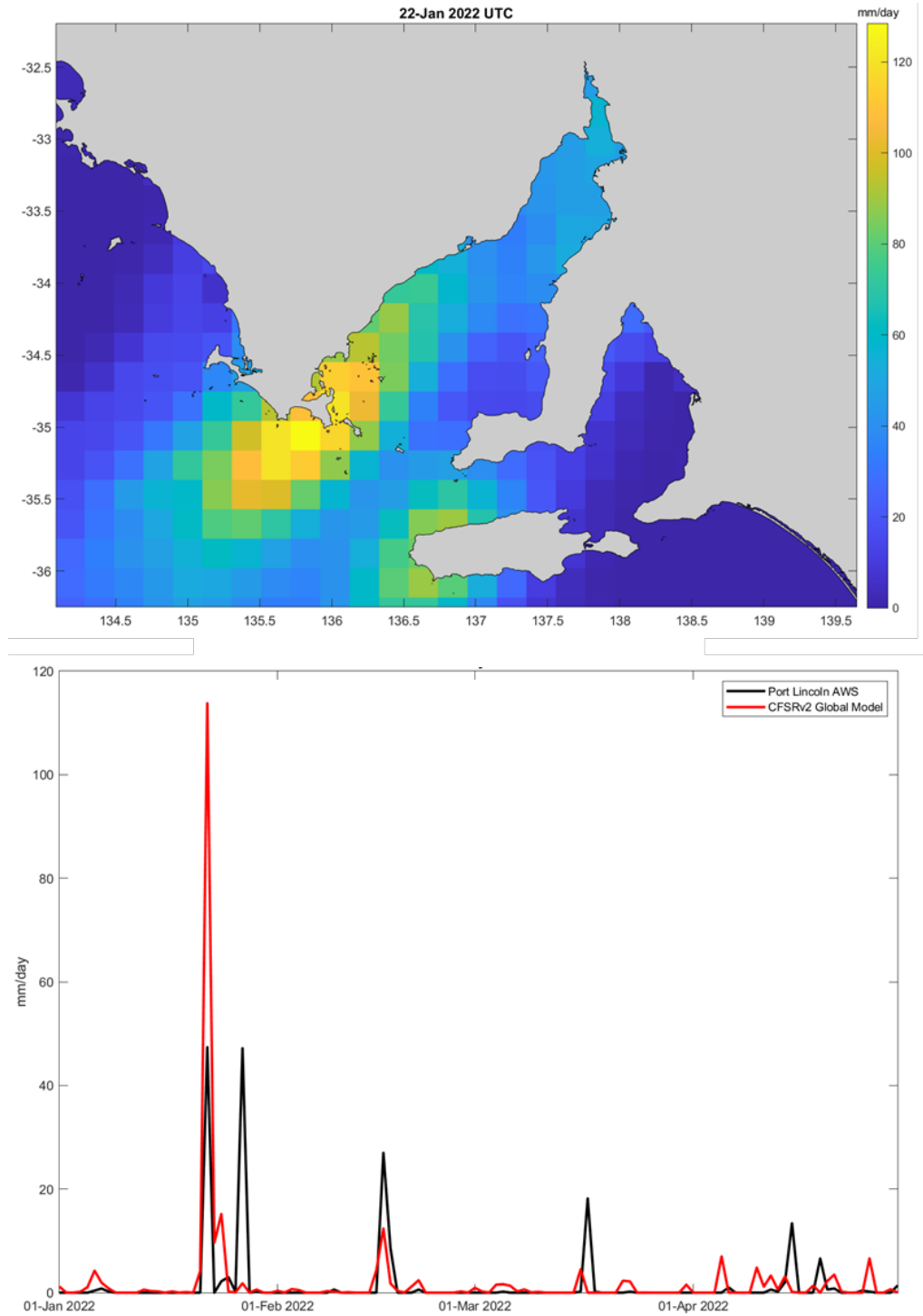
Figure 18. Measured and modelled freshwater fluxes. (Top) Distribution of precipitation (mm/day) in atmospheric model used to force the hydrodynamic models on 22-January 2022. (Bottom) Comparison of the precipitation (mm/day) measured at the Port Lincoln automated weather station (AWS) between 1-January and 1-April 2002 with the atmospheric model.

4. RESULTS: BRINE OUTFALL SCENARIOS

Figure 19 shows the seasonal circulation patterns averaged over the five-year model simulation without desalination. The observed patterns provide a climatological picture of the region's long-term net flow and are expected to be important to the flushing and transport of passive tracers and, potentially, brine discharges and planktonic larvae.

Seawater circulation is characterised by flows which enter from the offshore region into the centre of the embayments and leave against both the north and south coasts. The penetration of these flows into embayments surrounding Port Lincoln is typically weak but increases in winter (when it is directed towards Louth Bay) relative to other seasons. In the embayments there are two main flow regimes. The first involves flows in and around Boston and Proper Bay. Flows generally enter Boston Bay from the north of Boston Island, setting up a clockwise circulation in northern Boston Bay, with waters exiting beside Point Boston, and an anti-clockwise circulation in southern Boston Bay, with outflow south of Boston Island. This changes in summer, when inflow from south of Boston Island results in a clockwise circulation throughout Boston Bay. Water enters centrally into shallow Proper Bay and exits along either the north coast, past Billy Lights Point, or the south coast, toward Cape Donington. Within Proper Bay, circulation is variable being dependant on wind direction, strength and channelling. A weak persistent anticyclonic gyre is centred a few kilometres offshore to the northeast of Cape Donington. The second main flow regime describes the circulation in Louth Bay. Water predominantly flows into Louth Bay past Point Boston, south of Louth Island, and moves northwards along the coast, into and past Peake Bay, before exiting past Point Bollingbroke. In winter, though, water enters north of Louth Island and flows south along the coast to exit past Point Boston. A small, clockwise, cyclonic gyre persists year-round to the north of Louth Island. Other permanent circulation features predicted by the model included stronger year-round flows directed northwards of Point Bollingbroke and eastwards near Cape Donington.

To examine and compare the effect of hydrodynamics on the far-field dispersal of desalination brine discharges from different outfall locations, 5-year hydrodynamic model hindcast simulations with and without desalination outfalls were undertaken. Figure 20 shows a snapshot of the modelled bottom salinity predicted on March 17, 2017, showing discharges from each outfall site relative to the model run without desalination. A full animation of the 5-year hindcast is provided in Appendix 3. Comparison of model predictions with and without desalination were used to

estimate the far-field increases in salinity (i.e., anomalies) across a range of temporal and spatial scales and are presented for each outfall location as follows.

Maps of the seasonally-averaged maximum salinity anomalies are shown in Figure 21, Figure 24, Figure 27, Figure 30 and Figure 33. Using the three-day averaged results over the 5-year hindcast, seasonal-average maps were calculated by averaging the maximum anomaly predicted at each model grid point over the calendar months corresponding with the Australian seasons: Summer (December, January and February), Autumn (March, April and May), Winter (June, July and August) and Spring (September, October and November). Maximum anomalies provide a 'worst case' estimate of the predicted salinity increase across the water-column. Seasonal-averaging filters out positive and negative anomalies associated with dynamically driven changes in the circulation resulting from the injection of brine into the model, while preserving the positive anomalies associated with the brine discharge itself. The maps provide a conservative estimate of the spatial distribution (i.e., footprint) of long-term salinity increases associated with outfalls and the seasonal circulation patterns shown in Figure 19.

The use of three-day averaged hindcasts filters out daily tides and transient anomalies (those lasting less than three days). An indication of the variability and magnitude of salinity anomalies at hourly timescales at the virtual monitoring stations and mooring sites (see locations in Figure 7) is provided by the 5-year hourly time-series of the water column mean and maximum salinity anomalies shown in Figure 22, Figure 25, Figure 28, Figure 31 and Figure 34. For stations and sites located within the footprint of the salinity anomalies shown in the seasonally-averaged maps, positive anomalies provide an estimate of the maximum salinity increases expected in the far-field at hourly timescales. At distances beyond the footprint of the positive salinity anomalies, the predicted positive and negative hourly anomalies are due to dynamic differences in the model circulation between simulations with and without desalination inputs.

To understand the influence of tides on the vertical and horizontal dispersal of brine discharges in the vicinity of the outfalls, lateral transects and vertical profiles of the salinity anomaly modelled during dodge and spring tide conditions are shown in Figure 23, Figure 26, Figure 29, Figure 32 and Figure 35.
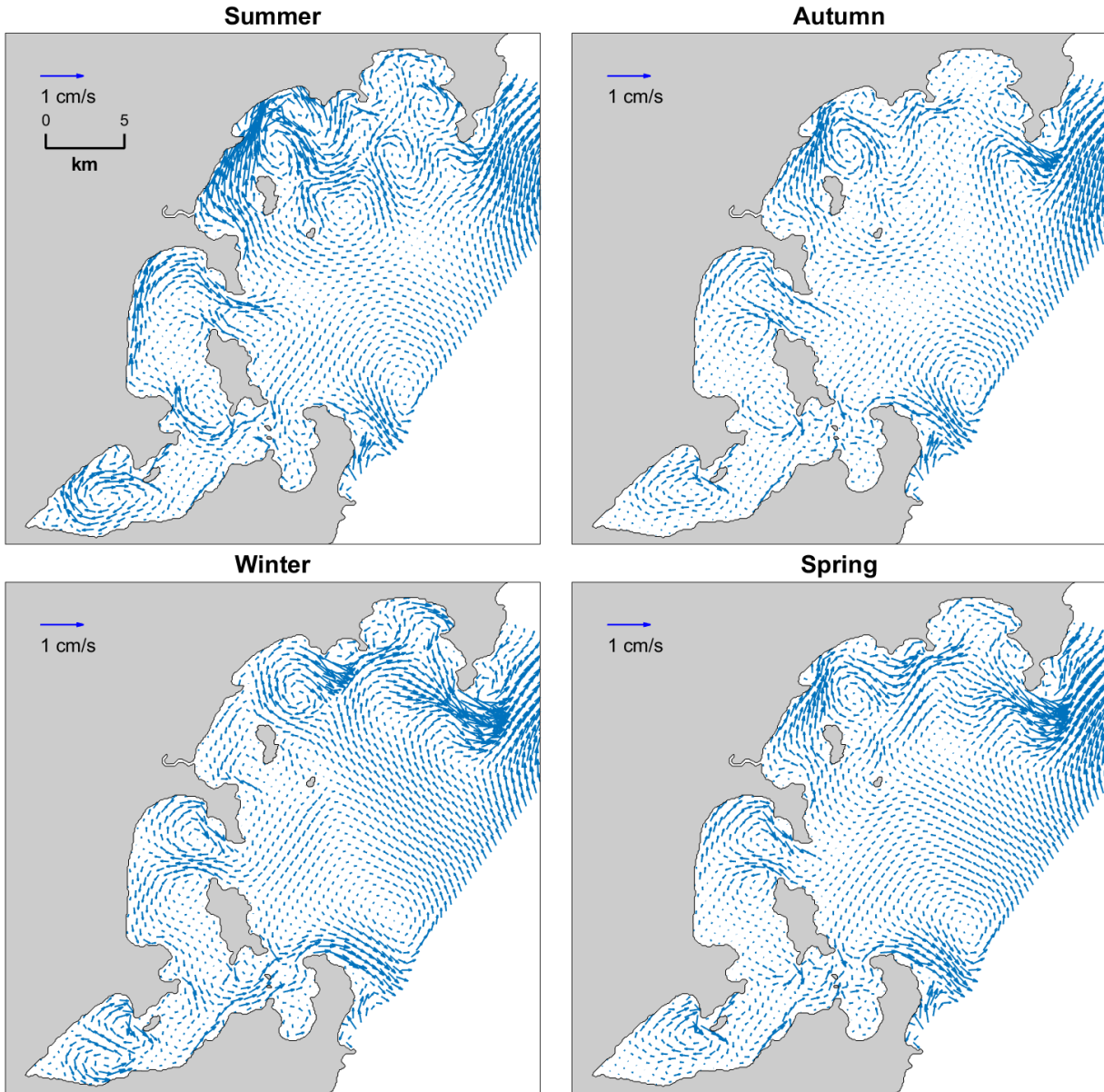
Figure 19. Time and depth averaged seasonal circulation patterns averaged over 5-years.
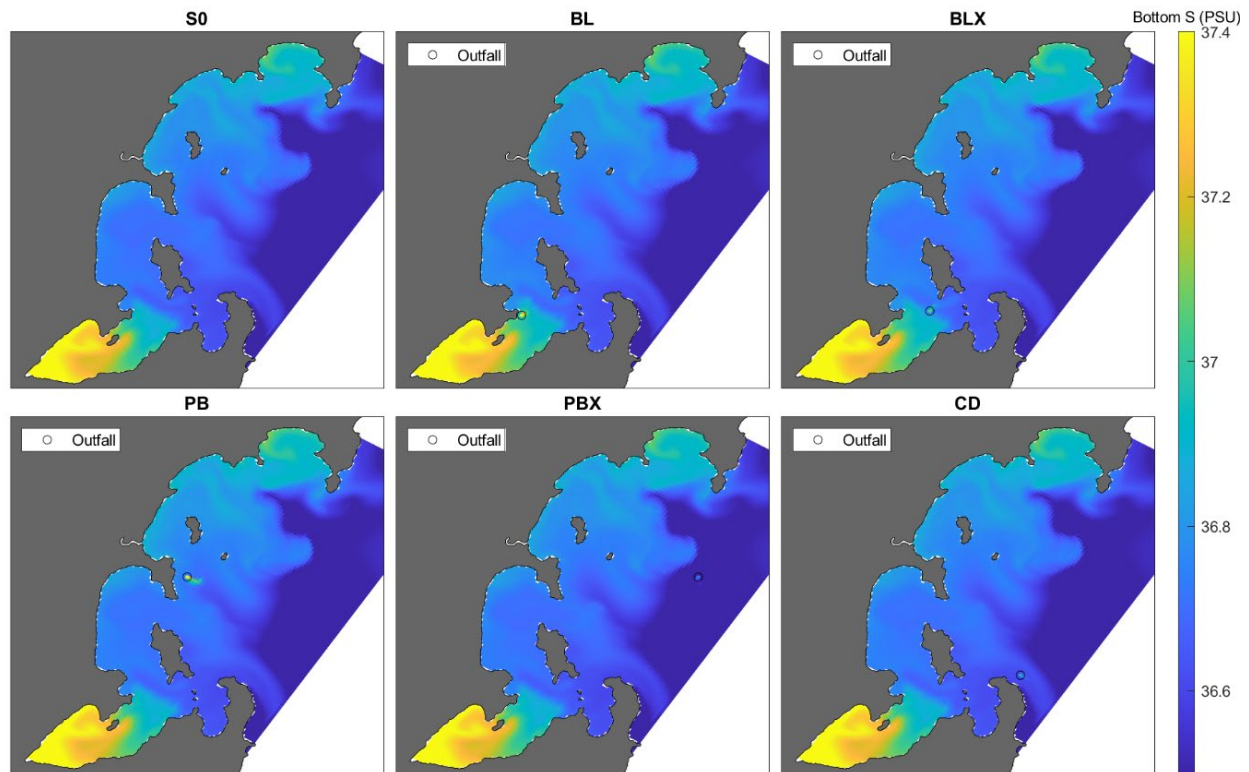
Figure 20. Snapshot of the bottom salinity on March 17, 2017, showing discharges from each outfall site relative to the default model run without desalination. SO = simulation without desalination, BL = Billy Lights Point, BLX = Billy Lights Point-extension, PB = Point Boston, PBX = Point Boston-extension, CD = Cape Donington.

4.1.   Billy Lights Point - inshore

The spatial distribution of seasonally averaged maximum salinity anomalies calculated from 5-years of model predictions for the Billy Lights Point inshore outfall are shown in Figure 21. Seasonally-averaged maximum salinity anomalies decreased from 0.76 PSU in the bottom layer of the model grid cell corresponding with the outfall location to 0.26 PSU and 0.07 PSU (Figure 21,Table 4) at distances of 0.5 and 1 km from the outfall. Assuming an average, ambient salinity of 36.2 PSU these increases correspond to salinity changes of ≤2%, ≤0.7% and ≤0.3% in the ambient salinity, respectively. The dispersion of salinity was influenced by the long-term net flow (Figure 19). For example, in winter, salinity increases were largely restricted to Proper Bay and Billy Lights Point. In summer, flows directed north along the shore of Boston Bay were predicted to disperse brine throughout Boston Bay and offshore past Point Boston and Boston Island. Smaller anomalies of

≤0.05 (<0.15% of the ambient salinity) were predicted up to 5 km from the outfall and encroached on the intake year-round.

Figure 22 shows the far-field increases in salinity predicted at hourly intervals at the virtual monitoring stations and mooring sites (shown in Figure 7). Hourly anomaly values never exceeded 0.4 PSU and were typically <0.2 PSU (<0.6% the ambient salinity). During cooler months anomalies were effectively zero. Consistent with the seasonally averaged maps shown in Figure 21, the largest anomalies were consistently predicted to occur at locations within 5 km of the outfall (e.g., V2, SAW1, SAW3). At greater distances (e.g., virtual monitoring station V7), anomalies of up to ~0.2 PSU occurred at various depths across the water column due to dynamical changes resulting from the injection of brine into the model rather than from direct connectivity with the brine discharge. Mean hourly anomalies averaged across the 5-year hindcast (highlighted to the right of each timeseries in Figure 22) ranged from <0.01 to 0.035 PSU (i.e., always <0.1% of the ambient salinity), and were relatively steady on annual timescales.

At a distance of approximately 300 m from the outfall (a map showing the location of the measurement point relative to the outfalls is provided in Appendix 1, Figure 42), maximum salinity anomalies of 0.55 PSU (1.5% of the ambient salinity) were predicted to occur intermittently on the seafloor (Figure 23) and were modulated by the tides. In the vertical plane, anomalies were mixed towards the surface during spring tides but were largely restricted to the bottom 2 m during dodge tides. Lateral transects (see Appendix 1 for the transect locations) of the salinity anomaly averaged over 3-days indicated increased bottom salinities of >0.1 PSU extended approximately 600 m downslope from the outfall, consistent with increased density of the brine discharge. Slightly increased salinity anomalies were predicted on the seafloor during the dodge tide relative to the spring tide.
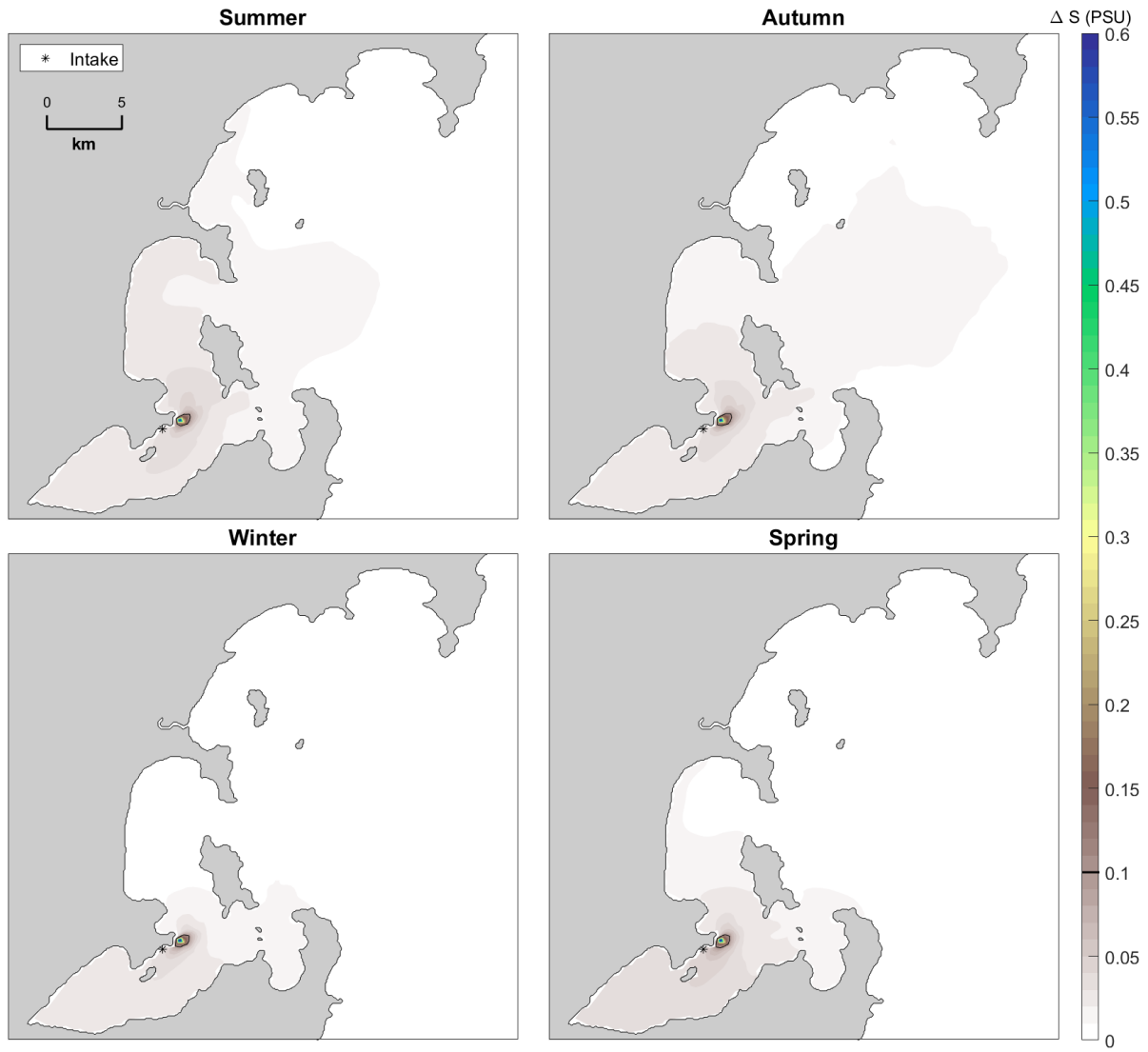
Figure 21. Maps of the seasonally-averaged maximum salinity anomaly for the Billy Lights Point inshore outfall. The map limits are set to 0.6 PSU for visualisation purposes and actual anomalies may exceed 0.6 PSU at the grid cell corresponding with the outfall site.
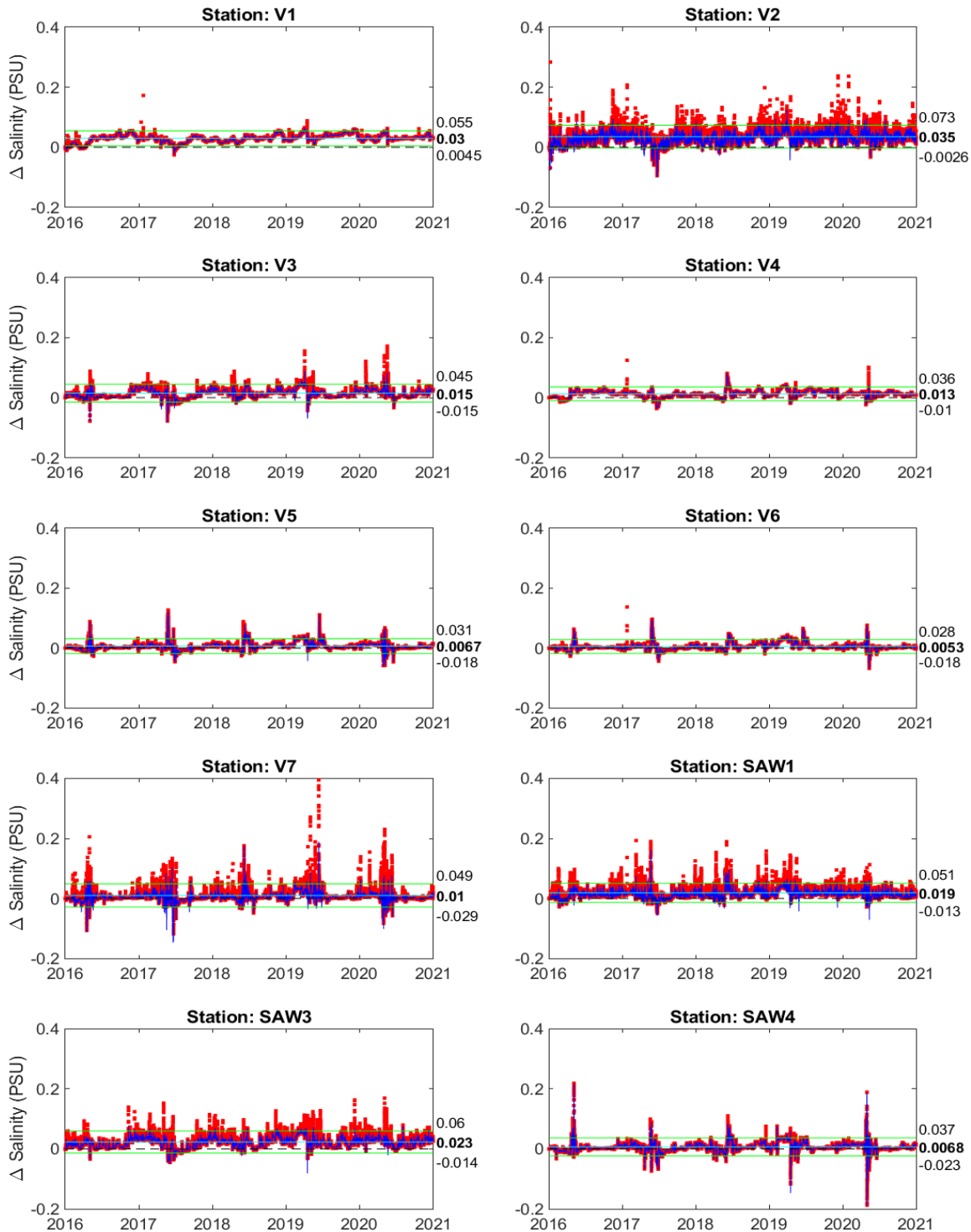
Figure 22. Far-field salinity anomalies predicted every hour over the 5-years hindcast at multiple locations for the Billy Lights Point inshore outfall. Blue line is the depth averaged anomaly. Red marker the maximum anomaly. Light blue and green lines show the timeseries mean ± 2 standard deviations, respectively. Figure 7 provides a map showing the corresponding locations.
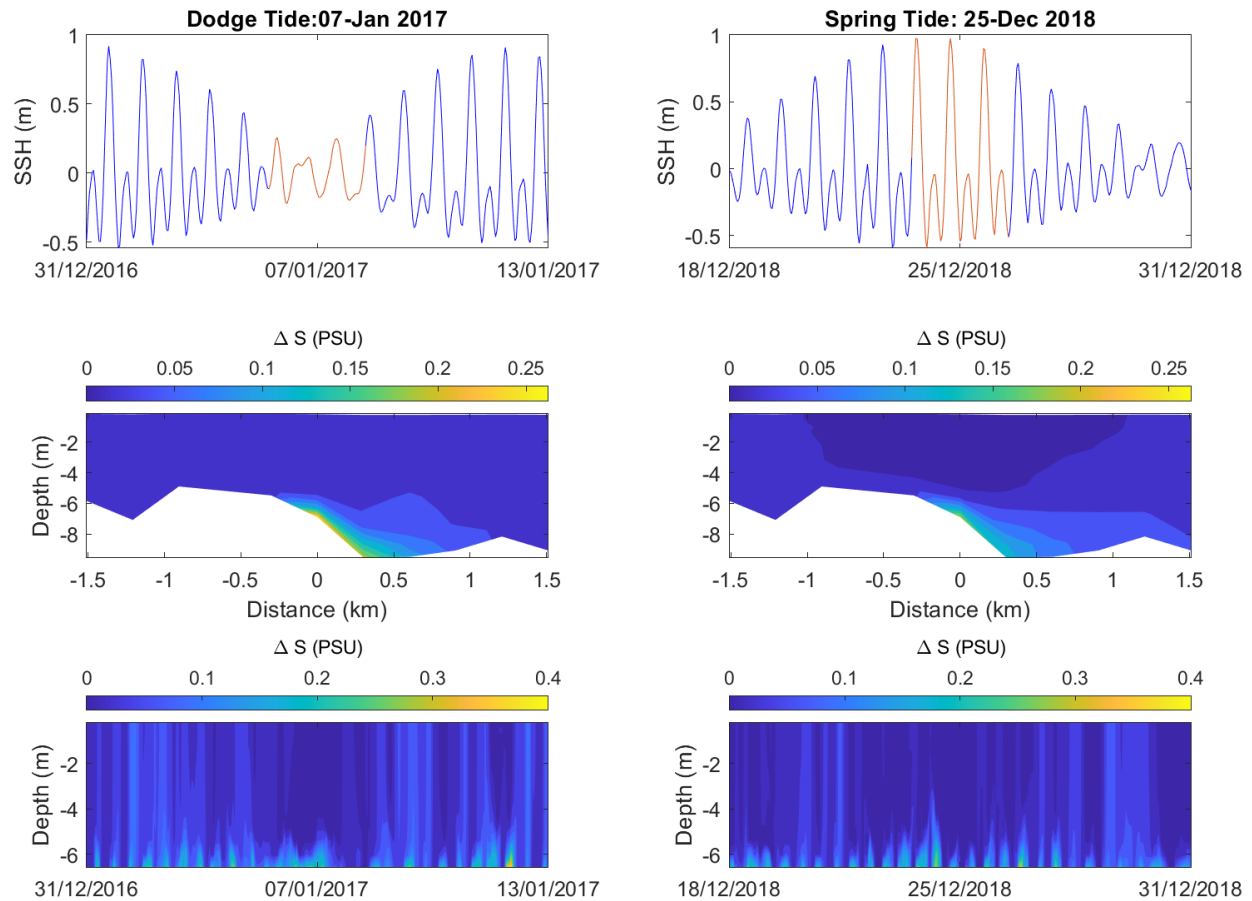
Figure 23. Snapshots of the salinity anomalies predicted in the vicinity of the Billy Lights Point inshore outfall during a (left panels) dodge and (right panels) spring tide. Top panels – 14-day timeseries of sea surface height (SSH, m) 300 m from the outfall. Middle panels – lateral transect of the 3-day average salinity anomaly (PSU) centred 300m from the outfall and corresponding with the SSH highlighted in red. Bottom panels – hourly changes in the salinity anomaly throughout the water column 300 m from the outfall. Figure 42 in the Appendix provides a map showing the locations corresponding with the plotted transect and timeseries. The map limits are set for visualisation purposes and actual anomalies may exceed these limits.

4.2.   Billy Lights Point - extension

The spatial distribution of seasonally averaged maximum salinity anomalies calculated from 5-years of model predictions for the Billy Lights Point extension outfall are shown in Figure 24. Salinity anomalies decreased from 0.43 PSU in the bottom layer of the model grid cell corresponding with the outfall location to 0.17 PSU and 0.06 PSU (Figure 24,Table 4) at distances of 0.5 and 1 km from the outfall. These increases correspond to salinity changes of ≤1.2%, ≤0.5% and ≤0.2% in the ambient salinity, respectively. Smaller anomalies of ≤0.5 PSU were predicted up to 20 km from the

outfall and, except for winter, showed connectivity with the intake and Proper Bay. The observed distribution of salinity anomalies can again be explained by seasonal circulation patterns (Figure 19). In winter, salinity increases were dispersed offshore with the offshore outflow of water on the southern side of Boston Island. In summer, coastal flows were predicted to disperse brine into Proper Bay and northward along the coast of Boston Bay.

Figure 25 shows the far-field increases in salinity predicted at hourly intervals at the virtual monitoring stations and mooring sites (shown in Figure 7). Maximum anomalies were predicted to be greater during warmer months and rarely exceeded 0.2 PSU at stations within 5 km of the outfall (e.g., V2, SAW1, SAW2). During cooler months, anomalies typically reduced to zero. Mean anomalies averaged across the 5-year hindcast ranged from <0.01 to 0.02 PSU (<0.1% of the ambient salinity) and were relatively steady on annual timescales.

The maximum salinity anomaly within 300m of the outfall was predicted to reach up to 0.37 PSU at times on the bottom (Figure 26) and was modulated by the tide. In the vertical plane, bottom anomalies associated with the discharge were predicted to be mixed towards the surface and diluted by the tides. Lateral transects of the salinity anomaly averaged over 3 days corresponding to dodge and spring tides showed anomalies between 0.1 and 0.37 PSU during dodge tides and spring tides, respectively. Anomalies ≥0.1 PSU extended out to approximately 0.6 km from the outfall.
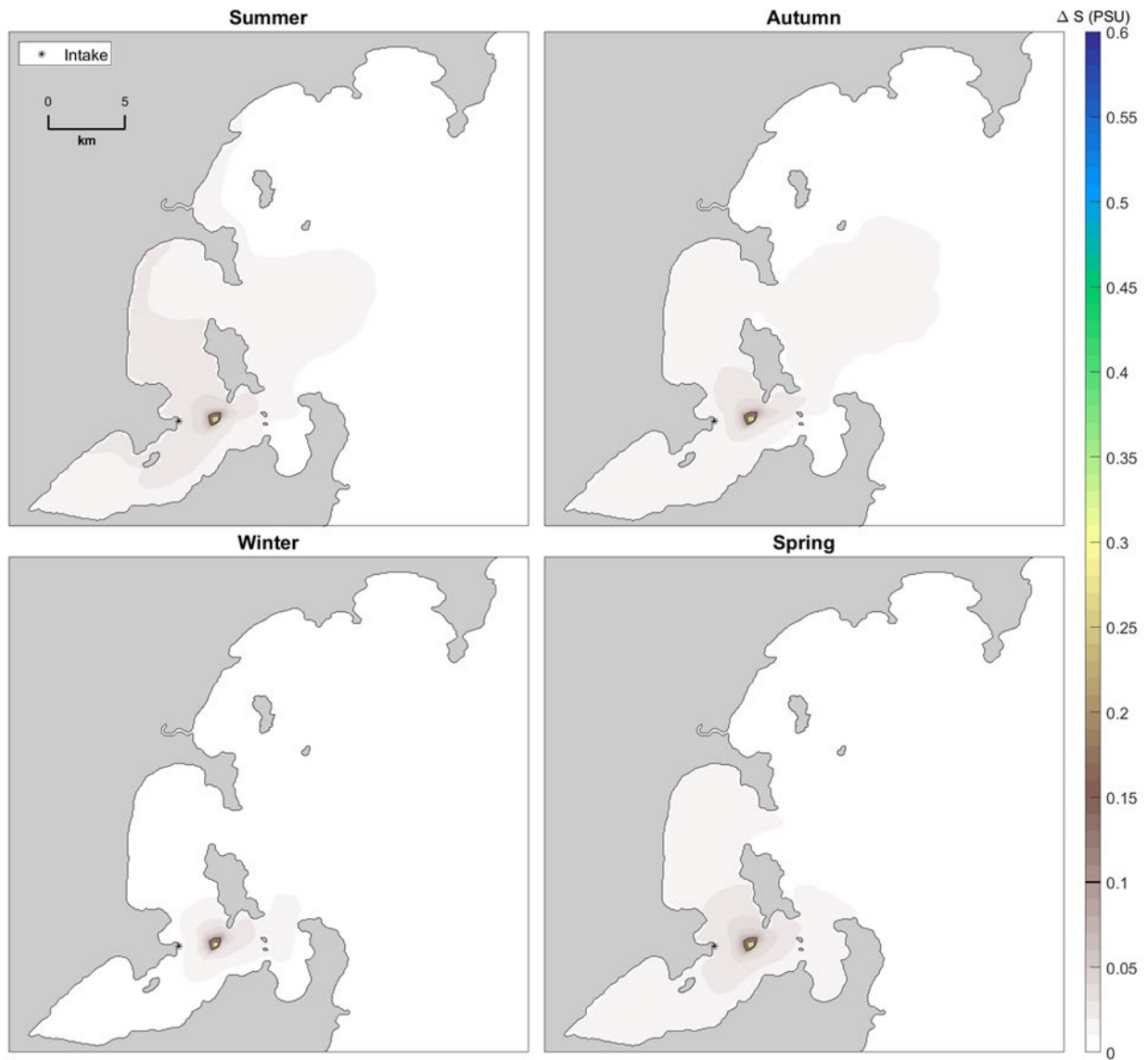
Figure 24. Maps of the seasonally-averaged maximum salinity anomaly for the Billy Lights Point extension outfall. The map limits are set to 0.6 PSU for visualisation purposes and actual anomalies may exceed 0.6 PSU at the grid cell corresponding with the outfall site.
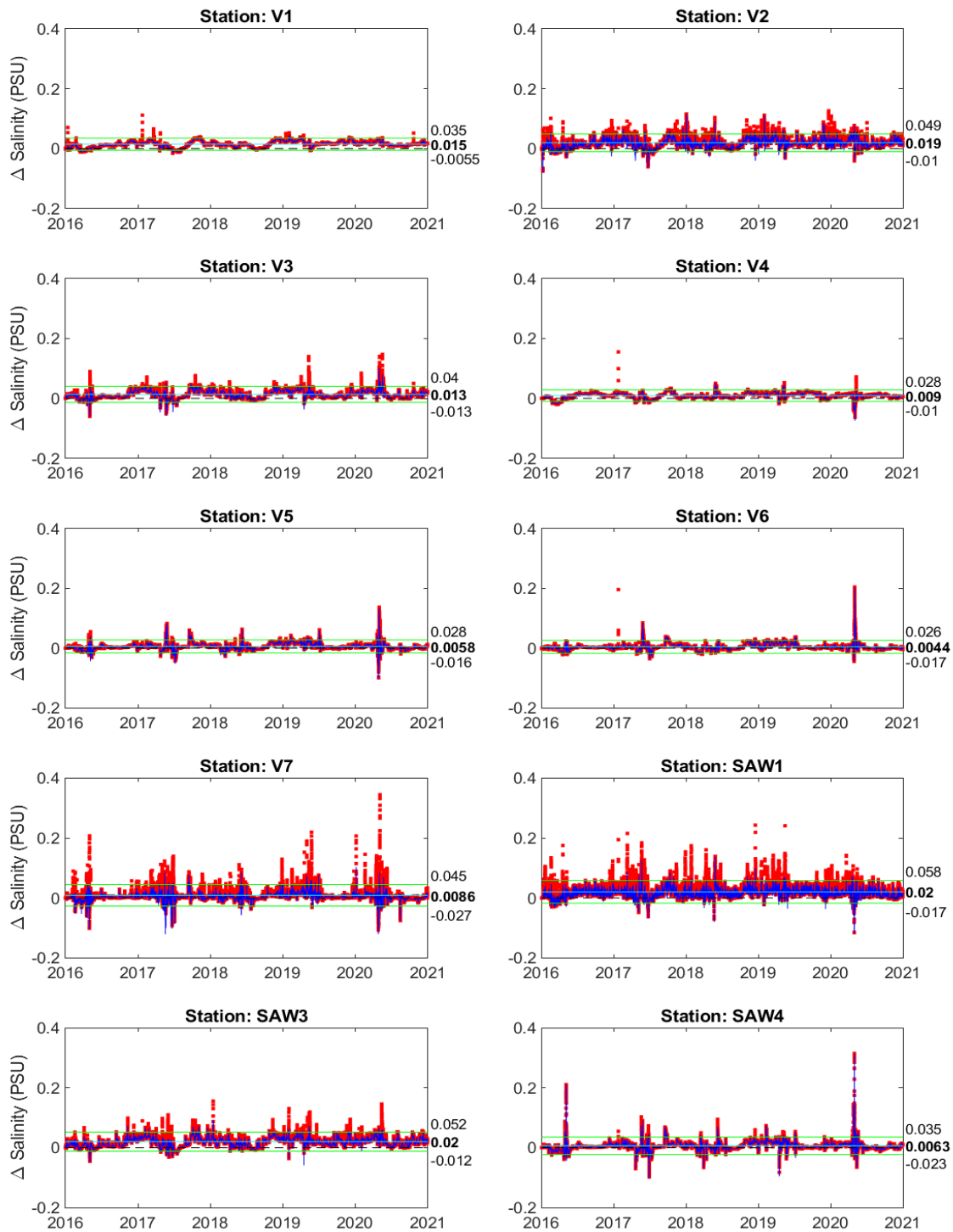
Figure 25. Far-field salinity anomalies predicted every hour over the 5-years hindcast at multiple locations for the Billy Lights Point offshore outfall. Blue line is the depth averaged anomaly. Red marker the maximum anomaly. Light blue and green lines show the timeseries mean ± 2 standard deviations, respectively. Figure 7 provides a map showing the corresponding locations.
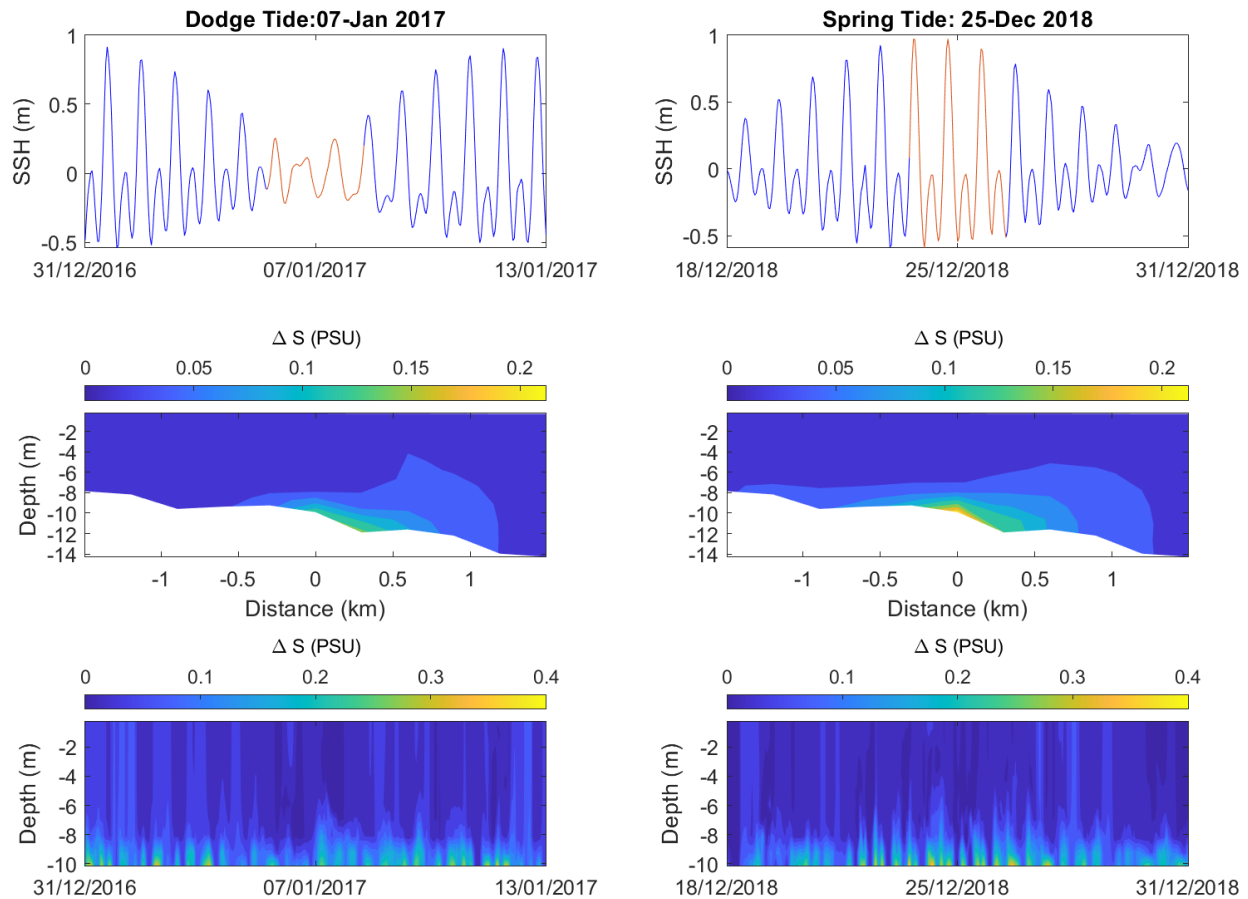
Figure 26. Snapshots of the salinity anomalies predicted in the vicinity of the Billy Lights Point extension outfall during a (left panels) dodge and (right panels) spring tide. Top panels – 14-day timeseries of sea surface height (SSH, m) 300 m from the outfall. Middle panels – lateral transect of the 3-day average salinity anomaly (PSU) centred 300m from the outfall and corresponding with the SSH highlighted in red. Bottom panels – hourly changes in the salinity anomaly throughout the water column 300 m from the outfall. Figure 42 in the Appendix provides a map showing the locations corresponding with the plotted transect and timeseries. The map limits are set for visualisation purposes and actual anomalies may exceed these limits.

4.3.   Point Boston - inshore

The spatial distribution of seasonally-averaged maximum salinity anomalies calculated from 5-years of model predictions for the Point Boston inshore outfall are shown in Figure 27. Salinity anomalies decreased from 0.97 PSU in the bottom layer of the model corresponding with the outfall location to 0.44 PSU and 0.1 PSU (Figure 27,Table 4) at distances of 0.5 and 1 km from the outfall. These increases correspond to salinity changes of ≤2.7%, ≤1.2% and ≤0.3% in the ambient salinity.

Smaller anomalies ≤0.05 PSU were predicted to be dispersed northwards along the coast into Louth Bay and Peake Bay in Autumn, consistent with the long-term net flow (Figure 19).

Figure 28 shows the far-field increases in salinity predicted at hourly intervals at the virtual monitoring stations and mooring sites (shown in Figure 7). Maximum anomalies rarely exceeded 0.1 PSU at stations within 5 km of the outfall (e.g., SAW4). At the V7 site located about 10 km offshore from the outfall, anomaly spikes >0.1 PSU predicted each autumn were associated with dynamical changes resulting from the injection of brine into the model and the greater dispersal of the brine plume in autumn (Figure 27) due to changes in the regions seasonal circulation patterns (Figure 19). Mean anomalies averaged across the 5-year hindcast were very small, <0.02 PSU, and anomalies at all sites were steady on annual timescales.

The salinity anomaly within 300m of the outfall reached 0.87 PSU on the bottom during both the dodge and spring tides (Figure 29). In the vertical plane, anomalies >0.4 PSU were largely restricted to the bottom 2 m and were mixed towards the surface on the spring tide. Lateral transects of the salinity anomaly averaged over 3 days showed negligible differences between dodge and spring tides with maximum anomalies ≥0.1 PSU extending out to approximately 0.75 km from the outfall.
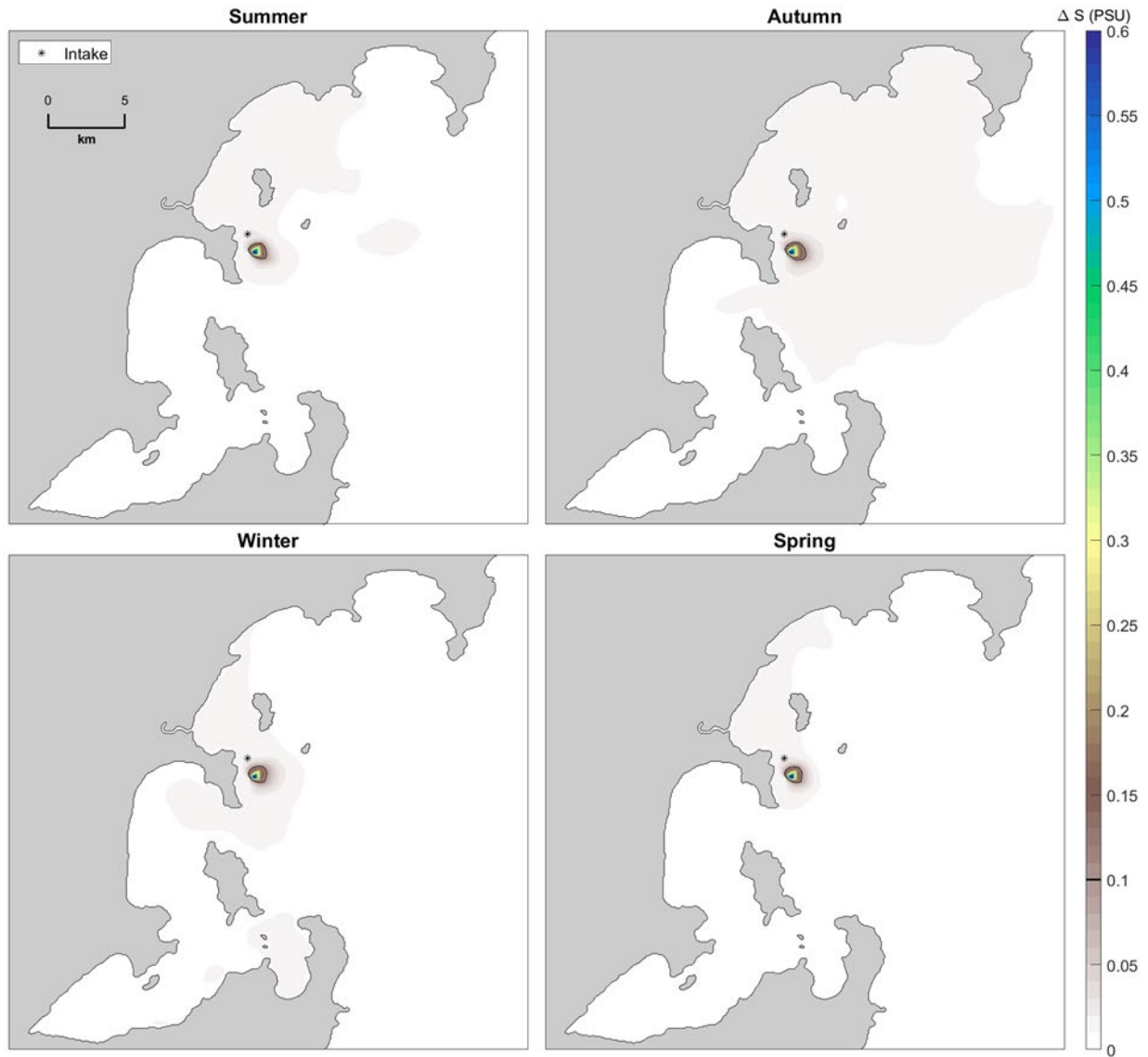
Figure 27. Maps of the seasonally-averaged maximum salinity anomaly for the Point Boston inshore outfall. The map limits are set to 0.6 PSU for visualisation purposes and actual anomalies may exceed 0.6 PSU at the grid cell corresponding with the outfall site.
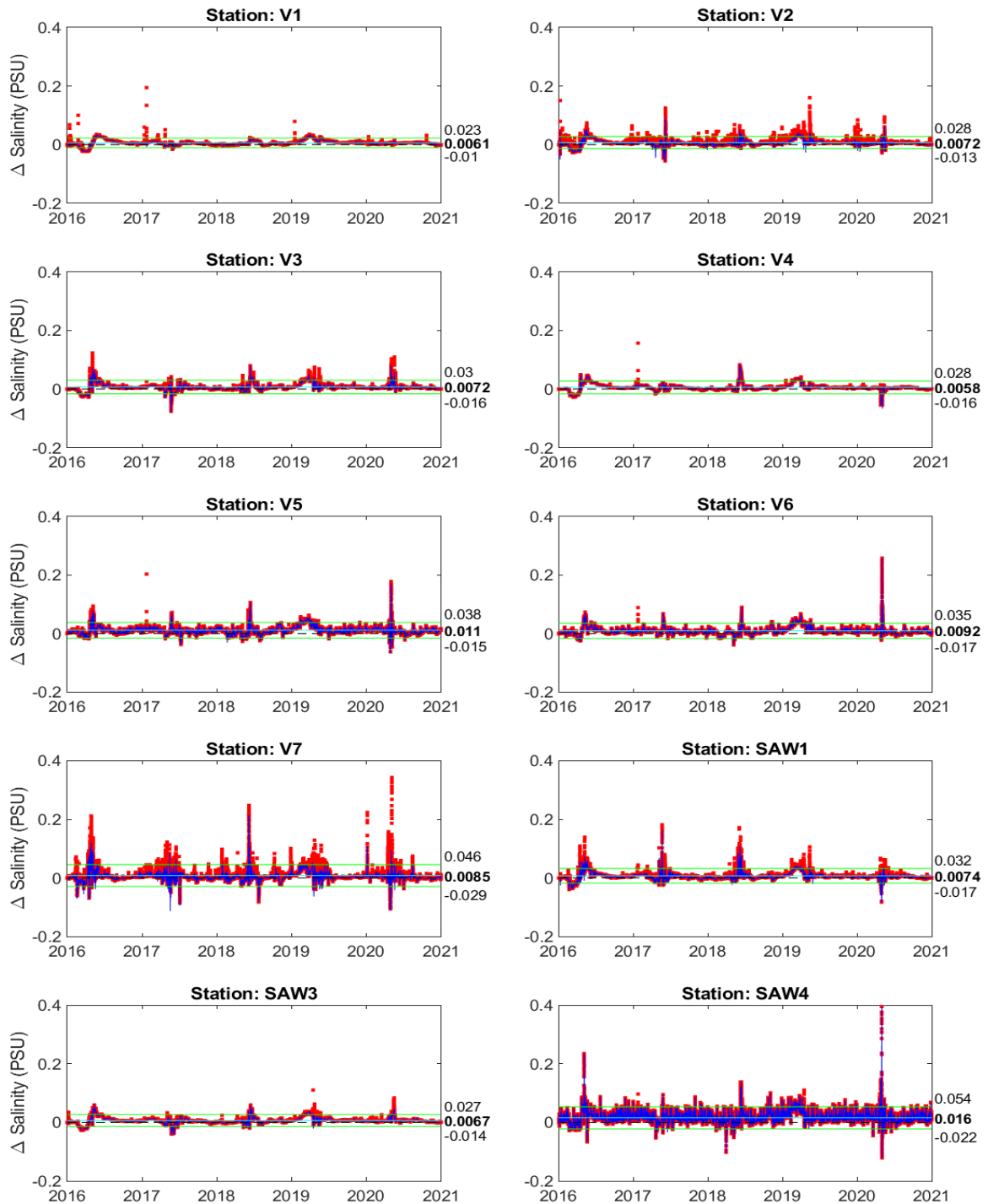
Figure 28. Far-field salinity anomalies predicted every hour over the 5-years hindcast at multiple locations for the Point Boston inshore outfall. Blue line is the depth averaged anomaly. Red marker the maximum anomaly. Light blue and green lines show the timeseries mean ± 2 standard deviations, respectively. Figure 7 provides a map showing the corresponding locations.
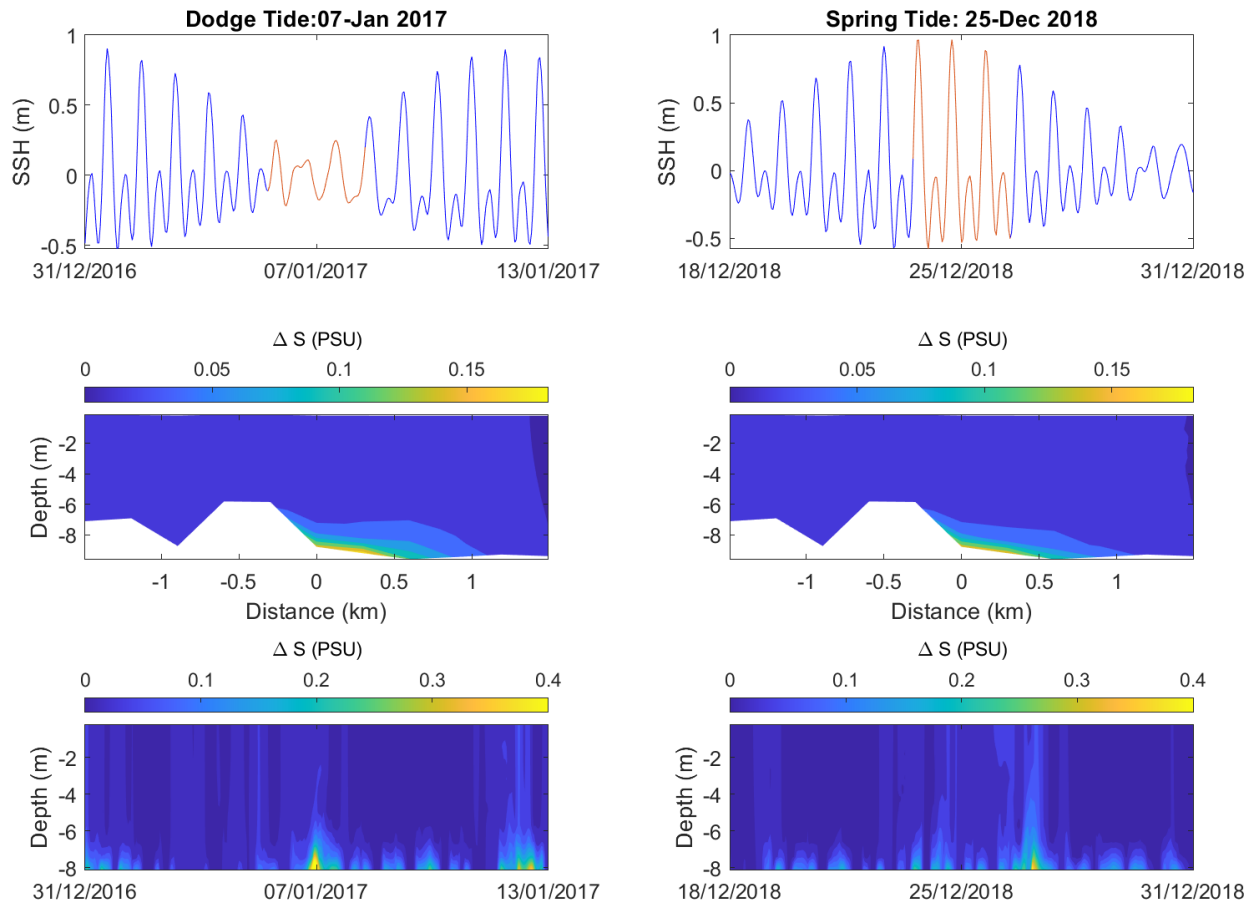
Figure 29. Snapshots of the salinity anomalies predicted in the vicinity of the Point Boston inshore outfall during a (left panels) dodge and (right panels) spring tide. Top panels – 14-day timeseries of sea surface height (SSH, m) 300 m from the outfall. Middle panels – lateral transect of the 3-day average salinity anomaly (PSU) centred 300m from the outfall and corresponding with the SSH highlighted in red. Bottom panels – hourly changes in the salinity anomaly throughout the water column 300 m from the outfall. Figure 42 in the Appendix provides a map showing the locations corresponding with the plotted transect and timeseries. The map limits are set for visualisation purposes and actual anomalies may exceed these limits.

4.4.   Point Boston - extension

The spatial distribution of seasonally-averaged maximum salinity anomalies calculated from 5-years of model predictions for the Point Boston extension outfall are shown in Figure 30. Salinity anomalies decreased from 0.36 PSU in the bottom layer of the model grid cell corresponding with the outfall location to 0.16 PSU and 0.08 PSU (Figure 30, Table 4) at distances of 0.5 and 1 km from the outfall. These increases correspond to salinity changes of ≤1%, ≤0.4% and ≤0.2% in the

ambient salinity, respectively. Smaller anomalies of ≤0.5 PSU were predicted up to 1.5 km from the outfall.

Figure 31 shows the far-field increases in salinity predicted at hourly intervals at the virtual monitoring stations and mooring sites (shown in Figure 7). Maximum anomalies predicted at any site rarely exceeded 0.1 PSU and mean anomalies across the 5-year hindcast were negligible and less than <0.001 PSU.

The maximum salinity anomaly within ~300m of the outfall on the bottom reached 0.44 PSU during the dodge tide and was reduced to a ≤0.2 PSU during the spring tide (Figure 32). In the vertical plane, anomalies were predicted to be restricted to the bottom 2 m during dodge and spring tides and quickly mixed to ambient levels. Lateral transects of the salinity anomaly averaged over 3 days showed salinity anomalies ≥0.1 PSU during dodge tides extending out to ~1 km of the outfall. Salinity anomalies were reduced to <0.05 PSU within 1 km of the outfall during spring tides.
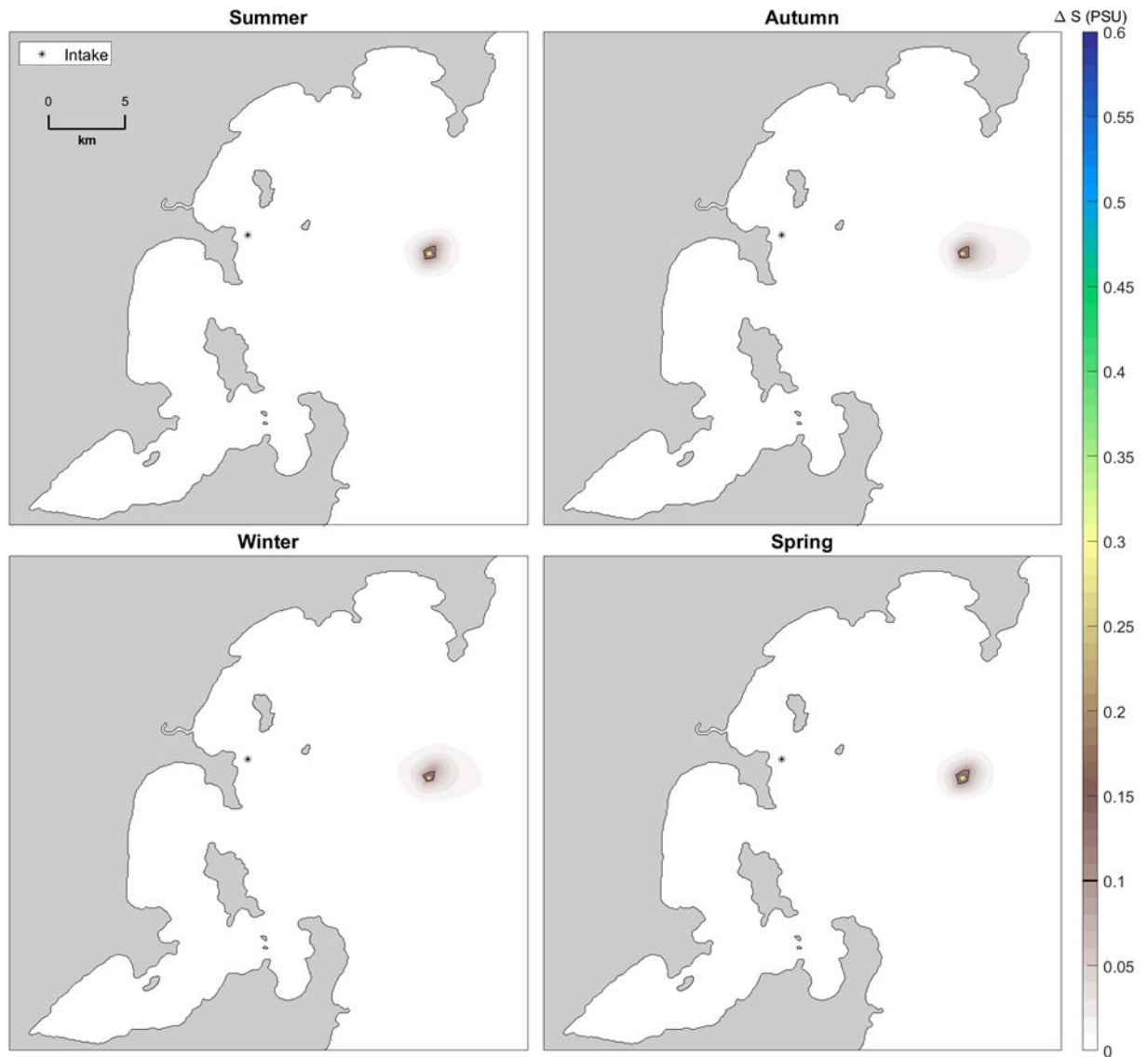
Figure 30. Maps of the seasonally-averaged maximum salinity anomaly for the Point Boston extension outfall. The map limits are set to 0.6 PSU for visualisation purposes and actual anomalies may exceed 0.6 PSU at the grid cell corresponding with the outfall site.
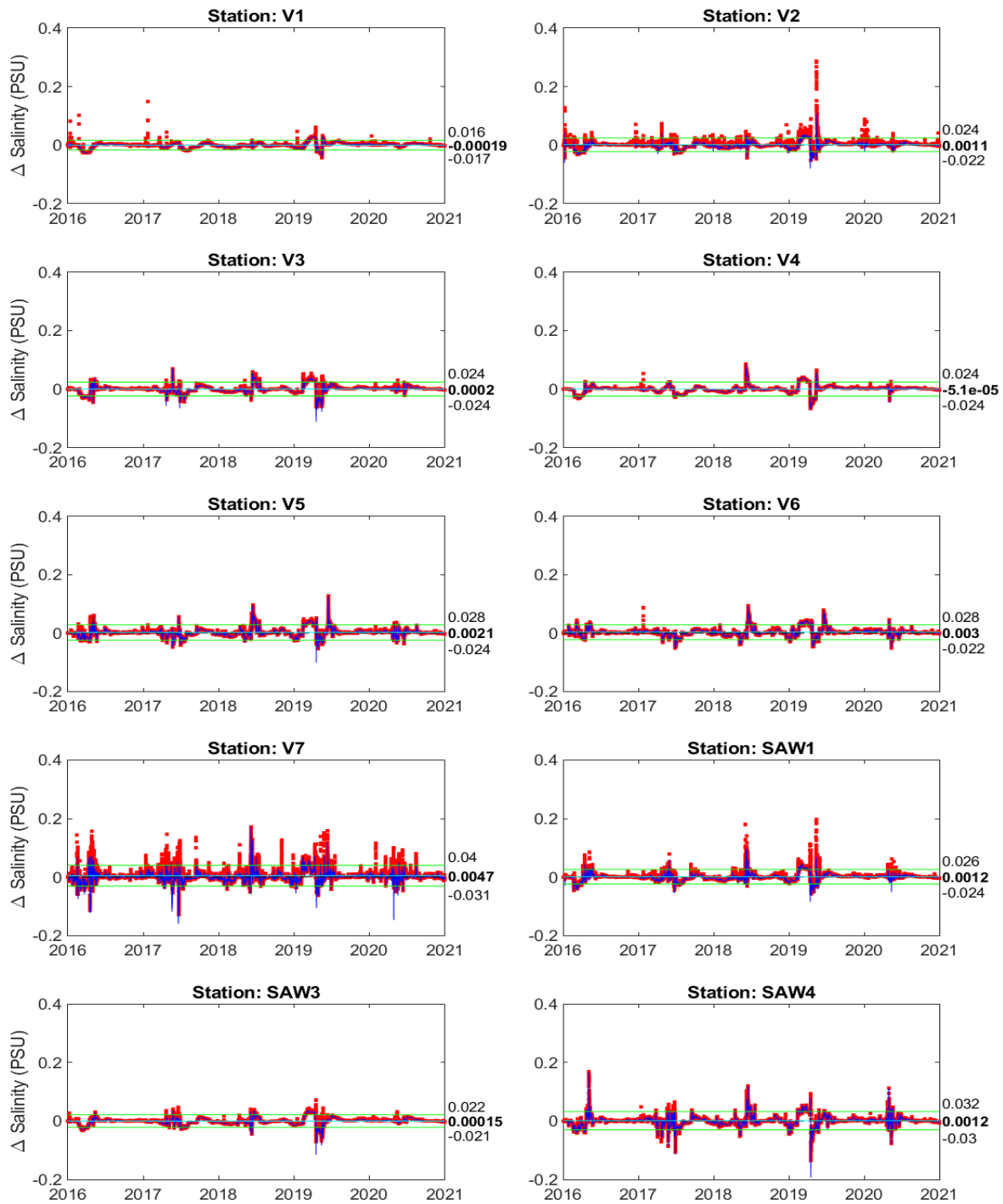
Figure 31. Far-field salinity anomalies predicted every hour over the 5-years hindcast at multiple locations for the Point Boston offshore outfall. Blue line is the depth averaged anomaly. Red marker the maximum anomaly. Light blue and green lines show the timeseries mean ± 2 standard deviations, respectively. Figure 7 provides a map showing the corresponding locations.
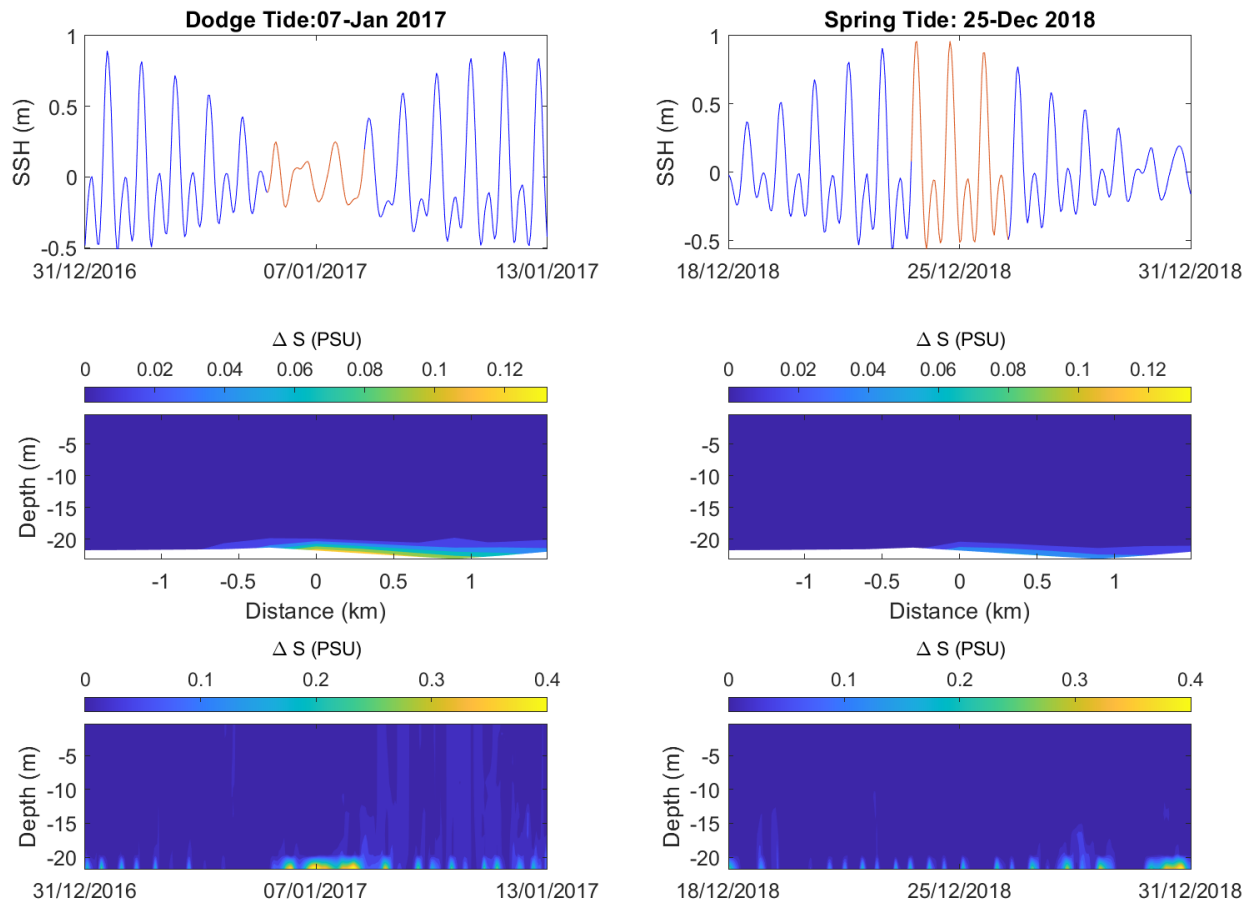
Figure 32. Snapshots of the salinity anomalies predicted in the vicinity of the Point Boston extension outfall during a (left panels) dodge and (right panels) spring tide. Top panels – 14-day timeseries of sea surface height (SSH, m) 300 m from the outfall. Middle panels – lateral transect of the 3-day average salinity anomaly (PSU) centred 300m from the outfall and corresponding with the SSH highlighted in red. Bottom panels – hourly changes in the salinity anomaly throughout the water column 300 m from the outfall. Figure 42 in the Appendix provides a map showing the locations corresponding with the plotted transect and timeseries. The map limits are set for visualisation purposes and actual anomalies may exceed these limits.

4.5.   Cape Donington

The spatial distribution of seasonally-averaged maximum salinity anomalies calculated from 5-years of model predictions for the Cape Donington outfall are shown in Figure 33. Salinity anomalies decreased from 0.36 PSU in the bottom layer of the model grid cell corresponding with the outfall location to 0.11 PSU and 0.03 PSU (Figure 33, Table 4) at distances of 0.5 and 1 km from the outfall. These increases correspond to salinity changes of ≤1%, ≤0.3% and ≤0.1% in the ambient salinity, respectively.

Figure 34 shows the far-field increases in salinity predicted at hourly intervals at the virtual monitoring stations and mooring sites (shown in Figure 7). Maximum anomalies predicted at any site rarely exceeded 0.1 PSU and mean anomalies across the 5-year hindcast were negligible and less than <0.001 PSU.

The maximum salinity anomaly within ~300m of the outfall on the bottom reached 0.3 PSU during the dodge tide and was reduced to a maximum of <0.15 PSU during the spring tide (Figure 35). During both tidal phases brine discharges were quickly mixed to ambient levels in the vertical. Lateral transects of the salinity anomaly averaged over 3 days show anomalies of ~0.05 to 0.1 PSU extending out to ~1 km from the outfall during the dodge tide. Salinity anomalies were reduced during spring tides to <0.05 PSU within 0.5 km of the outfall.

Figure 33. Maps of the seasonally-averaged maximum salinity anomaly for the Cape Donington outfall. The map limits are set to 0.6 PSU for visualisation purposes and actual anomalies may exceed 0.6 PSU at the grid cell corresponding with the outfall site.
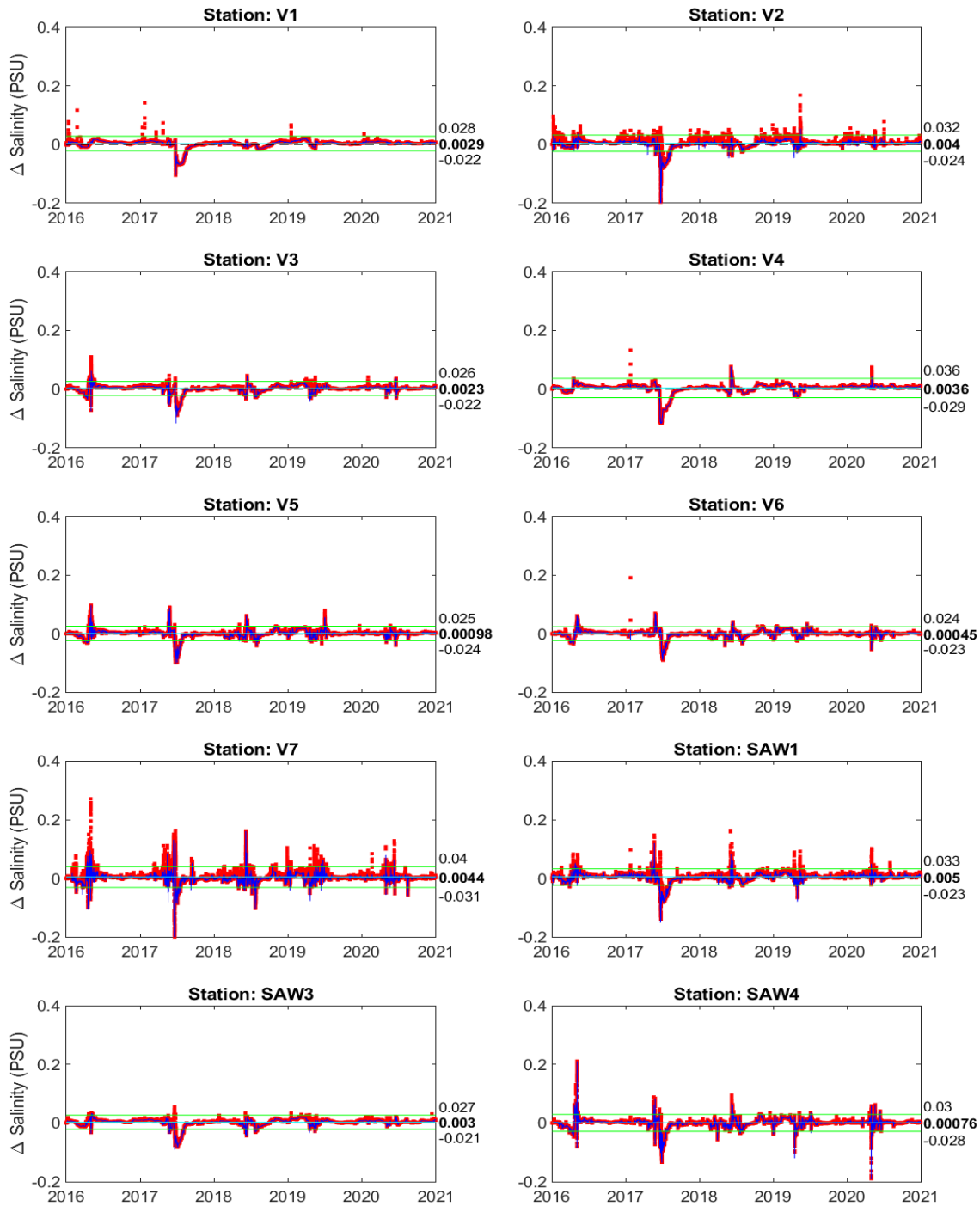
Figure 34. Far-field salinity anomalies predicted every hour over the 5-years hindcast at multiple locations for the Cape Donington outfall. Blue line is the depth averaged anomaly. Red marker the maximum anomaly. Light blue and green lines show the timeseries mean ± 2 standard deviations, respectively. Figure 7 provides a map showing the corresponding locations.
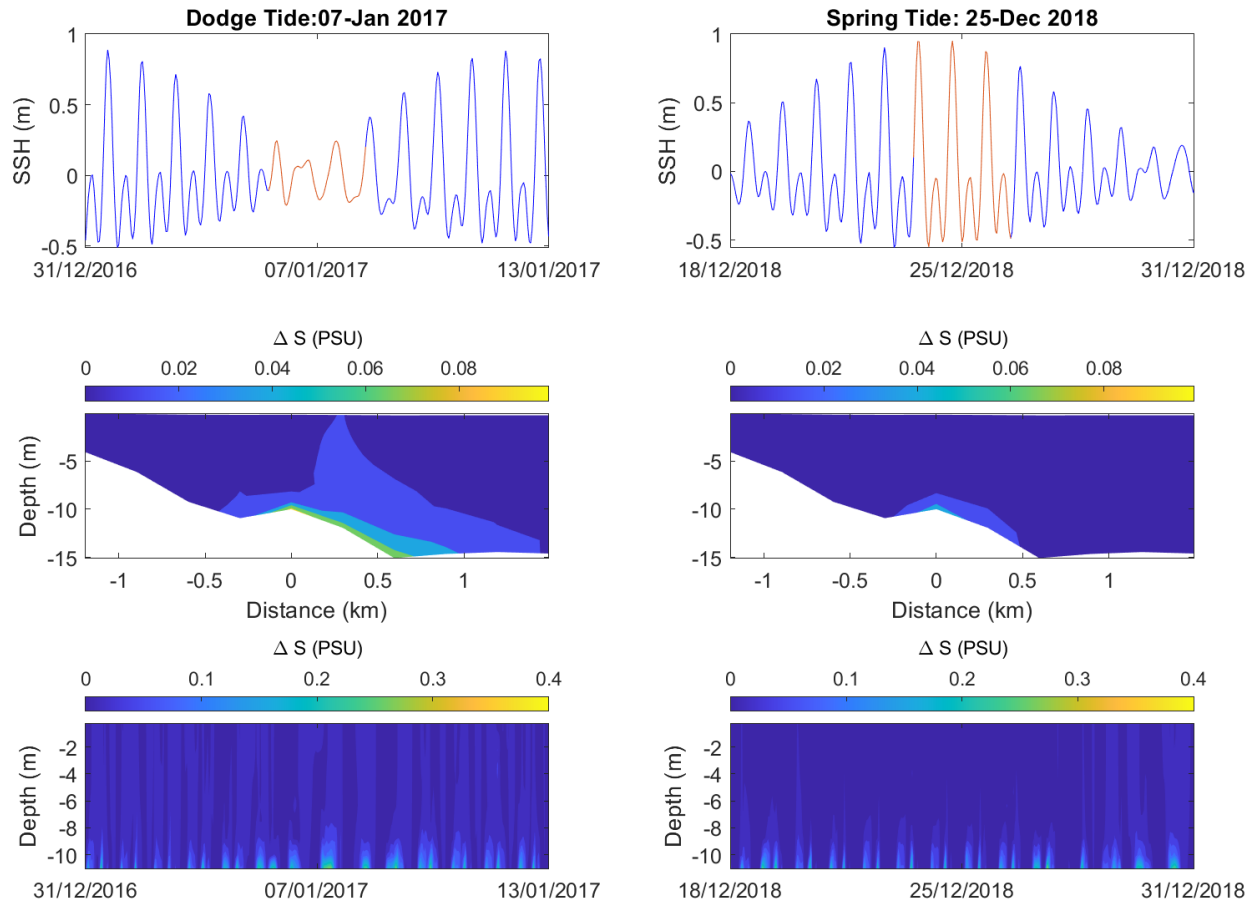
Figure 35. Snapshots of the salinity anomalies predicted in the vicinity of the Cape Donington outfall during a (left panels) dodge and (right panels) spring tide. Top panels – 14-day timeseries of sea surface height (SSH, m) 300 m from the outfall. Middle panels – lateral transect of the 3-day average salinity anomaly (PSU) centred 300m from the outfall and corresponding with the SSH highlighted in red. Bottom panels – hourly changes in the salinity anomaly throughout the water column 300 m from the outfall. Figure 42 in the Appendix provides a map showing the locations corresponding with the plotted transect and timeseries. The map limits are set for visualisation purposes and actual anomalies may exceed these limits.

4.6.   Site comparison summary

Figure 36 summarizes the decrease in maximum seasonally-averaged salinity anomalies with distance from each outfall. For each outfall, the maximum anomaly from each of seasonal maps (shown in Figure 21, Figure 24,Figure 27, Figure 30 and Figure 33) were determined at different distances from the outfall using a bin width of 250 m. Corresponding values are shown in Table 4. Except for the Billy Lights Point and Point Boston inshore outfalls, maximum long-term salinity

increases below 0.2 PSU were predicted within 0.25 - 0.5 km of outfalls. For all outfalls, long-term salinity increases ≤0.1 PSU were predicted within 0.75-1 km of outfalls.
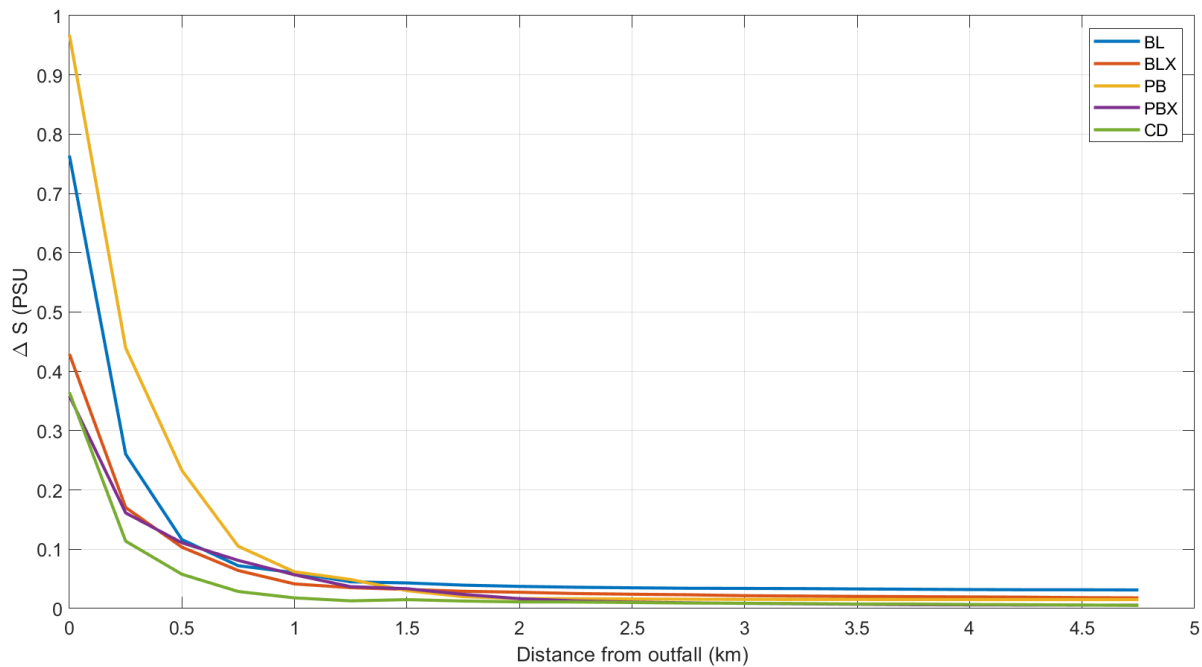
Figure 36. The maximum seasonally-averaged salinity anomaly (PSU) predicted at different distances from each outfall site. BL = Billy Lights Point inshore, BLX = Billy Lights Point extension, PB = Point Boston inshore, PBX = Point Boston extension, CD = Cape Donington. Salinity anomaly values on the x-axis corresponded with the minimum value of the bin shown inTable 4.

Table 4. Maximum seasonally-averaged salinity anomaly values predicted over the 5-year hindcast at different distances from each outfall site.

Site	0 - 0.25 km	0.25 - 0.5 km	0.75 - 1 km	1.25 - 1.5 km	1.75 - 2 km	2.75 - 3 km	4.75 - 5 km
Billy Lights Point inshore	0.76	0.26	0.07	0.05	0.04	0.03	0.03
Billy Lights Point extension	0.43	0.17	0.06	0.04	0.03	0.02	0.02
Point Boston inshore	0.97	0.44	0.10	0.05	0.02	0.02	0.02
Point Boston extension	0.36	0.16	0.08	0.04	0.02	0.01	0.01
Cape Donington	0.36	0.11	0.03	0.01	0.01	0.01	0.01

5. RESULTS: PARTICLE TRACKING MODELLING

Larval dispersal patterns simulated by the biophysical model predicted larvae will be largely transported along the coastal boundaries and away from the coast into offshore waters by the tidal and wind driven circulation (Figure 37). Maps showing the percentage of particles from each source location arriving within 25 m radius of the different intakes are shown in Figure 38, Figure 39, and Figure 40. The predicted spatial patterns were averaged over the three annual spawning events and demonstrate increased connectivity of larvae (≥0.3%) within 2 km of the intakes. This is consistent with tidal displacement distances of ~2 km estimated over 3 hours for a current speed of 0.2 m/s.

For the Billy Lights Point inshore and Cape Donington intake, connectivity was predicted to be dominated by larvae from Proper Bay, with slightly greater levels of connectivity early in the spawning season (May and June) relative to the later months (July-September) (Figure 38). Despite being located less than 2 km away, connectivity with the Billy Lights Point extension intake were distinct from those predicted from the inshore intake. Connectivity with the extension intake was characterised by increased connectivity with Boston Bay and Boston Island across the spawning season. There was a slight increase in connectivity with Proper Bay later in the spawning season (July-September) relative to the inshore intake (Figure 39). For the Point Boston intake, connectivity was dominated by larvae sourced from Louth Bay, Louth Island, the northern coastline of Boston Island and Boston Bay, across the spawning season. Connectivity with Peake Bay was predicted to be strongest in May (Figure 40).

The mean percentage of total particles (i.e., larvae) released each month estimated to come within 25 m of the intakes is shown in Figure 41. Less than 0.04% percent of each monthly spawning event was estimated to be at risk of entrainment by the Billy Lights Point inshore and extension intakes. For these intakes monthly connectivity was predicted to be slightly higher in May and June. Connectivity was greatest with the Point Boston intake, with up to 0.06% of the total particles released each month estimated to be at risk of entrainment. As for the previous intake sites, connectivity was predicted to be slightly higher early in the spawning season (May and June) compared to the later months.
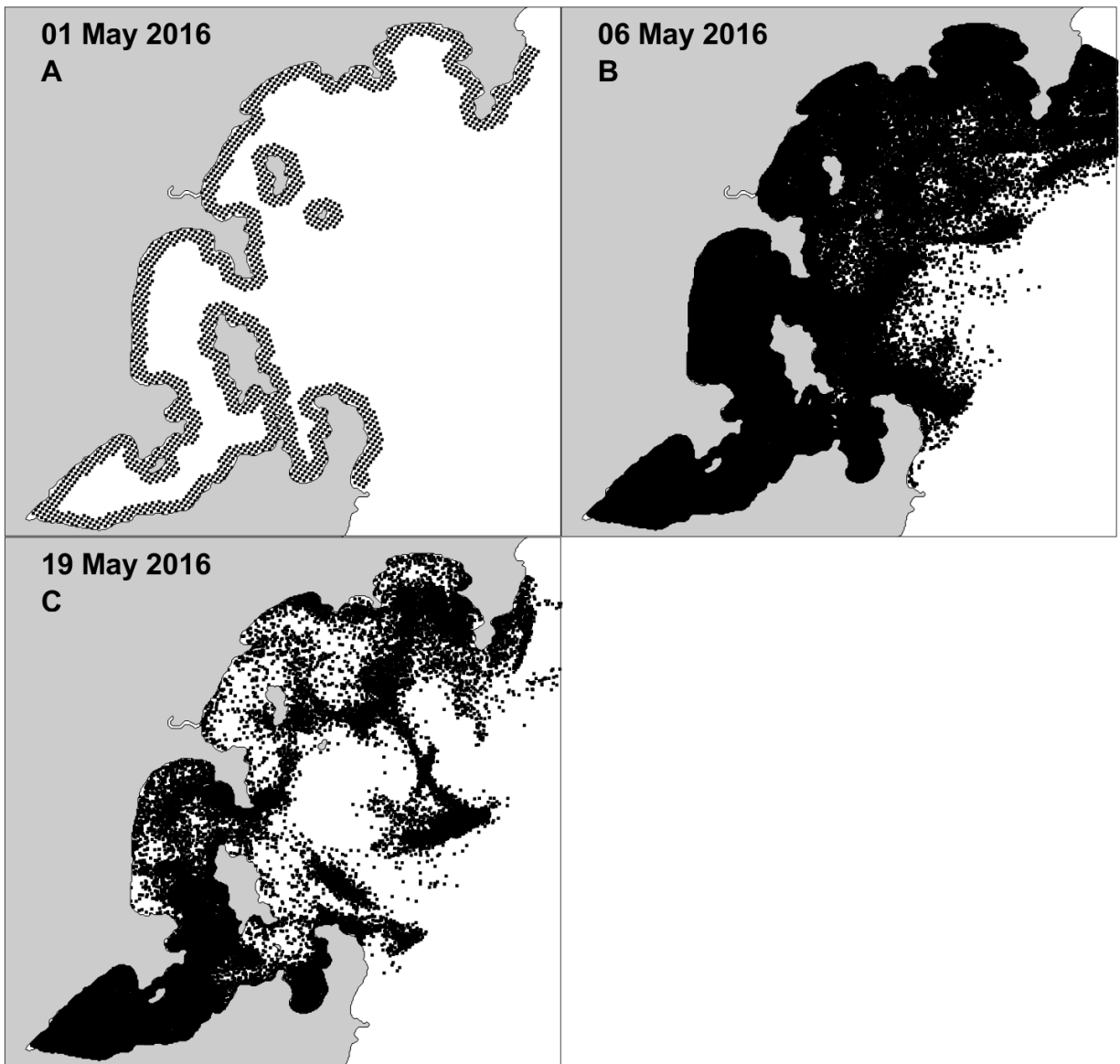
Figure 37. Snapshots of larvae distribution simulated during the May 2016 spawning event. (A) Initial distributions corresponding to model grid cell within 1 km of the coast 1, (B) distributions on day 6 following the release of all larvae and (C) distributions on day 20.
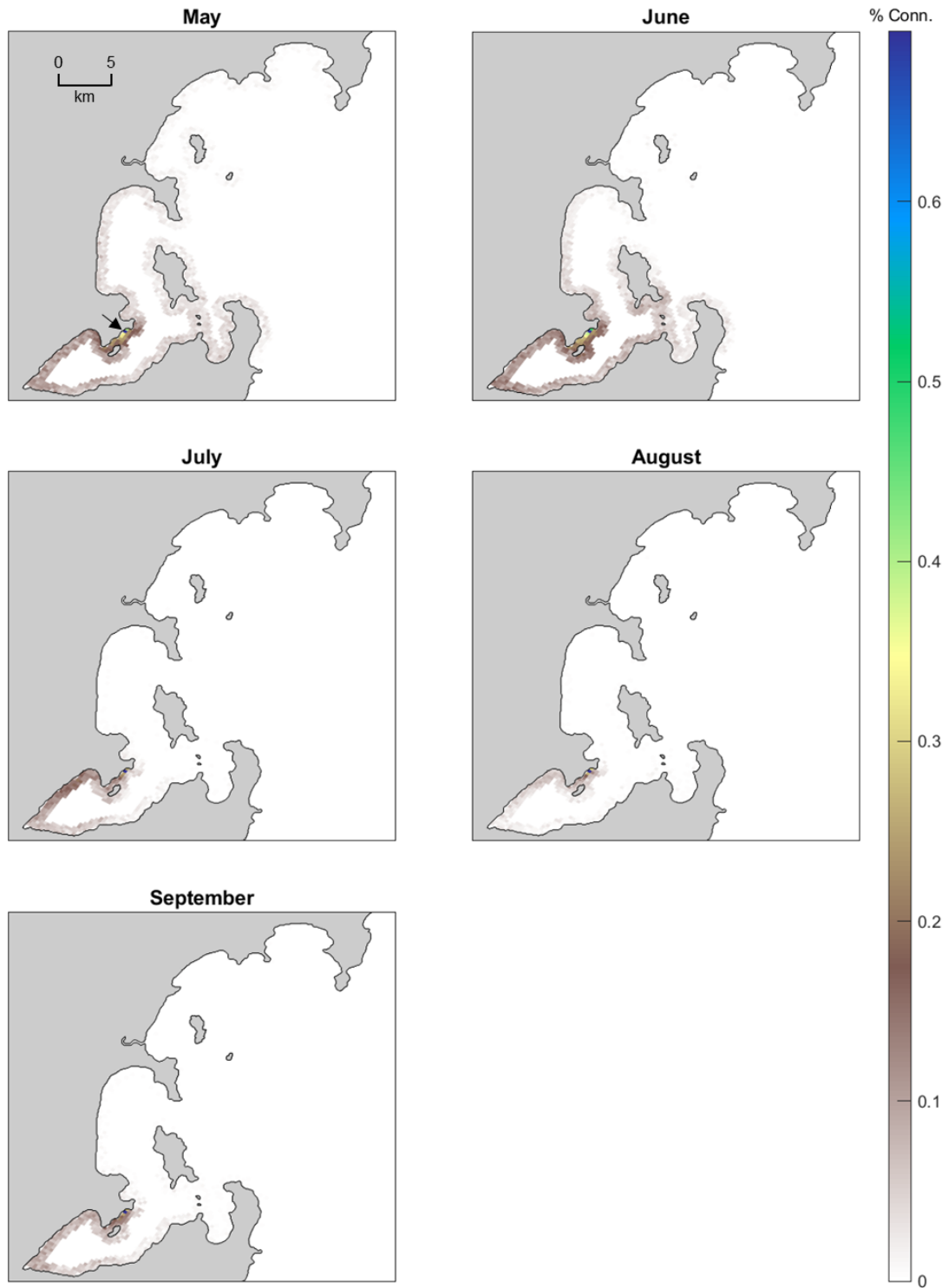
Figure 38. Modelled connectivity of larvae with Billy Lights Point inshore and Cape Donington intake showing the percentage of larvae from each release point which came within a 25m radius of the intake. Results are the monthly averaged distributions for each monthly spawning events averaged over three years (2016-2019). Black arrow in the top left plot indicates the intake location.
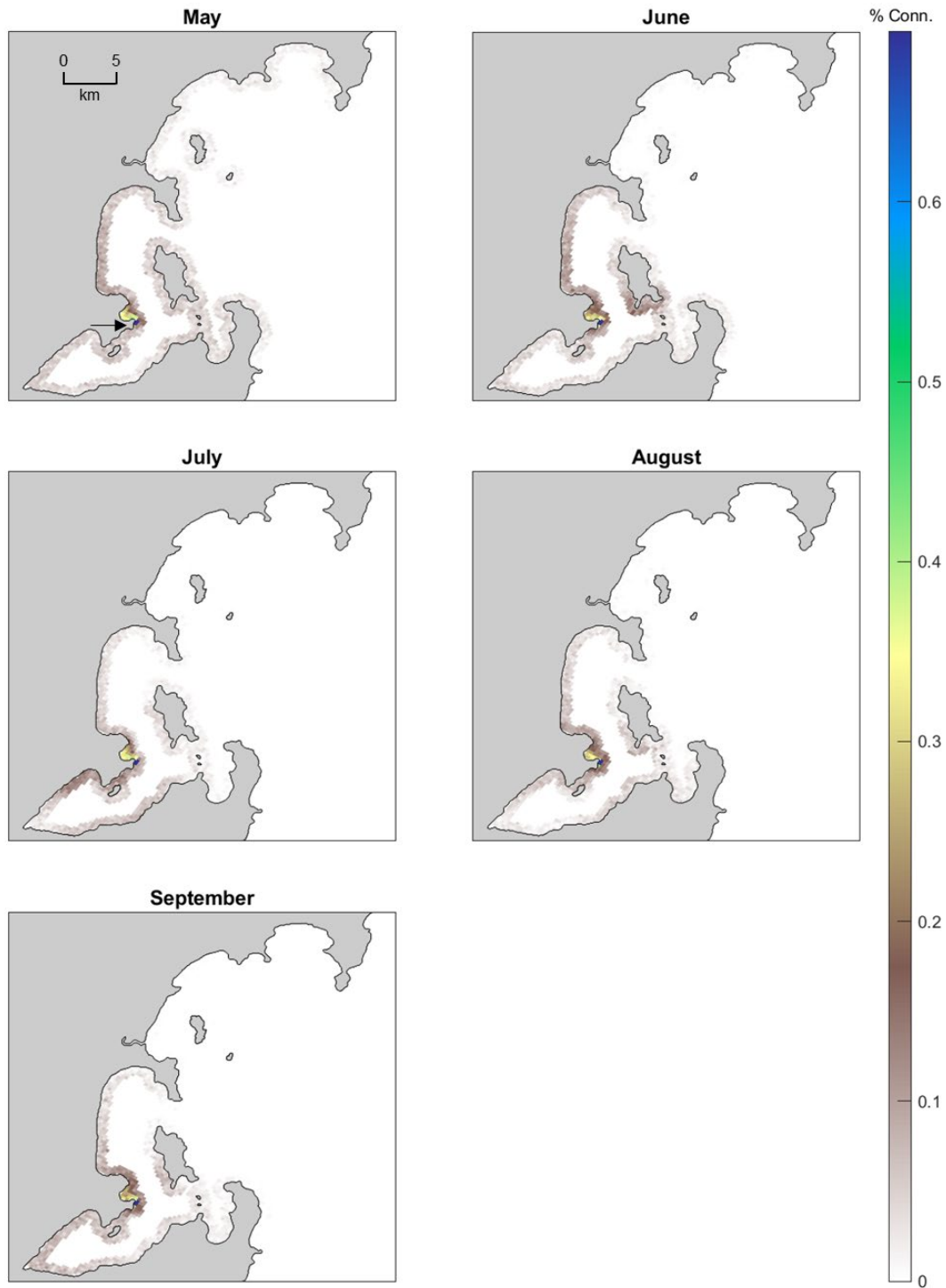
Figure 39. Modelled connectivity of particles (representative of larvae) with Billy Lights Point extension intake showing the percentage of larvae from each release point which came within a 25m radius of the intake. Results are the monthly averaged distributions for each monthly spawning events averaged over three years (2016-2019). Black arrow in the top left plot indicates the intake location.
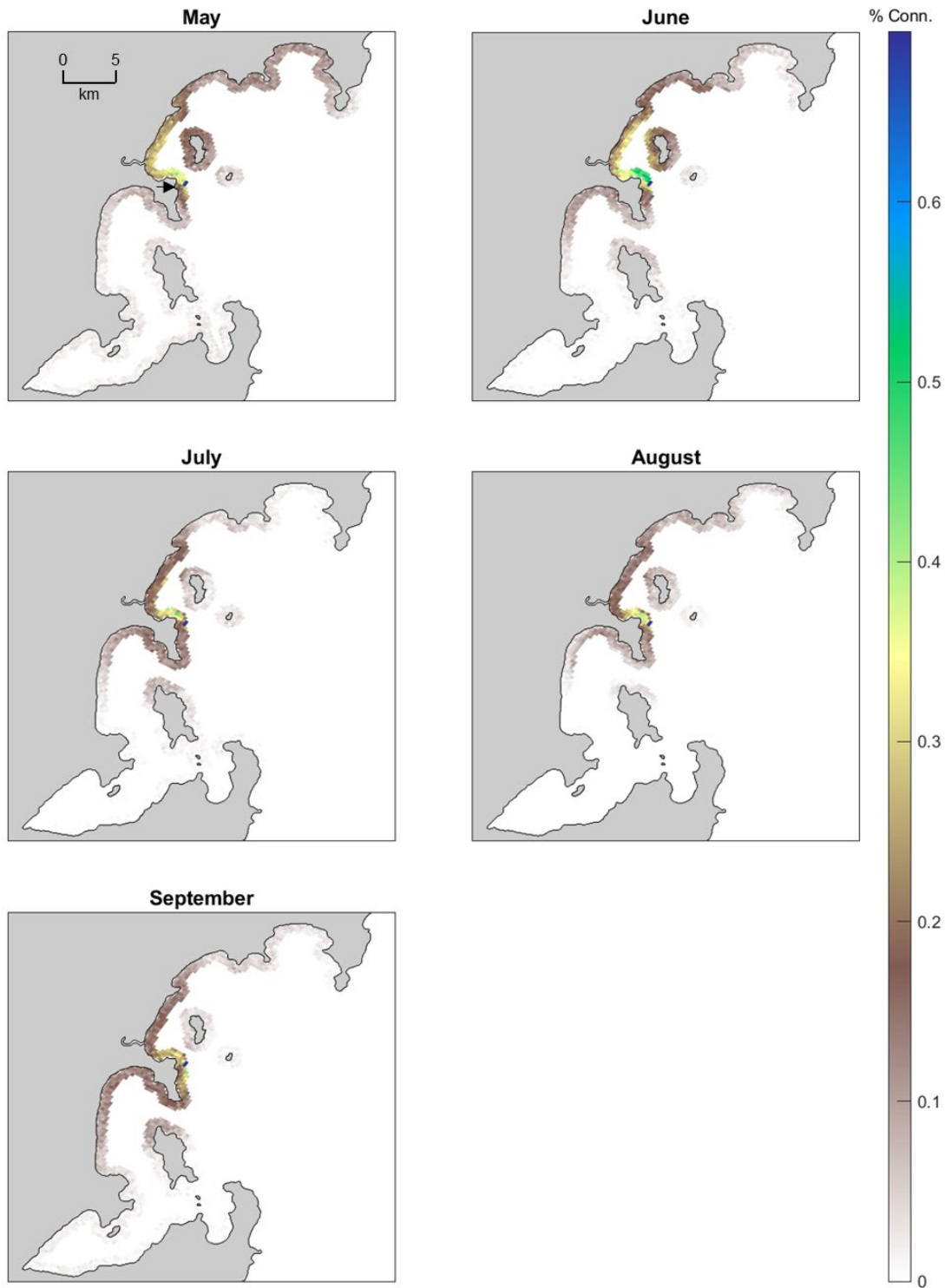
Figure 40. Modelled spatial connectivity of particles (representative of larvae) with the Point Boston inshore and Point Boston extension intake showing the percentage of larvae from each release point which came within a 25m radius of the intake. Results are the monthly averaged distributions for each monthly spawning events averaged over three years (2016-2019). Black arrow in the top left plot indicates the intake location.
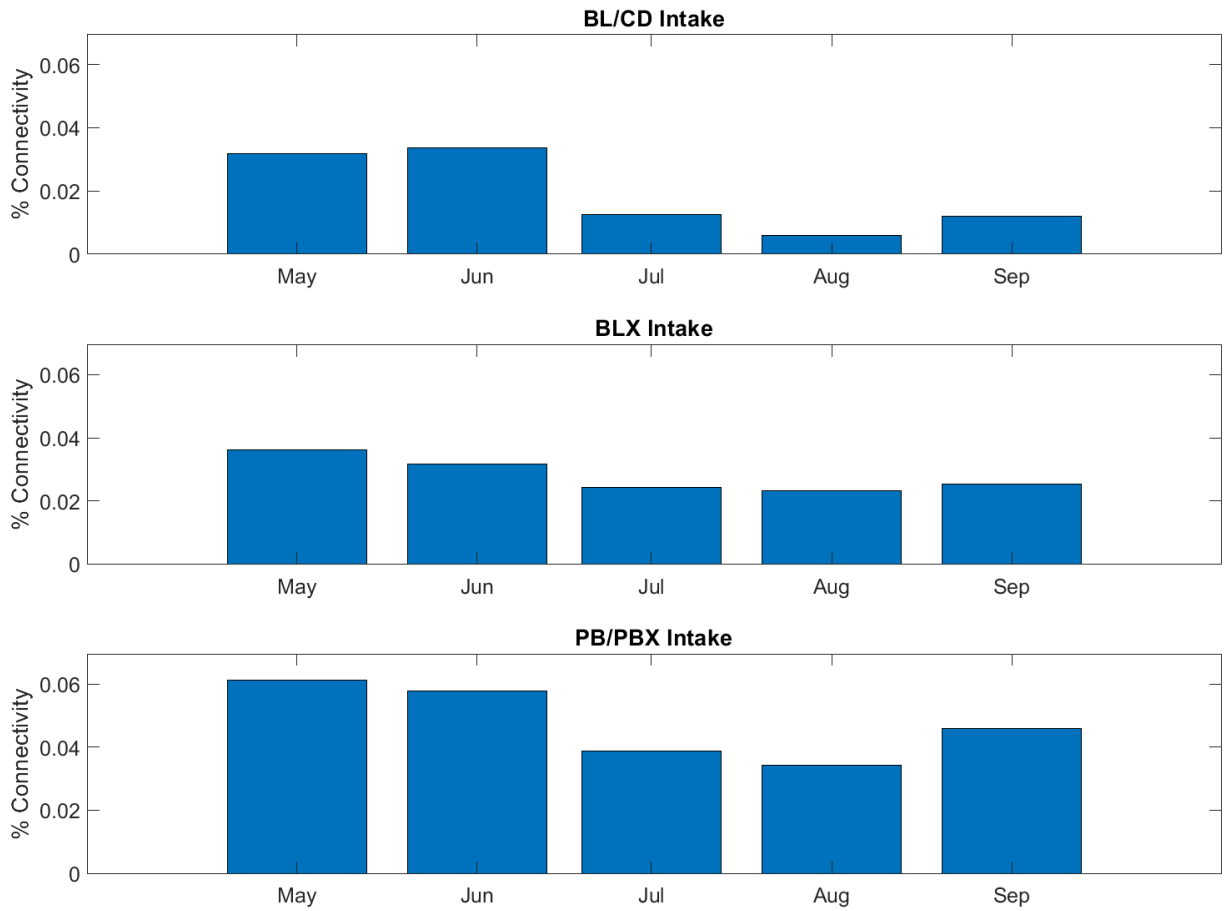
Figure 41. Modelled temporal connectivity showing the estimated percentage of particles (representative of larvae) released in each monthly spawning event which came within 25m radius of the (Top) Billy Lights Point inshore/Cape Donington (BLP / CD), (Middle) Billy Lights Point extension (BLX) and (Bottom) Point Boston (PB) intakes. Results are the average for the three annual spawning events (2016-2019).

6. CONCLUSIONS

A high-resolution 3D hydrodynamic model was developed for the Boston Bay region to examine the effect of hydrodynamics on the dispersal of brine outfall and connectivity of planktonic larvae (i.e., blue mussel) with intakes for several possible desalination plant outfall/intake locations.

Comparison with field measurements showed that the model was able to reproduce tidal and lower-frequency (i.e., weather-band and seasonal) variations in currents, sea level (including dodge and spring tides), temperature and salinity. The model predictions were consistent with, and improve on, existing oceanographic modelling for this region (Herzfeld et al. 2009; Middleton et al. 2013, Middleton and Doubell 2014; Middleton et al. 2014) that have been used to aid developing management for local aquaculture industry and fisheries sectors. The measurements and model results showed strong tidal currents (~0.2 m/s) and weaker (<0.05 m/s) weather-band currents. The model therefore had predictive capability for determining the mixing, diffusion, long-term transport and flushing of brine outfalls and planktonic larvae (Herzfeld et al. 2009; Middleton et al. 2014).

Using a 5-year model hindcast, far-field predictions of the salinity increases (anomalies) for a 12 GL per year desalination plant indicated maximum seasonally-averaged anomalies within 250-500m of the outfalls ranged between 0.11 and 0.44 PSU (≤1.2% change in the ambient salinity) depending on the outfall location. For all locations, maximum seasonally-averaged anomalies decreased to ≤0.1 PSU (≤0.3 % change in the ambient salinity) within 1km from the outfalls and were steady on annual timescales. The predicted changes are within the range of natural salinity variability determined from the measured data which showed an annual range of 1.46 PSU, equivalent to a 4% annual change in ambient salinity concentrations, and variations of 0.1 and 0.5 PSU observed over periods of several hours to weekly, respectively.

Although the predicted increases from the modelled outfall sites were low and within natural salinity variability, increases in salinity and the potential for long-term accumulation were smaller when outfalls were sited in better flushed locations. Consistent with previous estimates of flushing at the site (Middleton et al. 2014) scale and the scale of the bays within the Port Lincoln region (Herzfeld et al. 2009), the reduced flushing and the far-field transport brine from outfalls located inshore at Billy Lights Point was predicted to result in long-term mean increases of <0.05 PSU across Boston and Proper Bay. The spatial extent of this impact, and the potential for long-term accumulation in Proper Bay and Boston Bay, was lower when the outfall was located at the Billy

Lights extension outfall or Point Boston inshore outfall. Predicted salinity increases in the embayments were lowest when outfalls were in well flushed offshore waters east of Boston Island (i.e., Point Boston extension or Cape Donington).

At shorter timescales, hourly predictions of the far-field increase in salinity at distances >250m from the outfalls investigated in this study were always <0.9 PSU and remained below the 5% change in ambient salinity (~1.8 PSU) recommended by the Australian and New Zealand Guidelines for Fresh and Marine Waters. More recent studies on the impacts of desalination recommend environmental or ecological tolerance limits of 1 PSU for flora and fauna (Lattemann and Höpner 2008; Panagopoulos and Haralambous 2020; Omerspahic et al., 2022) including local aquaculture species (Tanner and Drabsch 2021). Given that the proposed plant is small (8 GL per year maximum), the modelling results from this study predicted for a 12 GL per year plant operating at full capacity suggest there is unlikely to be any substantial environmental impacts from brine discharges on salinity increases in the far-field. To further minimise environmental impacts, it is important sufficient mixing and dilution is achieved by optimising the design and application of diffuser systems in the near-field.

Biophysical modelling of planktonic larvae, based on the spawning characteristics of blue mussel larvae, indicated that less than 0.1% of the particles released (i.e., spawned biomass) are likely to be at risk of entrainment by the proposed desalination plant's intakes. Assuming larvae are passive and are sourced uniformly from the coastline of the surrounding embayments, spatial connectivity with proposed intakes was demonstrated to be strongly influenced by tides and the long-term mean circulation patterns. Connectivity patterns identified that mussels sourced from Proper Bay and the Boston Bay area inshore from Boston Island had increased connectivity with intakes located near Billy Lights Point and reduced connectivity with the intake located near Point Boston. Similarly, mussels sourced from Louth and Peake Bays had increased connectivity with the intake located near Point Boston and reduced connectivity with intakes located near Billy Lights Point. These results are based on a very limited understanding of the pelagic larval duration, development characteristics and source areas of the local blue mussel. Improved estimates of the total amount of larvae possibly removed by entrainment requires larval sampling to better understand source regions and concentrations. Additional model improvements could also be achieved with a better understanding of the pelagic larval duration and development characteristics (e.g., extent of vertical migration (McLeay et al. 2016)) for local blue mussels and other commercially important species.

This study suggests that the impact of salinity increases resulting from brine discharges associated with a 12 GL per annum plant on the receiving marine ecosystems and co-located aquaculture is likely to be small and within the regions natural variability. In part, this would be due to the small scale of the proposed plant. Initially, this is planned to be 4-5.3 per year, but up to a maximum of 8 GL per year, which compares, for example, with the 100 GL annual capacity desalination plant in Adelaide. A caveat for this conclusion is that slight increases in salinity could add an additional cumulative stress to some species that may be already stressed. For example, there are currently existing concerns that the cumulative effects of dissolved nutrient emissions from tuna and finfish aquaculture, wastewater treatment plants, and other sources may be potentially impacting the regions planktonic (Tanner at al. 2020) and seagrass (Tanner at al. 2019) ecosystems. These could potentially be compounded by stresses caused by climate induced changes in sea temperature, salinity, and water quality (Harley et al. 2006; Roberts et al. 2019; Chenoweth et al. 2022).

The hydrodynamic model developed here provides an improved tool that can be used to optimise desalination plant intake and outfall location determinations (and other anthropogenic point sources) to minimise potential and asses potential impacts from multiple sources to ensure the health and sustainability of the Port Lincoln region.

REFERENCES

ANZECC & ARMCANZ. 2000. Australian and New Zealand guidelines for fresh and marine water quality. National Water Quality Management Strategy Paper No 4, Australian and New Zealand Environment and Conservation Council & Agriculture and Resource Management Council of Australia and New Zealand, Canberra, Australia.

Chenoweth, J., P. Hadjinicolaou, A. Bruggeman, J. Lelieveld, Z. Levin, M. A. Lange, ... and M. Hadjikakou. 2011. Impact of climate change on the water resources of the eastern Mediterranean and Middle East region: Modeled 21st century changes and implications. Water Resources Research **47**(6).

Chin, T.M, J. Vazquez-Cuervo and E.M. Armstrong. 2017 A multi-scale high-resolution analysis of global sea surface temperature, Remote Sensing of Environment **200**:154-169.

Coolen, J. W., A.R. Boon, R. Crooijmans, H. Van Pelt, F. Kleissen, D. Gerla, ... and P.C. Luttikhuizen. 2020. Marine stepping-stones: Connectivity of *Mytilus edulis* populations between offshore energy installations. Molecular Ecology, **29(4)**: 686-703.

Davis, C., B. Brown, and R. Bullock. 2006. Object-Based Verification of Precipitation Forecasts. Part II: Application to Convective Rain Systems, Monthly Weather Review **134(7)**: 1785-1795.

Demmer, J., P. Robins, S. Malham, M. Lewis, A. Owen, T. Jones, and S. Neill. 2022. The role of wind in controlling the connectivity of blue mussels (*Mytilus edulis* L.) populations. Movement Ecology **10(1)**: 1-15.

Dobretsov, S. V., and G.Miron. 2001. Larval and post-larval vertical distribution of the mussel Mytilus edulis in the White Sea. Marine Ecology Progress Series **218**: 179-187.

De Vooys, C.G.N. 1999. Number of larvae and primary plantigrades of the mussel *Mytilus edulis* in the western Dutch Wadden Sea. Journal of Sea Research **41(3)**:189–201.

BDO EconSearch. 2020. Economic indicators for the commercial fisheries of South Australia summary report 2019/20. A Report for the Department of Primary Industries and Regions 30 June 2021 Prepared by BDO EconSearch.

Erofeeva, G., and L. Egbert. 2014. TPXO8-ATLAS, v1. Oregon State University, College of Earth, Ocean, and Atmospheric Sciences.

Harley, C. D., A. Randall Hughes, K.M. Hultgren, B.G Miner, C.J. Sorte, C.S. Thornber, ... and S.L. Williams. 2006. The impacts of climate change in coastal marine systems. Ecology letters **9(2)**: 228-241.

Herzfeld, M., J.F. Middleton, J.R. Andrewartha, J. Luick, W. Leeying. 2008. Numerical hydrodynamic modelling of Boston Bay, Spencer Gulf. Technical report, Aquafin CRC Project 4.6, FRDC Project 2005/059. Aquafin CRC, Fisheries Research & Development Corporation and South Australian Research & Development Institute (Aquatic Sciences), Adelaide. SARDI Publication No. F2008/000745-1, SARDI Research Report Series No 342, 100 pp.

Kämpf, J., C. Brokensha and T. Bolton. 2009. Hindcasts of the fate of desalination brine in large inverse estuaries: Spencer Gulf and Gulf St. Vincent, South Australia. Desalination and Water Treatment **2**: 325-333.

Lattemann, S., and T. Höpner, T. 2008. Environmental impact and impact assessment of seawater desalination. Desalination **220(1-3)**: 1-15.

Mavukkandy, M. O., C. M. Chabib, I. Mustafa, A. Al Ghaferi, and F. AlMarzooqi. 2019. Brine Management in Desalination Industry: From Waste to Resources Generation. Desalination **472**: 114187. doi: 10.1016/j.desal.2019.114187

McLeay, L., M.J. Doubell, S. Roberts, C. Dixon, L. Andreachhio, C. James, J. Luick, and J.F. Middleton. 2016. A biophysical model to optimise recruitment and sustainable harvest in southern Australia's largest prawn fishery. Fisheries Oceanography **25(2)**: 164-182. doi: 10.111/fog.12143

Middleton, J.F., M. Doubell, C. James, J. Luick, and Van Ruth, P. (2013). PIRSA Initiative II: Carrying Capacity of Spencer Gulf: Hydrodynamic and Biogeochemical Measurement Modelling and Performance Monitoring. Final report for the Fisheries Research and Development corporation. South Australian Research and Development Institute (Aquatic Sciences), Adelaide. SARDI Publication No. F2013/000311-1. SARDI Research Report Series No. 705.

Middleton J.F., M. Doubell. 2014. Carrying capacity for finfish aquaculture. Part I—Near-field semi-analytic solutions. Aquacultural Engineering **62**:54-65.

Middleton, J.F., J. Luick, and C. James. 2014. Carrying capacity for Kingfish aquaculture, Part II – Rapid Assessment using hydrodynamic and semi analytic solutions. Aquacultural Engineering, Aquacultural Engineering **62**: 66-78.

Middleton, J.F., D. Griffin, J. Luick, M. Herzfeld, C. James, and P. Oke. 2017. Physical oceanography of the Great Australian Bight: the science that underpins. Final Report GABRP Project 1.1. Great Australian Bight Research Program, GABRP Research Report Series Number 20, 109pp.

North, E. W., R. R. Hood, S.Y. Chao, and L. P. Sanford. 2006. Using a random displacement model to simulate turbulent particle motion in a baroclinic frontal zone: a new implementation scheme and model performance tests. Journal of Marine Systems **60**: 365-380.

North, E. W., Z. Schlag, R. R. Hood, M. Li, L. Zhong, T. Gross, and V. S. Kennedy. 2008. Vertical swimming behavior influences the dispersal of simulated oyster larvae in a coupled particle-tracking and hydrodynamic model of Chesapeake Bay. Marine Ecology Progress Series **359**: 99-115.

Oke, P. R., P. Sakov, M.L Cahill, J.R. Dunn, R. Fiedler, D.A. Griffin, ... and A. Schiller. 2013. Towards a dynamically balanced eddy-resolving ocean reanalysis: BRAN3. Ocean Modelling **67**: 52-70.

Omerspahic, M., H. Al Jabri, and I. Saadaoui, I. 2022. Characteristics of Desalination Brine and Its Impacts on Marine Chemistry and Health, With Emphasis on the Persian/Arabian Gulf: A Review. Frontiers in Marine Science 525.

Panagopoulos, A., and K.J. Haralambous. 2020. Environmental impacts of desalination and brine treatment-Challenges and mitigation measures. Marine Pollution Bulletin **161**: 111773.

Roberts, S.D., P.D. Van Ruth, C. Wilkinson, S.S Bastianello, and M.S. Bansemer. 2019. Marine heatwave, harmful algae blooms and an extensive fish kill event during 2013 in South Australia. Frontiers in Marine Science **6**: p.610.

Robins P., E., S.P. Neil, L. Gimenez, S.R. Jenkins, S.K. Malham. 2013. Physical and biological controls on larval dispersal and connectivity in a highly energetic shelf sea. Limnology and Oceanography **58(2)**: 505-524.

Rogers T.A., A. Redondo Rodriguez, A.J. Fowler, M.J Doubell, M.J. Drew, M.A. Steer, D. Matthews, C. James, B.M. and Gillanders. 2021. Using a biophysical model to investigate connectivity between spawning grounds and nursery areas of King George whiting (Sillaginodes punctatus: Perciformes) in South Australia's gulfs. Fisheries Oceanography **30(1)**:51-68.

Saha, S., S. Moorthi, X. Wu, J. Wang, S. Nadiga, P. Tripp, D. Behringer, Y.T Hou, H.Y. Chuang, M. Iredell, and M. Ek 2014. The NCEP climate forecast system version 2. Journal of Climate **27(6)**: 2185-2208.

Seed R. 1969. The ecology of *Mytilus edulis* L. (lamellibranchiate) on exposed rocky shore. Oecologia **3**:277–316.

Shchepetkin, A.F. and J.C. McWilliams. 2005. The regional oceanic modelling system (ROMS): a split-explicit, free-surface, topography-following-coordinate oceanic model. Ocean Modelling **9(4)**: 347-404.

Song, Y., and D.B. Haidvogel. 1994. A semi-implicit ocean circulation model using a generalized topography-following coordinate system. Journal of Computational Physics **115(1)**: 228-244.

Svane, I. 2011. An overview of the blue mussel in southern Australia–a serial invader, a blind passenger, or just a welcome addition to the menu? Transactions of the Royal Society of South Australia **135(2)**: 134-139.

Tanner, J.E., F. Bailleul, S. Bryars, M. Doubell, N. Foster, S. Gaylard, B.M. Gillanders, S. Goldsworthy, C. Huveneers, C. James, A.R. Jones, J. Maher, M. Nursey-Bray, P. van Ruth, and T.M. Ward. 2019. Potential social, economic and ecological indicators for integrated ecosystem assessment of Spencer Gulf. Goyder Institute for Water Research Technical Report Series No. 19/32, Adelaide, South Australia. ISSN: 1839-2725.

Tanner, J.E, M. Doubell M., P. van Ruth, C. James, J. and Middleton. 2020. Aquaculture Environmental Monitoring Program: 2015-2019. South Australian Research and Development Institute (Aquatic Sciences), Adelaide. SARDI Publication No. F2019/000334-1.

Tanner, J.E., and S. Drabsch. 2021. Literature review of potential impacts of desalination discharges in Boston Bay, with particular reference to Aquaculture. South Australian Research and Development Institute (Aquatic sciences) Adelaide. SARDI Publication No. F2021/0002999-1. SARDI Research Report Series No. 1105.17pp.

Thompson, R.O.R.Y. 1983. Low pass filters to suppress inertial and tidal frequencies. Journal of Physical Oceanography **13**:1077-1083.

Warner, J.C., Z. Define, K. Haas, and H.G. Arango. 2013. A wetting and drying scheme for ROMS. Computers and Geosciences **58**: 54:61.

Whiteway, T.G., 2009. Australian Bathymetry and Topography Grid: Geoscience Australia Record 2009/21, 46pp.

7. APPENDIX

7.1.   Appendix 1: Station transects

Figure 42 shows the locations of model stations and the transects from which model results were used to investigate the salinity increases in the vicinity of outfalls presented in Figure 23, Figure 26, Figure 29, Figure 32 and Figure 35.
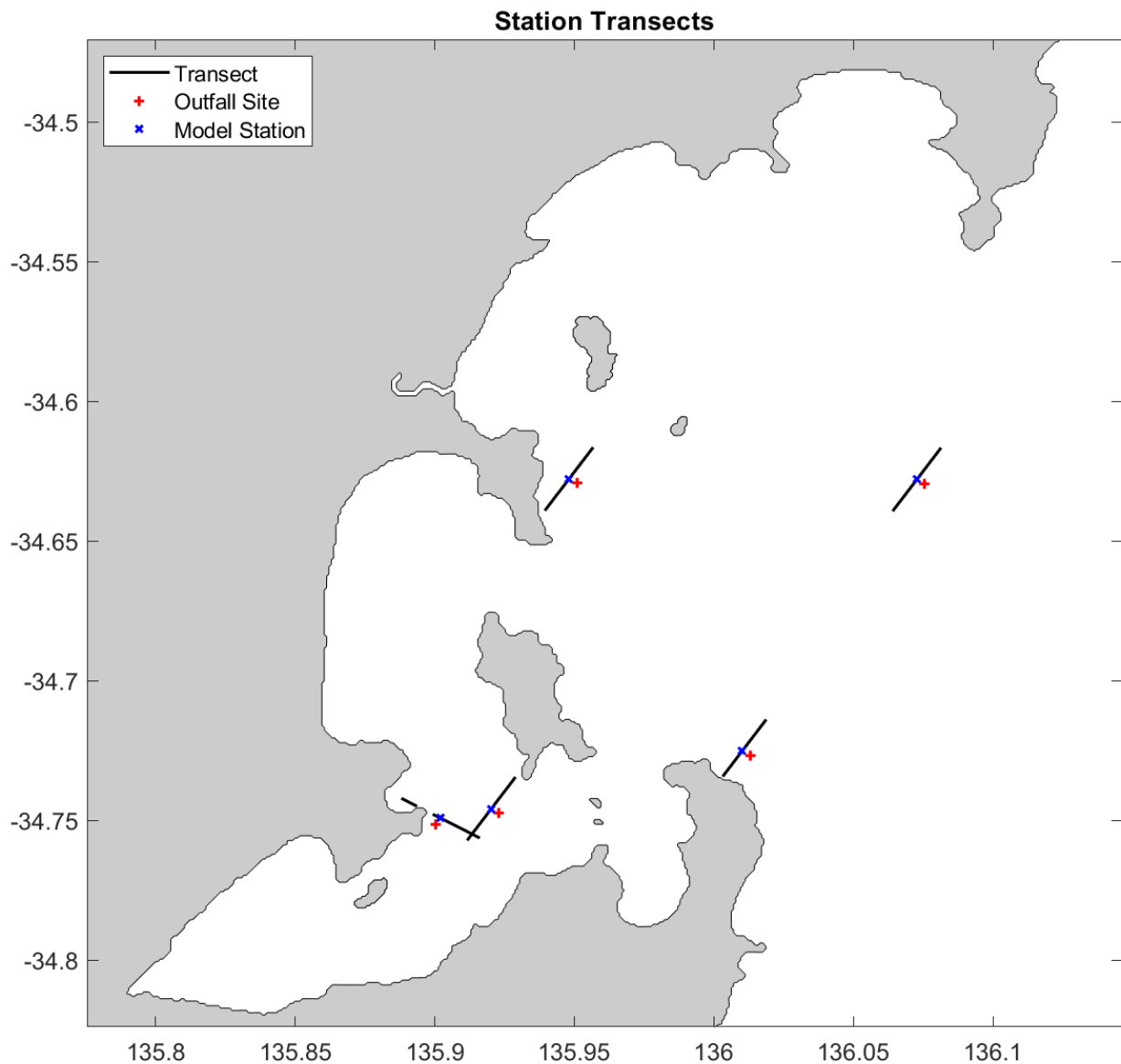
Figure 42. Location of transects (black lines) and model stations (blue markers) relative to potential outfall sites (red markers).

7.2. Appendix 2: Model sensitivity to the vertical distribution of brine discharges

As detailed in the methods (see section 2.3) desalination brine was discharged into the bottom (sigma) layer of the model at each outfall location. This provided a conservative approach to understand the potential 'worst case' increases in salinity. In reality, brine discharged through diffusers, which are designed to achieve a 40:1 dilution at the seabed under all conditions, are expected to achieve rapid mixing and dispersal of discharges over spatial scales of metres to several hundred meters.

To better understand the sensitivity of far-field salinity increases associated with a more realistic brine releases in the vertical, model simulations for the Billy Lights Point and Point Boston inshore outfalls were run for a period of 3 months from 1-January to 1-May 2016 with brine discharges spread across the bottom 1, 2 and 3 layers of the model, respectively. Figure 43 shows example time-series of the vertical salinity distribution at the Point Boston inshore outfall location corresponding with discharges spread over increasing distances in the vertical. Not surprisingly, dilution of the outfall was achieved by discharging brine into larger volumes. Maximum salinity anomalies averaged across the 3-month simulation at the Billy Lights inshore outfall reduced from 0.7±0.4 PSU (± 2 standard deviations of the mean) for discharges into the single bottom layer of the model to 0.39±0.25 PSU for discharges spread across the bottom three layers of the model (Figure 45). Similarly, for the Point Boston outfall, maximum salinity anomalies decreased from 0.98±0.5 PSU (± 2 standard deviations of the mean) for discharges into the single bottom layer of the model to 0.44±0.27 PSU for discharges spread across the bottom three layers of the model.

Figure 46 and Figure 47 show map views of the hourly-averaged bottom salinity distribution predicted for the different vertical discharge scenarios from the Billy Lights Point and Point Boston outfalls, respectively. A full animation of the 3-month period is provided in Appendix 3. The dilution of brine achieved by discharging across increasing distances in the vertical was predicted to have a small, localised impact on the far-field dispersion of salinity. This was evidenced by a ~50 % reduction in the size of the spatial footprint indicated by the 0.2 PSU anomaly contour, which decreased from a diameter of ~1-2 km for outfalls discharged into the bottom layer of the model to ≤1 km for discharges spread across the bottom three layers of the model.
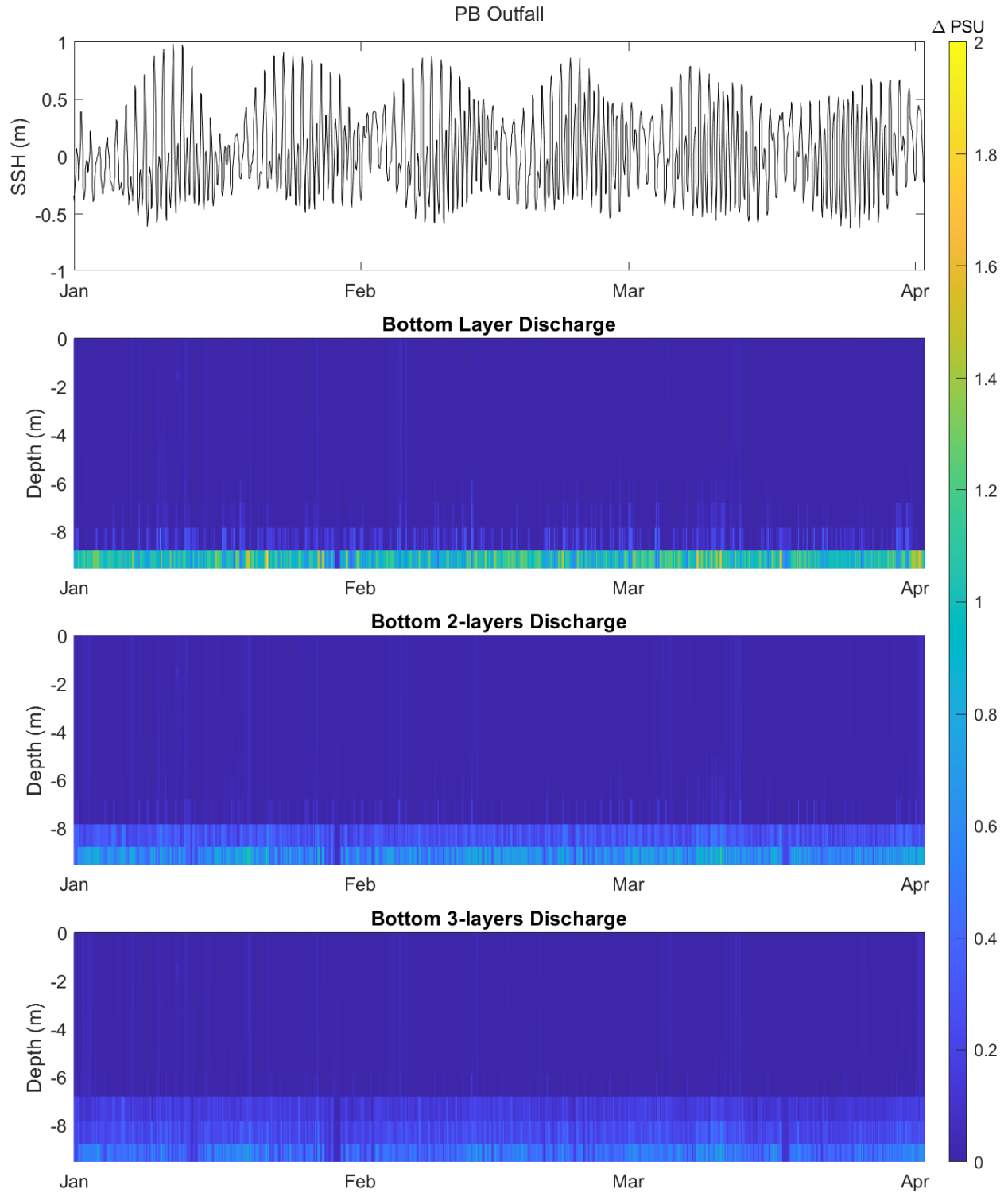
Figure 43. Hourly time-series of salinity (PSU) throughout the water column at the Point Boston inshore outfall associated with brine discharged into the bottom 1, 2 and 3 layers of the model, respectively.

Figure 44. Hourly salinity anomalies (PSU) at the Billy Lights Point outfall associated with discharges spread across the bottom 1, 2 and 3 layers of the model. Red markers show the maximum anomaly. Light blue and green lines show the timeseries mean ± 2 standard deviations, respectively. Dark blue line shown the vertically averaged salinity anomaly.

Figure 45. Hourly salinity anomalies (PSU) at the Point Boston outfall associated with discharges spread across the bottom 1, 2 and 3 layers of the model. Red markers show the maximum anomaly. Light blue and green lines show the timeseries mean ± 2 standard deviations, respectively. Dark blue line shown the vertically averaged salinity anomaly.
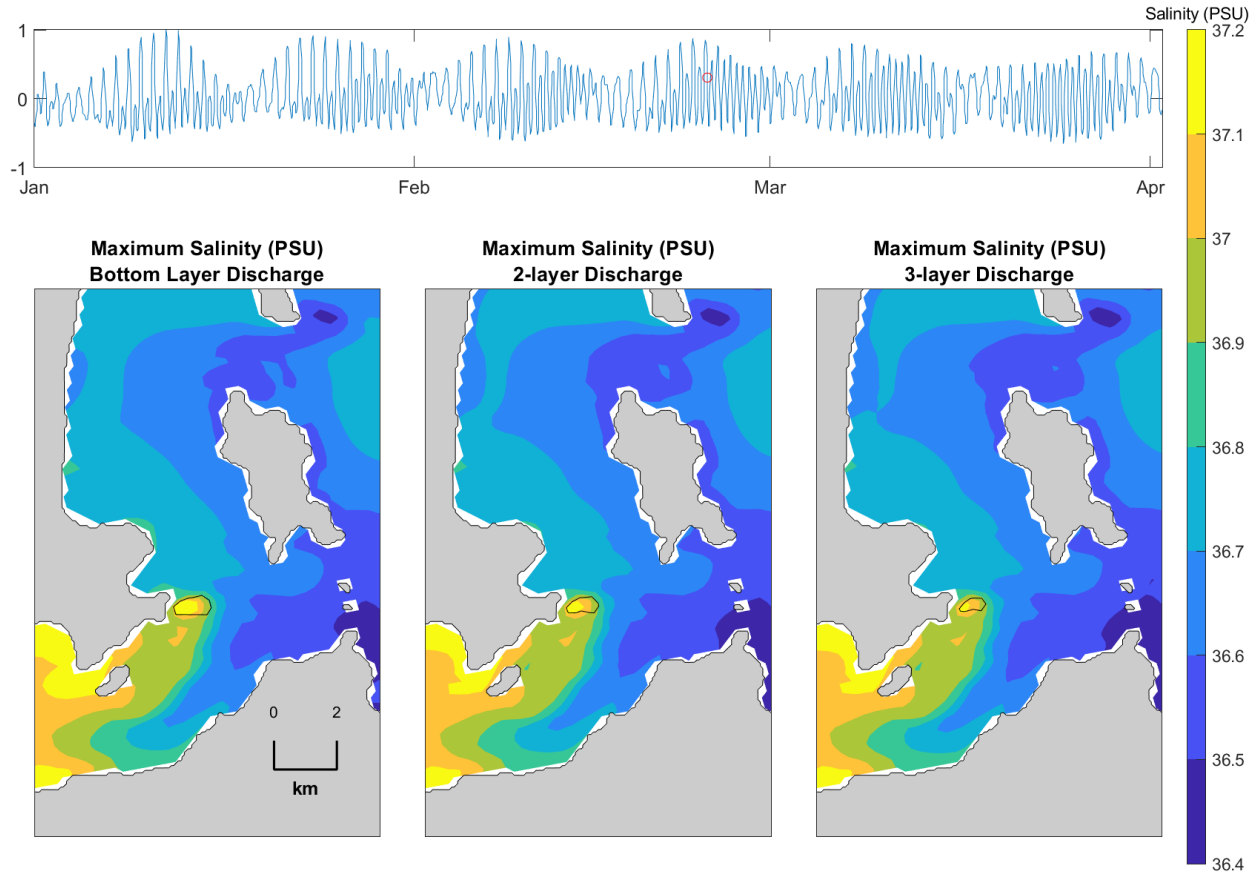
Figure 46. Snapshot of the bottom salinity in the vicinity of the Billy Lights Point outfall for discharges spread across the bottom 1, 2 and 3 layers of the model. Top panel - shows the sea level height (m). Red marker shows the point in time corresponding to the salinity maps shown in the bottom panels. Black line shows the 0.2 PSU salinity anomaly contour.
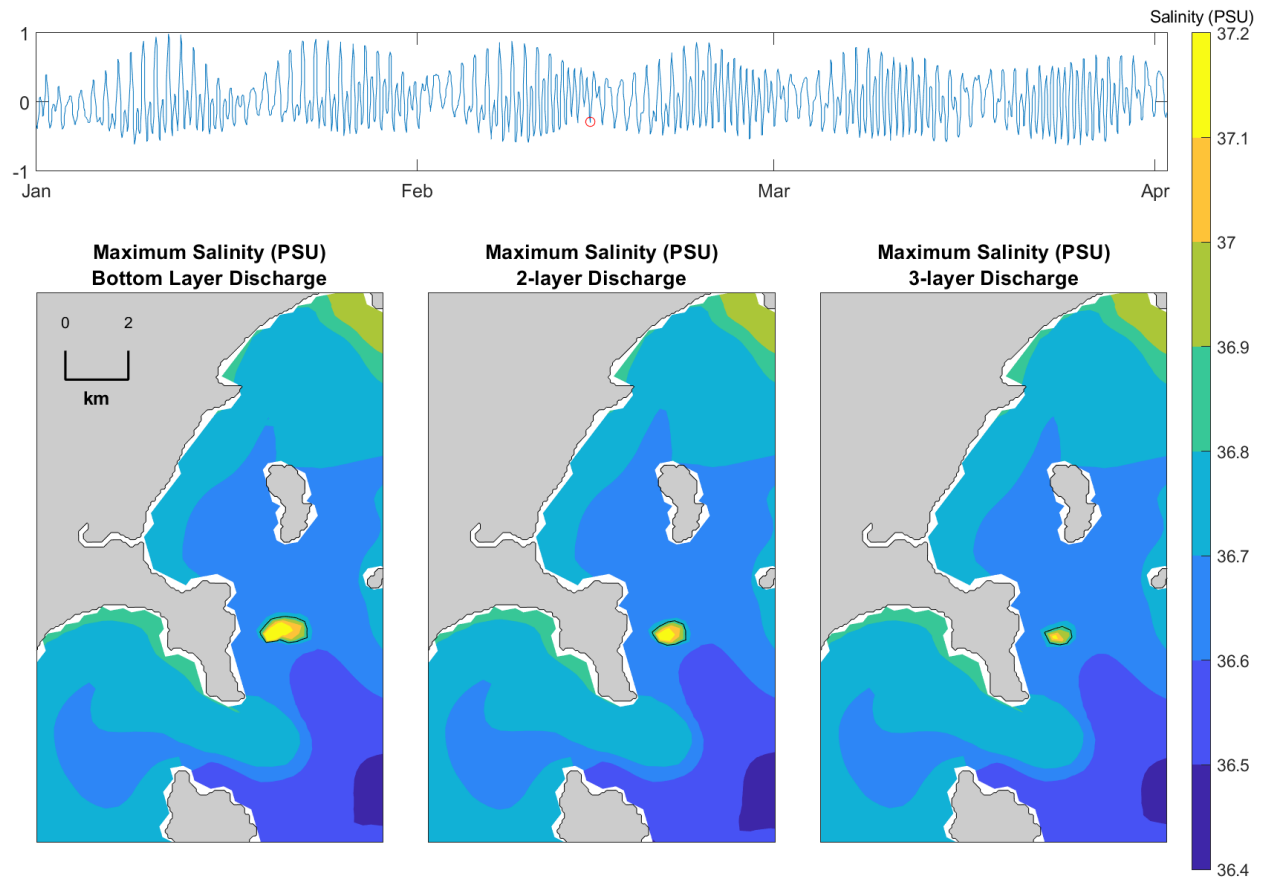
Figure 47. Snapshot of the bottom salinity in the vicinity of the Point Boston outfall for discharges spread across the 1, 2 and 3 bottom layers of the model. Top panel - shows the sea level height (m). Red marker shows the point in time corresponding to the salinity maps shown in the bottom panels. Black line shows the 0.2 PSU salinity anomaly contour.

7.3.   Appendix 3: List of supplementary model animations

Animation1. 5-year hindcast showing daily bottom salinity distributions for model scenarios with and without desalination and at each outfall location. S0 = default model run without desalination. BL = Billy Lights Point, BLX = Billy Lights Point-extension, PB = Point Boston, PBX = Point Boston-extension, CD = Cape Donington.

Animation 2a. 3-month hindcast of hourly-averaged bottom salinity in the vicinity of the Billy Lights Point outfall for discharges spread across the bottom 1, 2 and 3 layers of the model. Top panel - shows the sea level height (m). Red marker shows the point in time corresponding to the salinity maps shown in the bottom panels. Black line shows the 0.2 PSU salinity anomaly contour.

Animations 2b. 3-month hindcast of hourly-averaged bottom salinity in the vicinity of the Point Boston outfall and for discharges spread across the bottom 1, 2 and 3 layers of the model. Top panel - shows the sea level height (m). Red marker shows the point in time corresponding to the salinity maps shown in the bottom panels. Black line shows the 0.2 PSU salinity anomaly contour.